

## High-resolution atomic force microscopy and spectroscopy of native membrane proteins

This article has been downloaded from IOPscience. Please scroll down to see the full text article.

2011 Rep. Prog. Phys. 74 086601

(<http://iopscience.iop.org/0034-4885/74/8/086601>)

View [the table of contents for this issue](#), or go to the [journal homepage](#) for more

Download details:

IP Address: 133.28.47.30

The article was downloaded on 03/09/2011 at 08:12

Please note that [terms and conditions apply](#).

# High-resolution atomic force microscopy and spectroscopy of native membrane proteins

Christian A Bippes and Daniel J Muller

ETH Zürich, Department of Biosystems Science and Engineering, 4058 Basel, Switzerland

E-mail: [daniel.mueller@bsse.ethz.ch](mailto:daniel.mueller@bsse.ethz.ch)

Received 9 March 2011, in final form 30 May 2011

Published 11 July 2011

Online at [stacks.iop.org/RoPP/74/086601](http://stacks.iop.org/RoPP/74/086601)

## Abstract

Membranes confining cells and cellular compartments are essential for life. Membrane proteins are molecular machines that equip cell membranes with highly sophisticated functionality. Examples of such functions are signaling, ion pumping, energy conversion, molecular transport, specific ligand binding, cell adhesion and protein trafficking. However, it is not well understood how most membrane proteins work and how the living cell regulates their function. We review how atomic force microscopy (AFM) can be applied for structural and functional investigations of native membrane proteins. High-resolution time-lapse AFM imaging records membrane proteins at work, their oligomeric state and their dynamic assembly. The AFM stylus resembles a multifunctional toolbox that allows the measurement of several chemical and physical parameters at the nanoscale. In the single-molecule force spectroscopy (SMFS) mode, AFM quantifies and localizes interactions in membrane proteins that stabilize their folding and modulate their functional state. Dynamic SMFS discloses fascinating insights into the free energy landscape of membrane proteins. Single-cell force spectroscopy quantifies the interactions of live cells with their environment to single-receptor resolution. In the future, technological progress in AFM-based approaches will enable us to study the physical nature of biological interactions in more detail and decipher how cells control basic processes.

(Some figures in this article are in colour only in the electronic version)

This article was invited by E Frey.

## Contents

<b>1. Introduction</b>	2		
<b>2. Overview of atomic force microscopy-based methods applied to membrane proteins</b>	2		
2.1. Contact mode imaging	2	3.1. Membrane proteins must reside in their functional environment	10
2.2. Oscillation mode imaging	4	3.2. Immobilization strategies for membrane proteins	10
2.3. High-speed imaging	5	3.3. Modification of AFM cantilevers for SMFS and SCFS	14
2.4. Limits, challenges and perspectives of high-resolution imaging	5	3.4. Current limitations, challenges and perspectives	16
2.5. Single-molecule force spectroscopy	6	<b>4. Imaging native membrane proteins at work</b>	17
2.6. Dynamic force spectroscopy	7	4.1. Imaging native membrane proteins at sub-nanometer resolution	17
2.7. Single-cell force spectroscopy	8	4.2. Identifying membrane proteins and their structural details	18
2.8. Limits, challenges and perspectives in SMFS and SCFS	9	4.3. Imaging the oligomeric state of native membrane proteins	20
<b>3. Sample preparation procedures</b>	10		

4.4. Oligomeric assembly can alter surface structures of membrane proteins	20	5.5. Mapping energy barriers and reconstructing the energy landscape of membrane proteins	28
4.5. Imaging the supramolecular assembly of membrane proteins	21	5.6. Current limitations, challenges and perspectives	29
4.6. Imaging membrane protein dynamics using time-lapse AFM	21	<b>6. Understanding function-related interactions in membrane proteins</b>	29
4.7. Imaging membrane proteins at work	23	6.1. Ligands establish specific interactions	30
4.8. Current limitations, challenges and perspectives	24	6.2. Inhibitors establish different interactions than ligands	30
<b>5. Quantifying and locating interactions of membrane proteins</b>	24	6.3. How do interactions influence conformation?	30
5.1. Pick and play with single membrane proteins	24	6.4. Quantifying how membrane proteins crosstalk	31
5.2. Unfolding individual membrane proteins	24	6.5. Current limitations, challenges and perspectives	32
5.3. Quantifying and mapping interactions of membrane proteins	24	<b>7. Conclusions and outlook</b>	33
5.4. Refolding membrane proteins	26	<b>Acknowledgments</b>	34
		<b>References</b>	34

## 1. Introduction

Membrane proteins are essential for life. They reside in lipidic membranes that form the boundaries of cells and their compartments. Membrane proteins are highly specialized molecular machineries that provide cellular membranes with unique functions. Cellular membranes peppered with membrane proteins not only separate chemically and physically different environments from each other but also actively create and maintain such differences. As such, they are involved in crucial processes such as energy conversion, signal transduction and amplification, enzymatic activities, molecular transport, anchoring of the cytoskeleton, formation of adhesion and motility.

*In vivo*, membrane proteins are involved in various networks providing and controlling cellular functionality. Consequently, timed and spatial organization of membrane proteins and their binding partners are crucial to fulfil their functional tasks. Inter- and intramolecular interactions spatially organize membrane proteins and determine their structure and function. But it is still not understood how cells establish, direct and control such interactions to, for example, determine the dynamic assembly and modulate the functional state of membrane proteins. Malfunction of these mechanisms that control membrane protein structure, assembly and function often causes severe diseases. Understanding the processes leading to malfunction is critical for the development of new therapies. It is therefore not surprising that over the past decades many scientists aimed to characterize the mechanisms that determine the structure, assembly and function of membrane proteins.

Since its invention in 1986, the atomic force microscope [1] has evolved into a multifunctional tool [2] in membrane protein research [3,4]. Here, we will review atomic force microscopy (AFM)-based methods used to investigate structure, assembly, folding and interactions of membrane proteins. We exemplify how these techniques can be applied to membrane proteins. In particular, we will illustrate how high-resolution AFM imaging approaching a lateral resolution of  $\approx 1$  nm is used to gather information about the oligomeric state and assembly of membrane proteins and how time-lapse AFM

can be used to observe membrane proteins at work. AFM-based single-molecule force spectroscopy (SMFS) can be used to detect the inter- and intramolecular interactions that stabilize membrane proteins, determine their unfolding pathways, direct their assembly and guide ligand as well as inhibitor binding. Deciphering the physical and chemical nature of these interactions allows deeper understanding of how they can modulate protein structure and functional state. Unfolding proteins on different time-scales allows reconstruction of the unfolding energy landscape of membrane proteins and thus provides deeper insight into how different functional states are stabilized.

## 2. Overview of atomic force microscopy-based methods applied to membrane proteins

Most AFM-related applications share a common experimental setup consisting of three main elements [2]. (i) The heart of an atomic force microscope is a microfabricated cantilever with a molecularly sharp stylus at its end. It senses the interaction forces between the very apex of its stylus and the sample. The cantilever can be described as a Hookean spring. Its vertical displacement ( $d$ ) is proportional to the force ( $F$ ) applied or experienced:  $F = -k_c d$ , where  $k_c$  is the cantilever spring constant. (ii) An optical beam deflection detection system monitors the cantilever bending upon interaction with the sample. (iii) A piezoelectric actuator allows accurate three-dimensional positioning of the sample relative to the stylus. Computer-controlled hardware provides feedback mechanisms, records the deflection signal and piezo positions and drives the piezoelectric actuator. In the following, the most common imaging and probing techniques in membrane protein research will be described.

### 2.1. Contact mode imaging

Contact mode (CM) imaging was the very first AFM imaging mode. To reveal a sample's topography in CM, the cantilever stylus is raster scanned over the surface while being in contact with the sample and applying a pre-defined, non-destructive contact force. The contact force and thus the cantilever deflection are maintained by a feedback loop throughout the

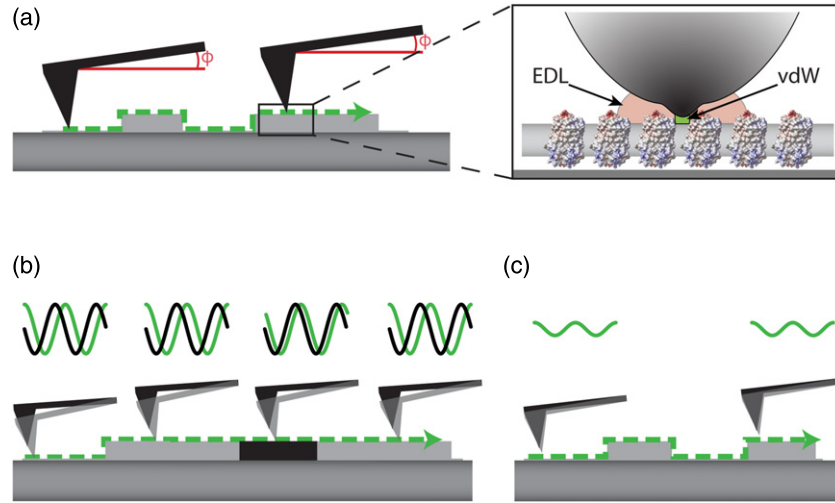


**Figure 1.** AFM modes used to image native membrane proteins at high resolution. (a) In CM, the atomic force microscope stylus contours the surface (green dashed line) while applying a constant force. The force, or bending of the atomic force microscope cantilever, is kept constant by a feedback loop. In high-resolution CM imaging, small protrusions at the apex of the atomic force microscope stylus contour the protein membrane. Interactions between stylus and protein membrane can be separated into long-range electrostatic double layer (EDL) and short-range van der Waals (vdW) forces. (b) In intermittent CM, the cantilever is oscillated (black curves) while scanning the sample surface. Ideally, the atomic force microscope stylus touches the sample surface at the end of every downward movement. Simultaneous to the sample topography, the intermittent CM can provide information on surface properties such as charges, hydrophobicity, roughness and elasticity. The phase mode records the phase shift between the oscillation driving the cantilever (black curve) and the actual cantilever oscillation (green curve). The scheme shows two surface areas (black and gray) that exhibit different mechanical properties and originate different phase shifts. (c) In NC mode AFM imaging, the cantilever is oscillated at its resonance frequency using low amplitudes. In contrast to the intermittent CM, the stylus does not touch the sample surface during its downward movement. Interactions between stylus and sample cause a distance-dependent resonance frequency change, which is used to infer the sample topography.

imaging process, i.e. if a surface feature deflects the cantilever the piezoelectric actuator vertically adjusts the sample (or stylus) position to maintain the cantilever deflection constant (figure 1(a)). The piezo's  $x$ -,  $y$ - and  $z$ -positions at each pixel of the raster scan are used to generate the topographic image. The deviation of the cantilever deflection from its setpoint is recorded as well and provides the error image. During imaging careful adjustment of imaging gains and deflection setpoint are required to precisely contour the soft biological surface without distortion.

Forces acting between the stylus and a complex biological macromolecule can have very different origins. Most interactions are based on steric, van der Waals (vdW) and electrostatic forces. In contrast to extremely short-range steric forces ( $\leq 1 \text{ \AA}$ ), vdW and electrostatic forces are effective over a range from a few to several hundreds of nanometers [5].

The surfaces of biological specimens as well as of most materials used as atomic force microscope supports and cantilevers expose net surface charges and thus an electrostatic surface potential. Magnitude and sign of the surface charges depend on the pH of the buffer solution and the pK values of functional groups on the material. Charges on surfaces immersed in buffer solution are screened by counterions that give rise to a diffuse electrostatic double layer (EDL). The EDL thickness is characterized by the Debye length,  $\lambda_D$ ,

$$\lambda_D = \sqrt{\frac{\epsilon_e \epsilon_0 k_B T}{e^2 \sum_i c_{e,i} z_i^2}}, \quad (1)$$

where  $e$  is the electronic charge,  $k_B$  is the Boltzmann constant,  $T$  is the absolute temperature,  $\epsilon_e$  and  $\epsilon_0$  are the permittivities

of solute and vacuum, respectively, and  $c_{e,i}$  and  $z_i$  are the concentration and valency of the  $i$ th electrolyte component. The Debye length thus highly depends on the concentration and valency of the electrolyte ions.

Approaching two charged surfaces causes the EDLs of both surfaces to overlap, which gives rise to long-range EDL forces ( $F_{el}$ ). At small separations in the order of a few nanometers, vdW forces ( $F_{vdW}$ ) also become relevant. The interplay between these two forces is described by the Derjaguin–Landau–Verwey–Overbeek (DLVO) theory. Both  $F_{el}$  and  $F_{vdW}$  depend on the shape and area of the interacting surfaces. Thus, an estimate for the stylus geometry is required to calculate the DLVO forces ( $F_{DVLO}$ ) between a membrane protein surface and a cantilever stylus. Styluses used for high-resolution imaging can be described as composed of a large macroscopic stylus (radius  $r_m \approx 40\text{--}200 \text{ nm}$ ) [6, 7] from which a small stylus (radius  $r_l \approx 2 \text{ nm}$ ) [8] protrudes (figure 1(a), magnified region). To calculate  $F_{DVLO}$ , interactions between the macroscopic stylus ( $r_m$ ) and the flat sample surface as well as interactions between a minimal protrusion of the stylus ( $r_l$ ), which is modeled as a hemisphere, and a protein of approximately the same radius ( $r_l$ ) have to be taken into account:

$$\begin{aligned} F_{DVLO}(d_{ts}) &\approx F_{DVLO}^m(d_{ts}) + \frac{1}{2} F_{DVLO}^l(d_{ts}) \\ &= F_{el}^m(d_{ts}) + F_{vdW}^m(d_{ts}) + \frac{1}{2} [F_{el}^l(d_{ts}) + F_{vdW}^l(d_{ts})] \\ &= \frac{4\pi \sigma_s \sigma_t r_m \lambda_D}{\epsilon_e \epsilon_0} e^{-(d_{ts}+r_l)/\lambda_D} - \frac{H_a r_m}{6(d_{ts} + r_l)^2} \\ &\quad + \frac{\pi \sigma_s \sigma_t r_l \lambda_D}{\epsilon_e \epsilon_0} e^{-d_{ts}/\lambda_D} - \frac{H_a r_l}{24d_{ts}^2} \end{aligned} \quad (2)$$

where  $\sigma_s$  and  $\sigma_t$  are the surface charge densities of sample and stylus, respectively,  $H_a$  is the Hamaker constant and  $d_{ts}$  is the distance separating stylus and sample. Based on equation (2) and underscored by experimental evidence, Muller *et al* showed that careful adjustment of pH and electrolyte concentrations are helpful to reveal high-resolution topographic images [7, 9]. For stable high-resolution imaging the electrostatic repulsion must be adjusted to compensate vdW attraction and most of the force applied to the scanning stylus (figure 1(a), inset) [9].

## 2.2. Oscillation mode imaging

Since the invention of AFM a multitude of imaging techniques other than CM have been developed. In these modes, the cantilever is not quasi-static as in CM AFM but is actively oscillated. These modes are also called dynamic modes. As the cantilever is either only temporarily or never in contact with the sample surface, these AFM imaging modes reduce sample disruption and displacement by lateral forces that can be exerted during CM imaging. Moreover, contamination of the scanning atomic force microscope stylus is also reduced. In the following sections some of these modes that were applied to membrane proteins will be briefly reviewed.

### 2.2.1. Intermittent CM imaging.

Intermittent CM AFM imaging is probably the most widespread AFM imaging technique. The cantilever is mechanically, acoustically or magnetically excited to oscillate close to its first resonance frequency ( $f_0$ ). Ideally, the stylus touches the sample surface only once during an oscillation cycle reducing lateral forces exerted on the sample. Several oscillation parameters are sensitive to interaction of the cantilever stylus with the surface: resonance frequency, oscillation amplitude and phase shift. Although any of these can be used as a feedback parameter, often the oscillation amplitude of the atomic force microscope cantilever is used as regulatory criterion to contour the sample surface by keeping the oscillation amplitude constant (figure 1(b), green curves). This so-called amplitude modulation (AM) AFM mode was shown to approach resolution close to CM AFM. However, it has been rarely used to image membrane proteins at high resolution [10, 11]. This is mainly due to the fact that CM AFM imaging still outclasses AM AFM imaging of membrane proteins in both speed and resolution.

*Beyond topographic imaging.* Apart from pure topographic imaging, intermittent CM AFM can be used to simultaneously image other sample properties. In AM AFM a phase shift between the driving signal and the actual oscillation of the cantilever indicates dissipative stylus sample interactions (figure 1(b), green and black curves). Such changes in dissipative interactions can indicate heterogeneous mechanical properties of the sample [12]. Recently, imaging modes that use excitation of higher harmonics or torsional modes extended the repertoire of dynamic modes [13–18]. These modes show higher sensitivity than conventional AM AFM and can provide nanomechanical properties of the sample. Moreover, imaging

modes simultaneously exciting multiple flexural modes of the cantilever have been developed [19–21]. Such multifrequency AFM imaging uses the different flexural modes to separate topography from other interactions that influence the stylus motion [19, 22]. For example, the amplitude signal of the first flexural mode of the cantilever oscillation contours the sample topography while the phase signal of the second flexural mode can be used to measure mechanical, magnetic or electrical properties of the sample [20]. Although multifrequency AFM imaging has been applied to image, e.g., DNA [19] and antibodies [23], so far none of these new dynamic imaging modes could reveal high-resolution ( $\approx 1$  nm) images of membrane proteins.

*Locating specific molecules by recognition imaging.* The location of specific membrane proteins within a complex sample can be determined using molecular recognition imaging (MRI). The mode relies on functionalization of the atomic force microscope stylus with molecules that specifically interact with the sample surface [24]. Such molecules can be ligands binding to their receptors [25–27] or antibodies binding to their antigens [28–30]. The fastest of the MRI modes simultaneously acquires topography and recognition (TREC) images. In TREC imaging, the upper and lower halves of the cantilever oscillation are analyzed separately. While the lower half provides topographic information, recognition information is revealed by the upper part. Upon specific binding of a molecule to the surface, the adhesion event and the concomitant linker stretching damp the upward movement of the cantilever. Resolution of TREC images is in the range 10–200 nm [28] and is therefore too low to localize binding sites within membrane proteins.

### 2.2.2. Non-contact imaging.

Problems arising from physical contact between atomic force microscope stylus and sample can be overcome by non-contact (NC) AFM [31], where the cantilever stylus is oscillated with small amplitude ( $\approx 0.5$ –10 nm) above the surface but never touches it (figure 1(c)). The distance between stylus and sample is quantified by changes in the cantilever's resonance frequency ( $\Delta f$ ) that is altered by stylus–sample interactions. Hoogenboom and co-workers recently developed an NC frequency modulation atomic force microscope capable of imaging membrane proteins at high resolution in aqueous solution [32, 33]. This imaging mode allows the use of stiff cantilevers with high resonance frequencies that are more stable when close to the sample surface than soft ones. The high resonance frequency of the cantilever also allows differentiating between conventional drift (low frequency) and the actual signal (high frequency). If  $\Delta f$  is known as a function of stylus–sample separation and the oscillation amplitude is kept constant by adjusting the drive power,  $\Delta f$  can be used to quantitatively determine the stylus–sample interaction. Using  $\Delta f$  as feedback parameter permits imaging the sample topography [32]. NC frequency modulation AFM showed its strength by imaging monomer, dimers, trimers, tetramers and hexamers of voltage dependent anion channels (VDAC, figure 11(e)) from potato mitochondrial outer membranes that were hardly resolved by CM AFM [33].

Although both AM and NC AFM showed potential to image membrane proteins at high resolution, these modes have so far not broken the resolution benchmark ( $\approx 0.5\text{--}1\text{ nm}$ ) set by CM AFM imaging. Hence, CM AFM is still the method of choice to obtain high-resolution topographs of membrane proteins (see section 4 for details).

### 2.3. High-speed imaging

**2.3.1. Conventional AFM imaging is a slow procedure.** The drawback of ‘conventional’ AFMs operating in any of the imaging modes described in sections 2.1 and 2.2 is their scanning speed. While recording an acceptable high-resolution image ( $512 \times 512$  pixels) in CM AFM requires about 100 s, it takes  $\approx 5\text{--}10$  min to acquire a similar image in AM AFM. However, in many biological systems dynamic molecular processes take place on the millisecond time-scale. Furthermore, the scanning procedure of the atomic force microscope implies that proteins imaged at the beginning of a scan are observed at significantly different time points compared with those imaged at the end of a scan. Consequently, researchers aimed to develop AFM instrumentation capable of imaging biological samples at much higher scanning speeds. Nowadays, different approaches reach this goal.

**2.3.2. How to increase the frame rate of imaging.** During AFM imaging the cantilever has to respond fast enough to precisely contour the sample surface. In 1993 Butt and co-workers calculated the speed limit of AFM imaging and showed that it strongly depends on the cantilever properties:

$$v_{\max} \ll \frac{\lambda}{2} \sqrt{\frac{k_c + S}{m_c} - \frac{D^2}{2m_c^2}}, \quad (3)$$

where  $v_{\max}$  is the maximal achievable stylus velocity,  $\lambda$  the surface feature periodicity,  $D$  the cantilever damping,  $m_c$  the effective cantilever mass and  $S$  the surface elasticity [34]. Using soft, short cantilevers that exhibit lower mass and higher resonance frequencies ( $10\text{--}14\ \mu\text{m}$  length,  $3\text{--}5\ \mu\text{m}$  width,  $100\text{ nm}$  thickness,  $k_c \approx 0.1\text{--}0.2\ \text{Nm}^{-1}$ ,  $f_{0,\text{water}} \approx 100\text{--}200\ \text{kHz}$ ) speed up CM imaging to a frame rate of  $\approx 0.6\ \text{s}^{-1}$  [35].

However, the cantilever is not the only part of the atomic force microscope that limits imaging speed. The dynamic behavior of piezoelectric scanners and the feedback bandwidth set additional speed limits. Within the last decade, development of improved feedback control mechanisms [36, 37] and new piezoelectric scanner designs [38] addressed these issues. The proposed scanner designs include piezo stacks [39], high resonance flexure piezo scanners [40, 41] and quartz tuning forks [42].

**2.3.3. Current high-speed imaging approaches.** Three scientific groups—Miles, Hansma and Ando—contributed significantly to high-speed AFM instrumentation development. The Miles group employed a tuning fork as  $x$ -scanner [42, 43] and achieved frame rates of up to  $1300\ \text{s}^{-1}$ . However, in this approach the samples were scanned without feedback control

in the constant height mode [44]. Consequently, the force applied to the sample could not be controlled.

The Hansma group developed a variety of different components for high-speed AFM such as high-resonance frequency scanners [40, 41, 45, 46], soft small cantilevers exhibiting high resonance frequencies [45], fast data acquisition devices [45, 47] and optical deflection detection systems [35]. Their high-speed closed loop scanners were designed for scan ranges of up to  $13\ \mu\text{m} \times 13\ \mu\text{m}$  in the  $x$ - and  $y$ -directions and  $\approx 4.3\ \mu\text{m}$  in the  $z$ -direction. In combination with small fast responding cantilevers, these scanners allowed frame rates of up to  $8\ \text{s}^{-1}$  [40]. However, apparently the feedback controller was not optimized to maintain the imaging force constant during CM imaging because the error signal revealed most of the samples’ details [48].

Ando’s group has put emphasis on improving every part of the atomic force microscope for high-speed imaging by consequently increasing its bandwidth. Their atomic force microscope is today’s state-of-the-art instrument for high-speed AFM imaging of biological samples. In particular, their first high-speed atomic force microscope operating in the AM mode employed high resonance frequency cantilevers ( $f_{0,\text{water}} \approx 600\ \text{kHz}$ ) and piezo scanners ( $f_0 \approx 260\ \text{kHz}$ ). Moreover, the feedback-loop bandwidth was increased to about  $1\ \text{MHz}$  and the deflection detection system was adapted to the requirements of the small cantilevers [49]. Since then, all components have been further improved, thus providing low stylus–sample interaction forces and a frame rate of  $\approx 25\ \text{s}^{-1}$  ( $250\ \text{nm}$  frame size,  $100 \times 100$  pixels) ([50] describes the setup in detail). However, the maximal scan range had to be traded in for high scanning rates. Thus, the microscope provides fast scanning only on small frames of a few hundred nm.

The instrument developed by Ando’s group has been most successful in producing molecular-resolution images of biological samples at frame rates  $\geq 1\ \text{s}^{-1}$ . It was used to investigate both soluble [51, 52] and membrane proteins [53]. The latter studies provided, for example, insight into the structural dynamics of cytoplasmic polypeptide loops of the D96N mutant of *Halobacterium salinarum* bacteriorhodopsin during the photocycle [54].

### 2.4. Limits, challenges and perspectives of high-resolution imaging

Since its invention, the AFM has evolved from an instrument imaging hard surfaces in air toward imaging soft biological samples in buffer solution. Yet, the atomic resolution obtained for hard surfaces has not been reached for biological samples. The highest resolution achieved on membrane proteins was  $\approx 0.1\ \text{nm}$  vertically and  $\approx 0.5\ \text{nm}$  laterally, which allows the observation of substructural details of single membrane proteins [55]. The main factors limiting lateral resolution are the cantilever stylus sharpness and the control of stylus–sample interactions. As the cantilever stylus mechanically contours the sample surface, the resulting topography is a convolution of the sample’s surface structure and the stylus shape. Therefore, sharper styluses with smaller radii are capable of recording images at higher resolution. However, if the forces

between stylus and sample are not carefully adjusted, even sharp styluses will fail to provide high-resolution topographs. Development of more sensitive AFM instrumentation and imaging modes that allow the controlled application of small imaging forces ( $\leq 50$  pN) with pN precision will improve imaging of more fragile specimens.

So far, high-resolution AFM imaging requires experienced users that optimize the parameters of the AFM feedback loop and correct the deflection setpoint to compensate for thermal drift in CM AFM. Cantilevers coated with thin metal films are a major source of thermal drift. Their temperature sensitivity originates from the difference of the thermal expansion coefficients of the cantilever material and the thin metal coating. Because the feedback parameter in CM AFM is the cantilever deflection, drift of the cantilever deflection changes the force applied to the sample with time. Inappropriately applied force might lead to deformation or disruption of the soft protein membrane. Recently, cantilevers with a high resonance frequency that show a radically different design have been developed. Compared with conventional atomic force microscope cantilevers, these cantilevers are not susceptible to drift originating from thermal expansion of the cantilever materials [56]. The suitability of such cantilevers for high-resolution imaging needs to be shown.

### 2.5. Single-molecule force spectroscopy

Understanding the mechanisms determining the folding, stability and function of membrane proteins is one of the important challenges in life sciences. Over the years it has been increasingly recognized that forces acting between and within membrane proteins play a pivotal role in cell adhesion [57], molecular recognition [24, 58–60], signal transduction [61], mechanotransduction [62–64], motor protein movement [65] and protein folding and stability [66–69]. The forces experienced and generated by biological macromolecules are of manifold nature and can range from the sub-piconewton range up to several nanonewtons [70]. Measuring such minute forces with high precision in both magnitude and position can provide information on intra- and intermolecular interactions and mechanical properties of single-molecules and macromolecular complexes [68, 71–76].

In AFM-based SMFS, the cantilever stylus is used to pick up single molecules that are attached to a support. Thereto, the stylus is brought into contact with the surface of the support and subsequently retracted. If a molecule adheres to the stylus, it is stretched while separating the stylus from the support. This deflects the atomic force microscope cantilever and applies a mechanical force to the molecule. The cantilever deflection signal is acquired along with the piezo displacement (figure 2(a)). The distance traveled by the piezo does not represent the stylus–sample separation (sss) because the cantilever bends toward the support during stretching the molecule (figure 2(b)). The cantilever deflection ( $d$ ) and the piezo movement ( $\Delta z$ ) allows calculation of  $sss = \Delta z - d$ , which equals the extension of the stretched molecule. Plotting the force as a function of sss yields the so-called force–distance (F–D) curve.

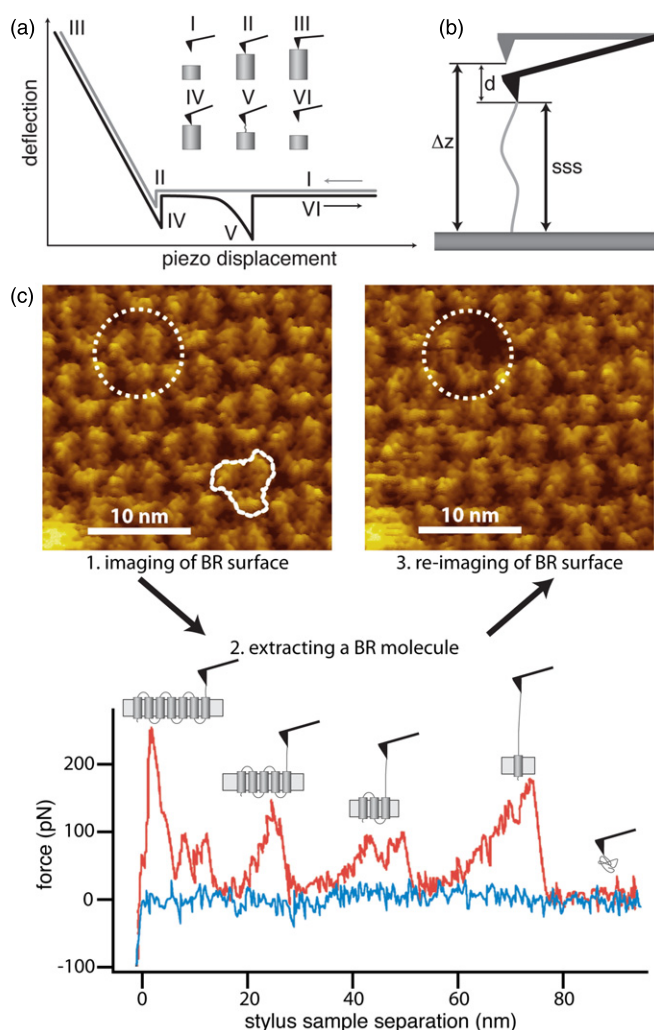


**Figure 2.** Principle of SMFS. (a) Schematic of an approach–retract cycle of a SMFS experiment. The sample surface is approached to the cantilever stylus until a certain contact force is reached (I–III). When approaching the surface, attractive forces pull the stylus toward the sample surface (‘snap in’, II). After allowing the stylus to establish interactions with the sample (III) the stylus is retracted. Non-specific adhesive stylus–sample interactions (IV) are stressed when establishing a stretching force upon retraction and deflection of the cantilever. As soon as the force suffices to break the interaction (V), the cantilever relaxes and the stylus is further separated from the sample (VI). (b) SMFS simultaneously records the cantilever bending ( $d$ ) and the movement of the piezoelectric transducer ( $\Delta z$ ). Subtracting the cantilever bending from the piezo movement results in the stylus–sample separation (sss) that reflects the length of the molecule tethered between the atomic force microscope stylus and sample surface. (c) Controlled unfolding of a single bacteriorhodopsin from native purple membrane. (1) High-resolution AFM topograph of the cytoplasmic surface of purple membrane clearly showing bacteriorhodopsin trimers (outlined). The atomic force microscope stylus was pressed for  $\approx 1$  s with  $\approx 0.5$ – $1$  nN onto one protein (circle). (2) Upon retracting the stylus from the purple membrane, an F–D curve exhibiting several force peaks was recorded. The distance at which the last force peak was recorded corresponds to the length of a completely unfolded and stretched bacteriorhodopsin molecule. (3) Topograph recorded after unfolding, which shows a missing bacteriorhodopsin molecule (encircled area).

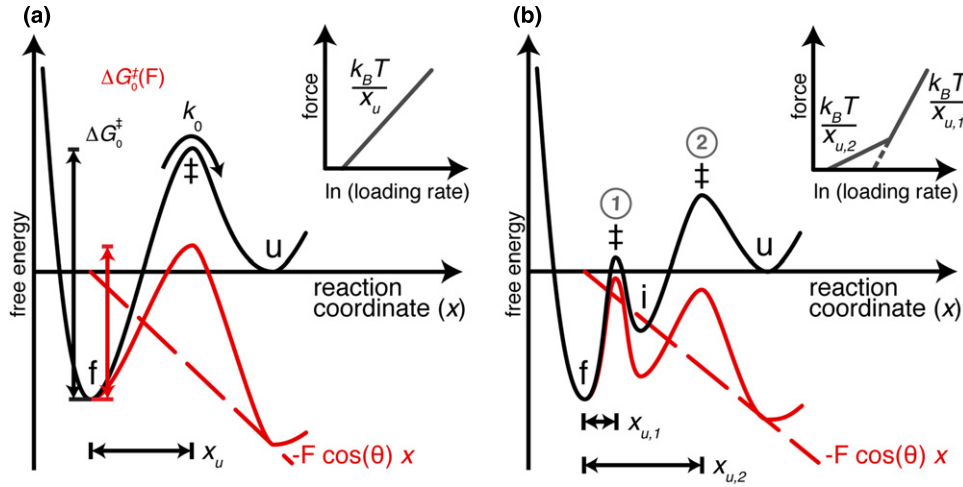


**Figure 3.** Free energy landscape deforming under externally applied force. (a) A single potential barrier separating the native (f, folded) and unfolded (u) states is characteristic for the free energy landscape of a two state unfolding process (black line). The activation free energy of unfolding is given by  $\Delta G_0^\ddagger$ , while  $x_u$  represents the distance between the native and the transition state ( $\ddagger$ ) along the reaction coordinate  $x$  and provides the width of the potential barrier. The energy barrier is spontaneously crossed at a transition rate  $k_0$ . Application of an external force,  $F$ , adds a mechanical potential  $-F \cos(\theta)x$  (dashed red line,  $\theta$  is the angle between the reaction coordinate and the vector of force) that tilts the energy landscape (solid red line). Therefore, the energy barrier is lowered. The inset sketches the theoretical dependence of the rupture force on the loading rate: the dynamic force spectrum, which is governed by a single linear regime, with a slope proportional to  $1/x_u$ . (b) Free energy landscape describing a three state unfolding process, in which an intermediate state (i) is populated during unfolding. Two energy barriers at  $x_{u,1}$  and  $x_{u,2}$  have to be crossed on the way from the native to the unfolded protein. Again, an externally applied potential (dashed red line) tilts the energy landscape (solid red line). At sufficiently high force, the outer barrier (2) is suppressed and the inner barrier (1) determines the transition kinetics. The inset shows the corresponding dynamic force spectrum with two linear regimes: at slow pulling velocities (lower force), the outer barrier determines the unfolding kinetics, while at higher pulling velocities (higher force) the inner barrier dominates.

For precise force measurements, a high force sensitivity of the cantilever is desirable. With sophisticated equipment, thermal motion of the cantilever is the only factor significantly limiting the smallest detectable cantilever deflection. Taking thermal motion as well as viscous damping and measurement bandwidth into account, the minimal detectable force,  $F_{\min}$ , is given by

$$F_{\min} \geq \sqrt{\frac{4k_B T B k_c}{2\pi f_0 Q}}, \quad (4)$$

where  $Q$  and  $B$  are quality factor and measurement bandwidth, respectively [77].

Figure 2(c) shows an example of a SMFS experiment. After high-resolution imaging the cytoplasmic surface of purple membrane from *H. salinarum* (figure 2(c), upper left panel), the atomic force microscope cantilever was pushed onto the purple membrane applying a contact force of  $\approx 0.5$ – $1.0$  nN for  $\approx 1$  s and subsequently retracted. During retraction an F–D curve like the one shown in the bottom panel of figure 2(c) was recorded. Re-imaging the purple membrane surface revealed a vacancy (figure 2(c), upper right panel) confirming unfolding and extraction of a bacteriorhodopsin molecule [68]. Analysis of such F–D curves not only provides information about the strength of interactions established but also about the location of force-induced structural transitions within the molecule. Thereto, peaks in the F–D curve are fitted using the worm-like chain (WLC) model [78] of polymer (here polypeptide) elasticity, which is accurate up to stretching forces of several

hundred piconewtons [71, 73, 79]:

$$F(x) = \frac{k_B T}{l_p} \left[ \frac{1}{4} \left( 1 - \frac{x}{L_c} \right)^{-2} + \frac{x}{L_c} - \frac{1}{4} \right], \quad (5)$$

where  $L_c$  is the contour length of the polymer,  $x$  is the polymer extension and  $l_p$  is the persistence length of the polymer, which describes the rigidity of the polymer and the distance over which the chain orientation is lost [80].

## 2.6. Dynamic force spectroscopy

Applying sufficiently high mechanical stress by SMFS causes membrane proteins to unfold in subsequent steps. Each force peak in an F–D curve reflects the unfolding of a structural segment of the membrane protein. However, these experiments are far from equilibrium because the rapid increase in distance between sample support and cantilever stylus prevents rebinding or refolding of the protein. In a first approximation, unfolding of each structural segment can be considered as a two state process. A structural segment resides either in a low-energy conformation representing the folded state or in a high-energy conformation, the unfolded state. An energy barrier has to be overcome when switching between both states (figure 3(a), black line). Such a two state unfolding energy landscape is characterized by the distance from the native to the transition state,  $x_u$ , and by the free energy of activation,  $\Delta G_0^\ddagger$ .  $\Delta G_0^\ddagger$  determines the rate  $k_0 = 1/t_0 \exp(-\Delta G_0^\ddagger/k_B T)$  at which a structural segment

spontaneously unfolds in the absence of force.  $t_0$  is the diffuse relaxation time.

Based on Bell's phenomenological model for the off-rate [81], Evans and Ritchie [82, 83] showed that an externally applied force lowers the unfolding energy barrier (figure 3(a), red line). Furthermore, the force required for unfolding depends on the rate at which force is applied, the so-called loading rate,  $r_f = dF/dt$  [83]. In general, unfolding of proteins at higher pulling velocities requires higher forces. Evans and Ritchie [82–84] showed that the most probable unfolding force,  $F^*$ , is a function of  $\ln(r_f)$ :

$$F^* = \frac{k_B T}{x_u} \ln \frac{r_f x_u}{k_B T k_0}, \quad (6)$$

The inset in figure 3(a) shows such a theoretical dynamic force spectrum. Dynamic force spectroscopy (DFS) determines the most probable unfolding force at different pulling velocities, i.e. loading rates. Fitting such a dynamic force spectrum using equation (6) yields  $x_u$  and  $k_0$ . These parameters characterize the energy barrier underlying the unfolding reaction.

The energy landscape sketched in figure 3(a) is a simplification. Macromolecular complexes are stabilized by a huge number of different interactions. Consequently, the energy landscape is rough with energy barriers of different heights and widths [85–88]. DFS locates the prominent energy barriers along the reaction coordinate, which is given by the stressing force [82, 89]. Figure 3(b) shows both the energy landscape and the dynamic force spectrum of a three state unfolding process, in which an intermediate state is populated during the transition from the folded to the unfolded protein.

## 2.7. Single-cell force spectroscopy

Many biological processes such as embryonic and neuronal development, intercellular communication or viral and bacterial infection rely on cell adhesion coordinated in time and space. This process is generally perceived as binding of a cell to another cell, a surface or an organic matrix. Interactions between cell and substrate are commonly established by cell-adhesion molecules (CAMs), which are usually transmembrane receptors. Whereas the extracellular domains of CAMs sense and bind the cellular environment, the intracellular domains of CAMs interact with cytoplasmic proteins, e.g. the cytoskeleton, and participate in intracellular signaling processes [90].

Although much is known already about cell adhesion, some fundamental questions are still unanswered. Classical washing assays have been helpful in identifying CAMs and their binding partners but did not provide quantitative information about their adhesion strength. Approaches based on regulated flow of media including flow-chambers [91] and spinning-disks [92] were used to estimate adhesion forces. However, these assays are based on shear force that depends on many parameters such as cell size. Therefore, the forces obtained remain rough and in many cases contradicting estimates. AFM-based single-cell force spectroscopy (SCFS) turned out to be a versatile and valuable tool to measure cell adhesion forces and gain insight into the underlying mechanisms [93].

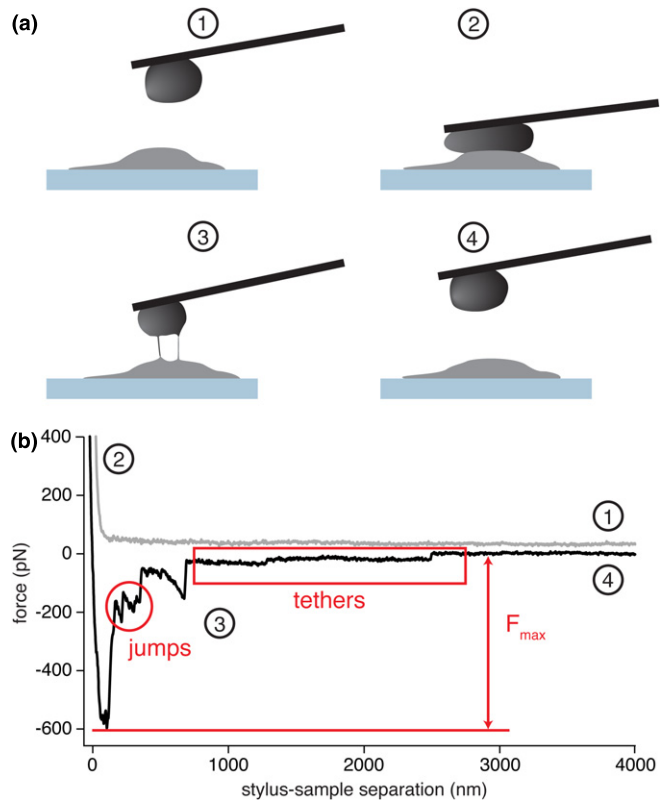


**Figure 4.** Principle of SCFS. (a) A living cell is attached to a functionalized cantilever (1) and lowered toward the substrate (2—here another cell). After reaching a certain contact force, the cell is kept in contact with the substrate for a predefined time before the cantilever is retracted from the substrate (3) until substrate and cantilever-bound cell are fully separated (4). (b) F–D curves recorded during approach and retraction of the cantilever-bound cell showing steps 1–4 explained in (a). Unbinding events classified as jumps and tethers can be assigned in the retraction F–D curve. Moreover, the maximum attachment force,  $F_{\max}$ , can be determined.

For SCFS, cells are seeded in a temperature-controlled liquid chamber of the atomic force microscope. A functionalized (stylus-less) cantilever is used to pick up a single cell. This cell can now be used to probe interactions with various substrates. Thereto, the cell is brought into contact with the substrate of interest, e.g. a functionalized surface or another cell, for a predefined contact time. Afterwards the cantilever is retracted at constant velocity (figure 4(a)). The cantilever movement is recorded during the approach and separation phase. The resulting F–D curves capture events occurring during cell detachment (figure 4(b)). As cell adhesion is a complex phenomenon involving a large number of molecules, F–D curves show an intricate spectrum of detachment events. The largest rupture force (figure 4(b), marked  $F_{\max}$ ) reflects the maximal adhesion strength. As the cell starts to detach from the substrate, small force steps (figure 4(b), marked jumps) can be observed which result from either breaking receptor–ligand interactions at the substrate or from the detachment of the receptor from the cellular cytoskeleton. In the latter case, a membrane tether is formed while the receptor is pulled away from the cell body. The final cell detachment events occur when the cell body is no longer in contact with the substrate and the membrane tethers are

stretched until remaining receptor interactions at the membrane tether tip rupture (figure 4(b), marked tethers) [94]. Extracting and extending such membrane tethers from cell membranes occurs at a constant pulling force that depends on the properties of the cell membrane and actomyosin cortex. Thus, tethers apply a constant force to receptors anchoring their end. This cellular force-clamp can be used to determine the lifetime of bonds established by cell surface receptors [95].

## 2.8. Limits, challenges and perspectives in SMFS and SCFS

### 2.8.1. Increased force sensitivity through small cantilevers.

SMFS relies on the detection of small stretching forces that induce sequential unfolding of the membrane protein. In modern thermal noise-limited SMFS instrumentation, the minimal detectable force ( $F_{\min}$ ) that determines the force resolution is set by the cantilever properties ( $k_c$ ,  $f_0$  and  $Q$ ) and the measurement bandwidth  $B$  (equation (4)). Consequently, at a given measurement bandwidth, small soft cantilevers with high resonance frequencies (for example, rectangular shaped cantilevers of  $10\ \mu\text{m}$  length,  $5\ \mu\text{m}$  width,  $100\ \text{nm}$  thickness,  $k_c \approx 0.064\ \text{N m}^{-1}$  and  $f_{0,\text{air}} > 500\ \text{kHz}$ .) offer higher force resolution and faster response than conventional cantilevers (for example triangular shaped cantilevers of  $200\ \mu\text{m}$  length,  $20\ \mu\text{m}$  width,  $k_c \approx 0.060\ \text{N m}^{-1}$  and  $f_{0,\text{air}} \approx 14\ \text{kHz}$ ) [96]. Unfortunately, such small cantilevers and specialized detection systems are currently not commercially available.

**2.8.2. Small cantilevers for DFS.** Small cantilevers would also offer advantages for DFS studies. To reconstruct an energy landscape the most probable interaction force should be captured over an as wide as possible range of loading rates, i.e. the speed at which the cantilever is separated from the sample surface has to be varied over a wide range. Because measurements are performed in aqueous solution, viscous drag forces ( $F_d$ ) act on the cantilever [97]:

$$F_d = \frac{6\pi\eta a_{\text{eff}}^2}{h + h_{\text{eff}}} v_{\text{stylus}}, \quad (7)$$

where  $\eta$  is the viscosity of the fluid and  $v_{\text{stylus}}$  is the velocity of the cantilever, which is not constant during an SMFS experiment due to cantilever deflection upon stretching a molecule.  $h$  represents the distance between the stylus and the sample,  $h_{\text{eff}}$  the effective stylus height and  $a_{\text{eff}}$  the effective radius of the cantilever.  $a_{\text{eff}}$  is an empirically determined parameter that also depends on the cantilever geometry. At high pulling velocities (above a few  $\mu\text{m s}^{-1}$ ) conventional cantilevers experience  $F_d$  comparable to the forces required for unfolding proteins or breaking receptor–ligand bonds. Moreover, viscous drag causes underestimation of the rupture force, which has to be corrected for [98, 99]. According to equation (7),  $F_d$  scales with both pulling speed and cantilever dimensions. Small cantilevers experience less viscous drag and as a result allow higher pulling velocities. Moreover, small cantilevers often show a higher resonance frequency and thus their noise level for a given bandwidth is significantly reduced compared with conventional cantilevers.

### 2.8.3. New approaches for SMFS near the equilibrium.

Force spectroscopy experiments are commonly far from equilibrium. Unfolding of membrane proteins often requires significant forces (several tens to a few hundred piconewtons). Refolding during an SMFS experiment requires the folding protein to generate a pulling force on the cantilever. This force is (at least) as high as the force required for prior unfolding. Moreover, the distance between cantilever stylus and sample surface rapidly increases in a SMFS experiment. Rebinding and refolding are thus inhibited. At very slow pulling velocities of  $\approx 0.5\text{--}1\ \text{nm s}^{-1}$  (water-soluble) proteins already unfold at low forces and also show refolding [100]. Under these conditions, switching between different folding states can be observed indicating that the protein is almost in equilibrium, at least on the timescale of the transitions. In these slow pulling experiments, which last several tens of seconds, cantilever drift may be problematic. Although the drift direction often shows a tendency, drift is an unpredictable process that superimposes with the cantilever deflection that is related to protein stretching [101]. To overcome drift-induced uncertainties drift-free cantilevers would be required. Cantilevers without any coating show less drift. Unfortunately, such cantilevers either poorly reflect the detection laser onto the atomic force microscope's photodiode, which results in a reduced signal-to-noise ratio, or exhibit a high spring constant reducing force resolution.

King *et al* proposed an alternative approach toward drift-free SMFS experiments [102]. In their setup, two lasers are used to monitor the position of the atomic force microscope cantilever stylus in space with respect to a fiducial mark engineered into the support. A feedback mechanism controls the stylus–sample distance and also keeps the stylus in register within the  $x$ ,  $y$ -plane at Ångström precision. Such ultra-stable atomic force microscopes will, in the future, allow new kinds of SMFS experiments where real equilibrium fluctuations of proteins under force can be investigated.

### 2.8.4. Large data sets demand high-throughput instrumentation.

For meaningful results from SMFS and SCFS experiments large data sets have to be acquired and analyzed. Today, throughput in both SMFS and SCFS is still low. Instruments that perform SMFS and SCFS automatically will increase the throughput. First automated SMFS robots are already commercially available. However, their use for SMFS on membrane proteins is currently limited as these automats lack the imaging capability that is usually required to locate suitable protein membranes. Cantilever arrays that permit simultaneous acquisition of multiple F–D curves might further increase throughput.

Today, most data analysis is still based on manual inspection and analysis of each F–D curve. In concert with automated data generation and acquisition [103, 104], data analysis routines have to be developed that reliably select, align and group F–D curves and beyond that identify and fit force peaks. First steps in this direction have been done. Some of these approaches mainly focus on selection [104], classification and alignment of F–D curves [105–107] while others automatically find and fit force peaks [108, 109].

### 3. Sample preparation procedures

Sophisticated sample preparation techniques are a prerequisite for AFM studies of membrane proteins. In this section we will focus on the importance of this issue starting with the separation of membrane proteins from the remainder of the cellular system. We will address methods to immobilize membrane proteins on different supporting substrates such as mica, gold and highly ordered pyrolytic graphite (HOPG) and to functionalize atomic force microscope cantilevers for SMFS and SCFS.

#### 3.1. Membrane proteins must reside in their functional environment

In addition to the plethora of structurally and functionally different membrane proteins present in cellular membranes, the lipid bilayer itself is multifaceted. The lipid composition of membranes strongly depends on organism, cell type and even the cellular organelle [110, 111]. The diversity of lipids allows individual cell to tailor membranes with specific physical and chemical properties. The vertical asymmetry of cellular membranes, i.e. different lipids are not equally distributed within the two leaflets of the membrane, gives each surface unique chemical and physical properties [112] and adds another level of complexity. Moreover, the amphipathic nature of lipids causes vertical anisotropy across the bilayer. Membrane surfaces facing the aqueous environment are hydrophilic while the membrane core is highly hydrophobic [113].

Membrane proteins adapt to this anisotropy of the lipid bilayer. Mostly, they expose, in contrast to water-soluble proteins, their hydrophobic surfaces to the hydrophobic core of the bilayer and face hydrophilic surfaces toward the aqueous solution. To maintain their structure–function relationship membrane proteins require an amphipathic lipid environment. Ideally, protein membranes are directly isolated from cellular membranes without changing their native and functionally important supramolecular assembly. Such examples are purple membranes embedding bacteriorhodopsin [114], gap junction plaques from HeLa cells [115, 116], rhodopsin-containing disk membranes from rod outer segments of the eye [117], mitochondrial outer membranes hosting voltage gated anion channels [33], bacterial membranes accommodating photosynthetic core complexes [118] or eye lens membranes showing the dense packing of aquaporins [119]. These membranes almost exclusively contain a single type of membrane protein or membrane protein complex at a high concentration. Unlike the proteins in the aforementioned examples, most membrane proteins cannot be extracted as densely packed arrays from cellular membranes. In these cases, membrane proteins are frequently solubilized, purified and subsequently reconstituted into lipid bilayers. When reconstituting, it is crucial to match the lipid composition with the requirements of the membrane protein, as it can influence protein folding, assembly and activity [120–122].

#### 3.2. Immobilization strategies for membrane proteins

3.2.1. *Immobilizing native protein membranes and reconstituted membrane proteins.* So far, most membrane proteins that have been imaged at sub-nanometer resolution were simply adsorbed to ultra-flat supporting surfaces such as mica [123], template-stripped gold [124], HOPG [125] and glass [126, 127]. These materials allow the imaging of subtle height differences of a few Ångströms. Generally, adsorption requires overcoming repulsive EDL forces to approach the protein membrane close enough ( $\approx 1$ – $5$  nm) to the supporting surface to be attracted and immobilized by vdW forces (figure 5(a)). Similar to the forces acting between a membrane protein and an atomic force microscope cantilever stylus, DLVO theory can be used to estimate the interaction forces between a protein membrane and the supporting surface:

$$F_{\text{DVLO}}(d_{\text{ms}}) = F_{\text{el}}(d_{\text{ms}}) + F_{\text{vdW}}(d_{\text{ms}}) \\ = \frac{2\sigma_s\sigma_m}{\epsilon_e\epsilon_0} e^{-d_{\text{ms}}/\lambda_D} - \frac{H_a}{6\pi d_{\text{ms}}^3}, \quad (8)$$

where  $\sigma_m$  is the protein membrane's charge density and  $d_{\text{ms}}$  is the distance between sample and membrane. Adjustment of electrolyte type and concentration as well as of the pH of the adsorption buffer are adequate measures to reduce EDL repulsion and improve sample adsorption [123]. On mica, which is the most commonly used atomic force microscope support, the adsorption energy of a single macromolecule is usually too low to prevent diffusion on the surface [128]. Such weakly attached molecules are easily swept away by the scanning atomic force microscope stylus. Because the adsorption energies of all molecules of a membrane sum up, the adsorption energy of a protein membrane composed of many proteins and lipids is much higher. Accordingly, much higher energies are required to detach a protein membrane from the supporting surface. When adsorbed onto a hydrophilic support in aqueous environment, a thin water layer of  $\approx 0.5$ – $2$  nm thickness is sandwiched between membrane and support (figure 5(a)) [129]. This distance is usually too small to avoid contact between the membrane protein and the supporting surface (figure 5(b)). In the case of mica, these non-native contacts are generally weak and do not disturb the integrity of the membrane proteins as long as they do not protrude too far ( $\approx 1$ – $2$  nm) from the lipid bilayer. Although the interaction of a single membrane protein with the supporting surface is relatively small, it can suffice to reduce its lateral mobility [130].

If the supporting surface is highly charged or hydrophobic, e.g. gold or HOPG, the interactions between membrane protein and surface change. As hydrophobic surfaces have been reported to denature water-soluble proteins [131–136], it may be speculated that their hydrophobic interactions can destabilize lipid-embedded membrane proteins.

3.2.2. *Direct incorporation of membrane proteins into supported lipid bilayers.* To observe purified membrane proteins in their native-like environment, they must be expressed at reasonably high level, purified and reconstituted into lipid bilayers [137, 138]. The development and

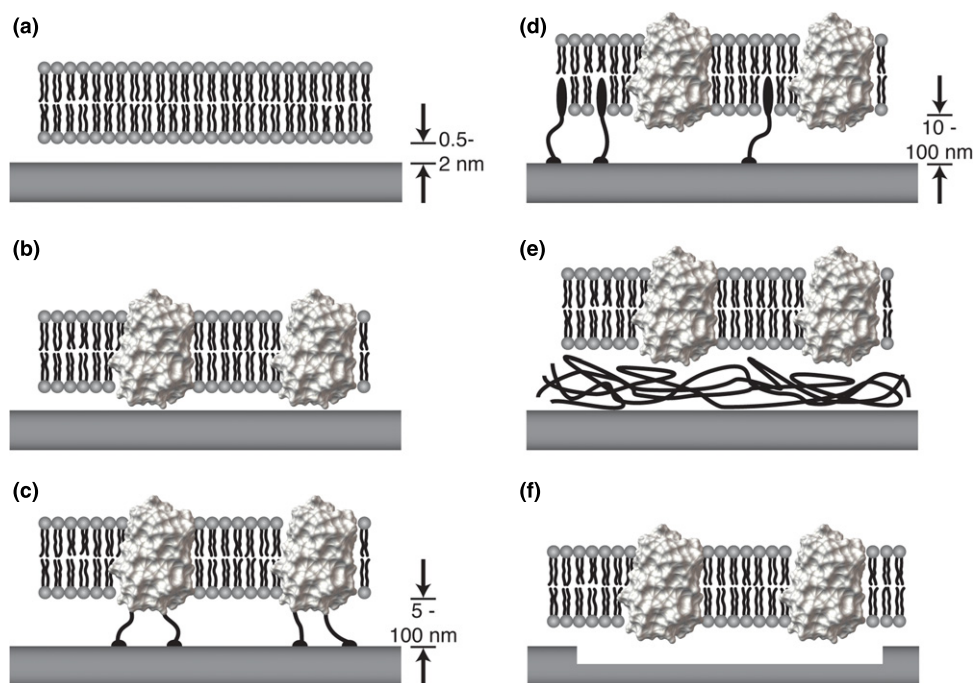


**Figure 5.** Strategies to immobilize protein membranes to solid supports for high-resolution AFM. In buffer solution, the gap between solid supported bilayers (a) and protein membranes (b) is only  $\approx 0.5\text{--}2$  nm. This might lead to non-specific interactions with the supporting surface. If the supporting material is chosen carefully, the structure of the membrane is not altered and the native structure–function relationship is preserved. (c) Protein tethered membrane. A functional group engineered into the extramembraneous regions of the protein allows attachment of the protein membrane to the support. The distance between protein membrane and support is adjusted via the tether length ( $\approx 5\text{--}100$  nm). (d) Functionally tethered lipid membranes. Lipo-polymers tether the membrane to the supporting surface by inserting their lipidic part into the membrane. The nature of the large hydrophilic polymer part tunes the distance ( $\approx 10\text{--}100$  nm) between supporting surface and membrane. (e) Polymer cushion supported membrane. The protein membrane is adsorbed onto a polymer covering the surface. Ideally, the cushion is prepared from a biopolymer that surrounds the investigated membrane *in vivo*. Such polymers are, e.g. cellulose, fibronectin or collagen. (f) Free spanning membranes. The protein membrane seals a nanoscopic hole of the supporting surface that could be used to establish an electrochemical potential or gradient.

optimization of each of this preparation steps requires highly specialized expertise, is in most cases specific to each membrane protein, and can take an unpredictable period of time. In an attempt to circumvent these difficulties, Milhiet *et al* developed a procedure to incorporate membrane proteins directly into mica-supported lipid bilayers (figure 6(a)) [139]. Their approach is comparable to the reconstitution of membrane proteins into detergent-destabilized liposomes [140, 141]. Briefly, a freshly cleaved mica surface was covered with a lipid bilayer. Then, solubilized membrane proteins were added to the buffer solution covering the lipid bilayer. Destabilization of the supported lipid bilayer by detergent (figure 6(a)) favored the insertion of membrane proteins into the lipid bilayer. After these preparation steps, the detergent was removed by exchanging the buffer solution. Subsequent high-resolution AFM imaging revealed the supramolecular structure and stoichiometry of light harvesting complexes (figures 6(b) and (c)) and reaction centers from three different organisms [139]. As this preparation method requires only picomole amounts of protein, it might be applied to proteins that cannot be produced in sufficiently high amounts for structural studies using x-ray and electron crystallography or nuclear magnetic resonance (NMR) spectroscopy. However, to what extent the procedure is applicable to other membrane proteins remains to be shown.

**3.2.3. Polymer tethers to separate protein membranes from solid supports.** The small thickness of the aqueous film between lipid membrane and support (figure 5(a)) might become problematic, particularly for membrane proteins containing large extramembraneous domains protruding more than 1–2 nm from the membrane [129]. In these cases, interactions of the supporting surface with both membrane proteins and the lipid bilayer can influence the mobility, stability, folding, assembly and function of membrane proteins and lipid bilayers [142–147]. These concerns led to the idea of spatially separating the protein membrane from the substrate.

**Tethered membrane proteins.** Surface modification for biosensors often involves tethering biomolecules to the biosensor surface through oligo- or polymeric linkers. These tethers provide a mechanically and chemically robust attachment of the target molecules. Further, such tethers separate proteins from the surface and retain them in their native state [148]. In SMFS, tethers are commonly used to functionalize atomic force microscope cantilevers or supports with nucleotides, peptides or proteins [149–152]. Tethered proteins and molecules are often used to probe, for example, specific receptor–ligand binding. Therefore, tether attachment must not interfere with the structure and function of the attached protein. Molecular dynamics simulations revealed stabilization as well as destabilization after tethering a protein

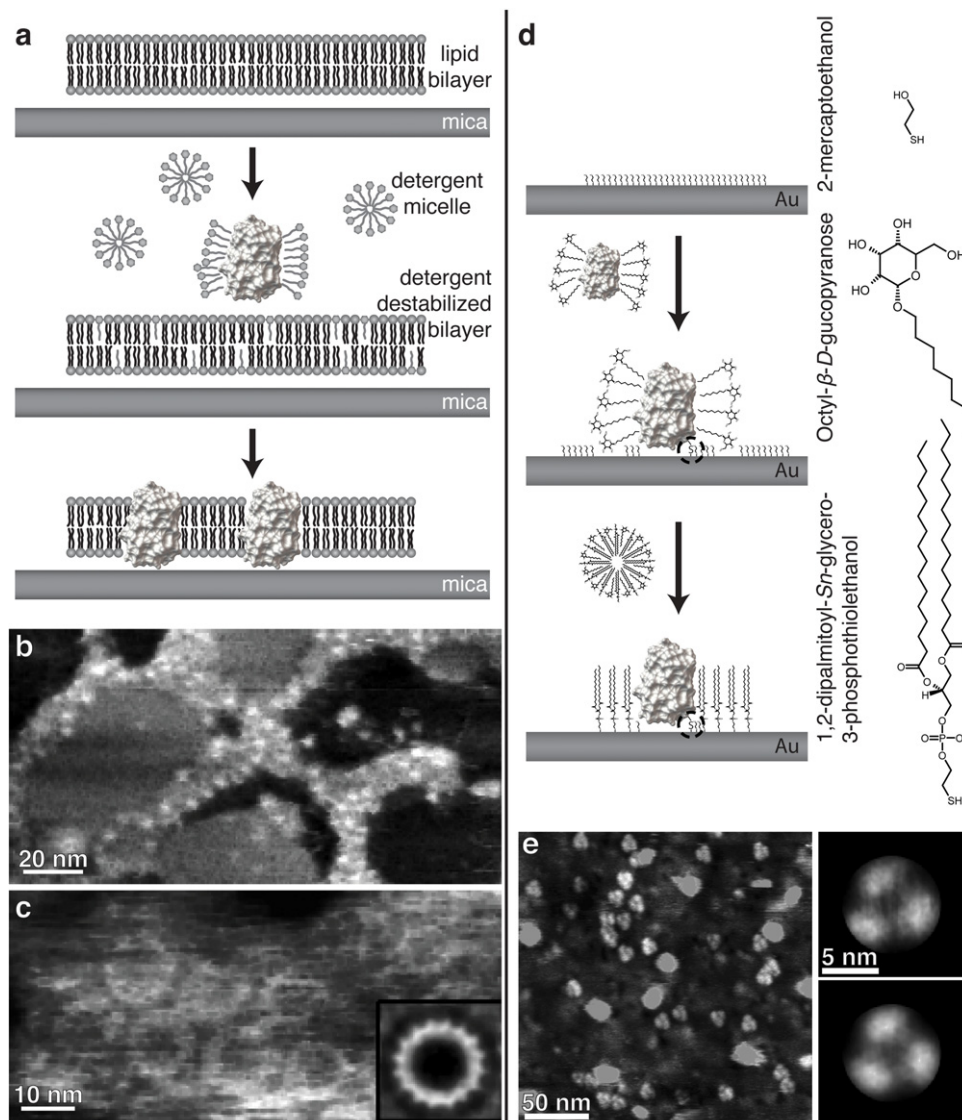


**Figure 6.** Alternative methods to prepare membrane proteins for high-resolution AFM imaging. (a) Direct incorporation of membrane proteins into supported, planar lipid bilayers. Planar lipid bilayers (top) are destabilized by detergent and incubated with detergent-solubilized membrane proteins (middle). After removal of detergent and excess solubilized proteins, the inserted membrane proteins remain in the membrane (bottom) and the sample is ready for AFM imaging [139]. (b) Intermittent CM AFM topograph showing the light-harvesting 1 complex reaction center (LH1-RC) complex from a *pufX*-deficient *Rhodobacter sphaeroides* strain. The sample was prepared as described in (a). (c) AFM topograph recorded in CM revealing the LH1-RC complex at higher resolution. Inset: correlation average revealing the 16  $\alpha/\beta$  heterodimers of LH1. (d) Preparation of membrane proteins on ultra-flat gold (Au) surfaces. Template-stripped Au is passivated using 2-mercaptoethanol and subsequently incubated with detergent-solubilized membrane proteins. Membrane proteins having an exposed cysteine residue can establish a covalent linkage to the Au surface. After binding the membrane proteins to the Au surface, the sample is incubated with a detergent/thio-lipid mixture. The thio-lipids form a self-assembled monolayer on the Au surface and provide the hydrophobic environment required to stabilize the membrane proteins. (e) High-resolution topograph of OmpF assemblies on template-stripped Au (left panel) that were prepared as described in (d). Non-symmetrized and symmetrized correlation averages (top and bottom right panel, respectively) of OmpF trimers observed in the topograph (left panel) [124]. Panels (b) and (c) adapted from [139] with permission from Elsevier.

to a surface. The effect depends on both the tether properties and the attachment site in the protein [145, 153], thus, clearly showing that care has to be taken when designing and using tethered molecules.

For AFM sample preparation tethers can serve to attach membrane proteins to a support (figure 5(c)), which requires engineering of a tether attachment site at a surface-exposed position of the membrane protein [154, 155]. This approach provides precise control of the density and orientation of

the tethered protein. Depending on the experimental needs, tethers and functional groups can be chosen that allow both reversible attachment via switchable affinity tags (e.g. His-tag [154, 156, 157]) or irreversible linkage via covalent bonds [158].

Recently, a first example of high-resolution AFM imaging of tethered membrane proteins was presented [124]. In this experiment, a single, surface-exposed cysteine was engineered into a periplasmic loop of the outer membrane

protein F (OmpF) from *Escherichia coli*. Then, the purified, solubilized OmpF was adsorbed onto a 2-mercaptoethanol-passivated ultra-flat template-stripped gold surface [159]. After extensive washing, detergent/lipid micelles containing synthetic thiolipids were added. The thiolipids self-assembled into a lipid monolayer on the gold surface and mimicked the natural lipid environment for OmpF (figure 6(d)). High-resolution AFM revealed individual OmpF trimers on the gold surface (figure 6(e)). Although located far from each other, the sub-structural details of single OmpF trimers could be revealed. All OmpF trimers attached to the gold surface via their periplasmic cysteine residue and exposed their extracellular surface to the scanning atomic force microscope stylus. The surface structures of the tethered OmpF corresponded well to that of the native OmpF trimer. This suggests that the folding and the structure of the OmpF trimers did not change upon covalent attachment to the gold surface. Functional studies confirmed the activity of these immobilized OmpF trimers [160]. The tether used was extremely short and so was the distance between membrane protein and the supporting surface. To date, no high-resolution AFM topographs of tethered membrane proteins that were separated far ( $\gg 1$  nm) from a supporting surface have been obtained.

*Tethered membranes.* Head-group functionalized lipids are widely used to separate lipid bilayers from supporting materials (figure 5(d)) [143, 161]. The structure of such lipopolymer tethers usually exhibits three distinct regions: (i) the amphiphilic region that inserts into and becomes part of the lower leaflet of the supported lipid bilayer, (ii) the linker region that decouples the membrane from the support and (iii) the functional group at the end of the linker that allows covalent linkage to the support. Depending on the chemical properties of the support, different functional groups can be used to attach lipopolymers. For gold surfaces, thiol [162, 163] or disulfide [158] groups are widely used for immobilization. On other supporting materials, hexahistidine (His<sub>6</sub>) sequence tags and nitrolotriactic acid (NTA) modifications [156], amino- and carboxyl-reactive as well as silane groups [164, 165] can be used.

Linker segments are commonly based on oligo(ethylene-oxide) [158, 166, 167], poly(ethyleneoxide) [165] and oligo-peptides [168]. The length of the linker segment but also the density of tethered lipopolymers allow fine-tuning of the distance between membrane bilayer and supporting surface (usually 10–100 nm) [164, 169]. The density of tethered lipids in the supported bilayer also influences the membrane viscosity and thus the membrane protein diffusion. Small matrix molecules that dilute the tethered lipoproteins on the support may be used to adjust their lateral density [143].

Supported membranes anchored to a solid support via lipopolymer tethers restrict membrane protein dynamics less than directly tethered membrane proteins. Such membranes might offer an appropriate environment to study insertion, assembly and interactions of membrane proteins [154, 165, 170, 171].

*3.2.4. Polymer cushion supported membranes.* Polymer-cushioned, supported membranes are another option to suppress non-native and non-specific interactions between the solid support and the proteins and lipids [129, 143, 172]. Ultra-thin polymer layers of 5–100 nm thickness form the cushions that ideally mimic the native environment of a cell membrane (figure 5(e)). To prevent non-specific contacts between membrane and support, careful design of such a multi-layered system is crucial [143, 172]. Relevant forces that have to be considered are vdW, electrostatic, long-range repulsion of the polymer and thermally induced undulation forces [172]. Carefully chosen polymer supports can maintain the native membrane properties, assist self-healing and provide an environment well suited for insertion of membrane proteins with large extramembranous domains [165, 173].

Instead of synthetic polymers [174–178], biological polymers may be used to imitate the native membrane environment such as given by the extracellular matrix. Regenerated cellulose [173, 179] and dextran [180] are examples of such biological polymers. Interestingly, when using a  $\approx 5$  nm thick layer of regenerated cellulose to support lipid bilayers, integrin  $\alpha_{11b}\beta_3$  showed a 3–10 fold higher adhesion free energy compared with similar experiments in solid-supported membranes. The increased adhesion free energy values match that inferred from the integrin–ligand dissociation constant, which suggests that integrins incorporated in polymer-cushioned membranes remain fully functional [173].

Both tethered membrane proteins and tethered lipid bilayers need to be chemically modified for immobilization. Polymer cushions, on the other hand, can be used to support any protein membrane or cell membrane fragment without further modification. Because the native cell membrane environment is specific to the type of membrane or cell, design and choice of polymers may be fine-tuned to improve the mimicry of cell-type specific environments.

*3.2.5. Free spanning lipid membranes.* An alternative to separating protein membranes from a supporting surface by means of polymeric tethers or cushions is to produce free spanning membranes [181–185]. In the simplest case, the protein membrane covers and ideally seals a buffer-filled hole or cavity (figure 5(f)). Such holes or cavities in the supporting material can be produced at micro- or nanoscale [186, 187] with defined regular patterns [188–191].

Porous silicon has been used to create and characterize the nanomechanical properties of free spanning lipid bilayers [192]. This study revealed that free spanning lipid bilayers behave more fluid than lipid bilayers on flat solid supports. Thus, free spanning bilayers are appealing systems to study membrane protein structure and function. In another approach, nanoporous substrates were used to adsorb fragments of cellular membranes in an oriented way [187]. Such cavities could be used to create molecular or ionic gradients across membranes by changing the buffer solution after membrane absorption. For example, ligands enclosed in cavities could activate transmembrane receptors on their extracellular side

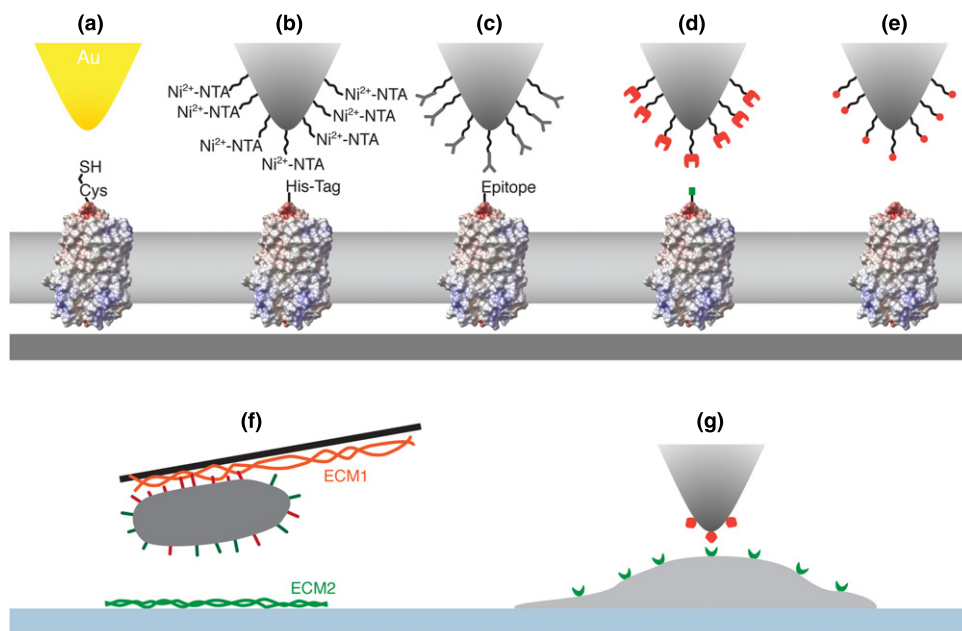


**Figure 7.** Cantilever and surface functionalization for specific protein attachment. (a) Gold-coated styluses can be used to specifically pick up membrane proteins at (engineered) cysteine (Cys) residues through formation of an Au–S bond. (b)–(e) Modification of gold-coated, silicon or silicon nitride styluses using linker molecules allows attachment of small molecules or proteins that specifically interact with the membrane protein. Such modifications include (b)  $\text{Ni}^{2+}$ -NTA binding to His-tagged proteins, (c) antibodies or antibody fragments binding their antigens, (d) receptors binding to ligands (e.g. streptavidin and biotin) and (e) (small) molecules or peptides serving as ligand for the protein. (f) Extracellular matrix (ECM) proteins can be used to attach cells via specific cell adhesion molecules to AFM cantilevers and to probe the interactions of these cells with other ECM proteins on the support surface. (g) Cantilever-bound molecules or proteins can be used to probe their interactions with the cell membrane down to the single molecule level.

while observing the receptors' response on the cytoplasmic surface by AFM.

So far, no high-resolution AFM imaging of membrane proteins from freely spanning membranes has been successfully performed. In the future, more sensitive and faster AFM imaging techniques may facilitate imaging soft membranes at sufficiently high resolution for structural and functional investigations.

### 3.3. Modification of atomic force microscope cantilevers for SMFS and SCFS

SMFS-based unfolding applies a stretching force to membrane proteins that are tethered between the lipid bilayer and the atomic force microscope stylus. For SMFS, the atomic force microscope stylus must pick up membrane proteins that are anchored to the lipid bilayer mainly by anisotropic hydrophobic and hydrophilic interactions. Atomic force microscope styluses are commonly made from silicon or silicon nitride and sometimes covered with a thin gold layer. Principally, these surfaces do not provide specific attachment sites for proteins. To simplify SMFS, membrane proteins are in most cases unspecifically attached to the stylus. This is achieved by pressing the atomic force microscope stylus for a short time (0.5–1 s) onto the membrane protein surface while applying a force of 0.5–1 nN. Although this attachment procedure does not result in a covalent bond, forces of >800 pN are necessary to detach the polypeptide from the atomic force microscope stylus [71]. Forces required to unfold membrane proteins are usually far below this threshold [193]. However,

some applications might require specific attachment of the protein to the atomic force microscope stylus. The following sections and figure 7 provide an overview of different methods to functionalize atomic force microscope cantilever styluses to enable specific attachment of a protein.

**3.3.1. Covalent attachment of membrane proteins to the atomic force microscope stylus.** Commercial gold-coated styluses can be employed to specifically attach proteins that carry a surface exposed cysteine residue via an Au–S bond (figure 7(a)). The strength of the Au–S bond was determined by force spectroscopy to be  $\approx 1.4$  nN [194]. It is not yet clear whether this force represents rupturing the Au–S bond or extracting the bonded Au atom from the gold layer [194]. The beauty of the approach is that only a single cysteine has to be engineered to one of the protein's termini. Oesterhelt *et al* [68] added a cysteine to the C-terminal end of bacteriorhodopsin and used gold-coated styluses to attach and mechanically unfold the membrane protein. As a result, the mechanical unfolding spectra of bacteriorhodopsin could be unambiguously assigned and co-existing unfolding pathways were discovered. Moreover, using this approach the probability of picking up membrane proteins from the membrane could be significantly increased.

**3.3.2. Non-covalent attachment of membrane proteins to the atomic force microscope stylus.** In addition to covalent attachment, proteins may be attached to the atomic force microscope stylus using specific non-covalent interactions.

These approaches rely on the interaction of different affinity tags engineered into the proteins with their cantilever-bound counterpart (figures 7(b)–(e)). However, such interactions are considerably weaker than covalent bonds and often not strong enough to withstand the forces required to unfold single membrane proteins ( $\approx 100$ – $300$  pN). Thus, such specific approaches are only of limited use for membrane protein unfolding experiments. Still, some of these specific interactions can be sufficiently strong to be used for adhesion mapping, recognition imaging and investigation of receptor–ligand interactions.

*The mechanical strength of the His<sub>6</sub>–NTA bond is controversial.* The coordination bond between His<sub>6</sub>-tags and complexes of transition metal ions (e.g. Ni<sup>2+</sup>) with NTA is chemically well understood and widely used for affinity chromatography of recombinant proteins [195]. The advantages of the His<sub>6</sub>–NTA interaction over conventional covalent cross-linking are its reversibility, its specificity and the directed attachment of molecules to the atomic force microscope stylus [196–198]. Therefore, the strength and thus suitability of the His<sub>6</sub>–NTA interaction was investigated soon after the advent of SMFS. The results obtained by different groups were controversial as the forces required to break a His<sub>6</sub>–NTA bond ranged between 38 and 500 pN [199–201]. A more systematic study estimated a loading rate-dependent bond strength between 139 pN (at 660 pN s<sup>-1</sup>) and 224 pN (at 46 200 pN s<sup>-1</sup>) [202]. Unfolding of membrane proteins often requires forces comparable to or exceeding the strength of the His<sub>6</sub>–NTA bond [193, 203]. Thus, His<sub>6</sub>–NTA interactions are not applicable to pick up membrane proteins for unfolding studies. On the other hand, NTA-modified cantilevers turned out to be valuable for recognition imaging of membrane receptor–ligand interactions that rupture at  $\approx 50$ – $100$  pN [197, 198, 200, 201].

*Recognition imaging can exploit weak receptor–ligand interactions.* Interactions between receptors and their ligands are highly specific. Examples include antibodies binding to their antigens (figure 7(c)), receptors interacting with their corresponding ligands (figure 7(d)) or small (organic) molecules specifically binding to a protein (figure 7(e)). Therefore, it is straightforward to functionalize atomic force microscope styluses with ligands to characterize receptor–ligand interactions [58, 204]. However, compared with the His<sub>6</sub>–NTA bond, most receptor–ligand interactions are considerably weaker [26, 28, 205], such as the bond between the Strep-tagII and Strep-Tactin, a streptavidin variant optimized for Strep-tagII binding, which withstands only 37 pN (at 337 pN s<sup>-1</sup>) [27]. Such weak interactions might be used for adhesion mapping and recognition imaging [26–29] but they are too weak to be exploited for membrane protein unfolding studies. Similarly, antigen–antibody bonds usually require 50–100 pN to be ruptured [197, 206, 207]. One of the rare exceptions amongst non-covalent interactions is the bond between streptavidin and biotin, whose affinity is one of the highest known in nature. This bond can bear forces exceeding 250 pN [58, 204]. Until now, this bond has been used to study polysaccharide elasticity by SMFS [72], but has not been applied to mechanically unfold membrane proteins yet.

### 3.3.3. Cantilever modification for SCFS.

*Non-signaling cantilever functionalization to pick up cells.* Unlike SMFS, the actual probe in SCFS is not a cantilever stylus but a living cell attached to a preferably stylus-less cantilever (figure 4). To ensure firm attachment of the cell, the cantilever has to be functionalized with molecules interacting with the cell surface (figure 7(f)). Ideally, cantilever modifications must not trigger signaling cascades within the cell as these might alter the interaction of the cell with the substrate. One such appropriate molecule is concavalin A (ConA), a lectin that binds *N*-linked oligosaccharides on the extracellular domains of membrane receptors [208, 209]. Modification of a clean cantilever with ConA is achieved by successively incubating it with biotinylated bovine serum albumin, streptavidin and finally biotinylated ConA [210–212]. After a final washing step, the cantilever is pressed onto a cell that was seeded onto a solid support. Thereby, the cell will attach to the cantilever.

Once firmly attached to the cantilever, the cell is used to probe the adhesive forces between the cell and a substrate. Such substrates can be cells or functionalized solid supports, e.g. surface patterned substrates [213–215], that interact with specific binding partners of the cell surface [57, 93].

*Cantilever modifications can trigger desired signaling pathways.* In some cases, triggering of cellular signaling cascades by the cantilever functionalization is desired. Assuming that the cantilever-modifying molecule specifically binds one kind of CAM, and the substrate on the support binds a second kind of CAM, one could study how initial binding of the first kind of CAMs modulates the binding of the second kind of CAMs. Such communication between membrane receptors is called crosstalk. Crosstalk between integrins (see section 6.4) was studied by coating cantilever and support with different ECM proteins (figure 7(f)). Deposition of ECM proteins on cantilevers and substrates only requires incubation with an ECM protein solution in a suited buffer [216].

*Single-molecule assays with live cells.* Cantilevers coated to capture cells for SCFS are also useful for single-molecule experiments probing receptor–ligand interactions of the native cell membrane (figure 7(g)). Krieg *et al* used a ConA-functionalized atomic force microscope stylus to probe the lifetime of the interaction between ConA and *N*-linked oligosaccharides of membrane receptors [95]. After gently touching a living cell the ConA-coated stylus was separated from the cell surface. After binding of ConA to *N*-linked oligosaccharides on the cell surface, the withdrawal of the stylus exerted a force on the glycosylated membrane receptors. In some cases, this pulling force was sufficient to extract a small membrane tether from the cell membrane. The force required to extract the tether from the membrane was constant throughout the experiment and solely depended on plasma membrane properties and extraction speed [95]. As ConA interacts only with a receptor at the very tip of the membrane tether, this natural force-clamp could be used to determine the lifetime of the receptor–ligand bond.

### 3.4. Current limitations, challenges and perspectives

**3.4.1. Sample preparation.** Sample preparation is crucial for high-resolution AFM imaging, SMFS and SCFS. Expression, solubilization, purification and reconstitution of membrane proteins are the major bottlenecks for membrane protein studies with any biophysical technique, including AFM-based methods [141, 217]. Therefore, techniques that provide membrane proteins fast and reliably are required. New cell-free *in vitro* expression approaches seem promising, as they avoid expression in bacterial or mammalian systems. Toxic or inhibitory effects of membrane protein overexpression are circumvented and reactions in small volumes often produce milligram amounts of protein. Moreover, these systems ease protein purification and solubilization [218–220].

Keeping in mind that high-resolution (<1 nm) AFM imaging usually still requires at least densely packed membrane proteins, methods to produce such samples have to be developed further. First examples of *in situ* sample preparation demonstrated that direct insertion of membrane proteins into lipid bilayers can be used for high-resolution AFM imaging [139]. Alternatively, tethering membrane proteins to solid supports allowed AFM imaging at molecular resolution although the protein density on the surface was very low [124]. In the future, such and similar approaches may guide the way to routinely prepare various native membrane proteins for high-resolution imaging.

**3.4.2. Separating membranes from solid supports.** New immobilization strategies for membrane proteins and lipid bilayers aim to separate membranes and proteins from the solid support. Eliminating unspecific interactions with the support through a properly adjusted distance between support and membrane provides unperturbed mobility and functionality of membrane proteins. However, tethering might influence both membrane protein function and properties of lipid bilayers [145, 153]. The mechanisms and origins of these alterations are still not well understood and require further investigation. Moreover, introducing attachment sites to membrane proteins may alter the protein function and folding. Thus, careful controls are a necessity.

A negative aspect of tethering membrane proteins to supporting surfaces is that they become physically immobilized. This will restrict the ability of membrane proteins to dynamically assemble into supramolecular complexes. Still, the approach might be valuable for high-resolution AFM to observe, for example, the stoichiometry of preformed membrane protein complexes or conformational changes in single membrane proteins. In contrast to tethering individual membrane proteins it may be beneficial to tether individual lipids of the protein membrane. Introducing a sufficiently long spacer between tethered lipid and support may ensure that the membrane proteins can freely diffuse within the membrane without being distorted by unspecific interactions with the support.

A variety of both synthetic and natural polymers have already been employed to support protein membranes. These cushions were usually composed of one type of polymeric

molecule. In the future, native-like polymers that mimic the native environment of cellular membranes more accurately should be developed.

Free spanning membranes enable a variety of new applications ranging from functionally related AFM imaging to SMFS of membrane proteins exposed to two different buffer compartments. To reveal more parameters of the studied membrane system, AFM-based experiments should be combined with other techniques such as fluorescence microscopy or electrophysiological approaches.

Despite all these encouraging developments, it should be kept in mind that both high-resolution AFM imaging and force spectroscopy have not been successfully demonstrated using free spanning or cushioned membranes. Polymer-cushioned and free spanning membranes are currently still too soft, flexible and rough for high-resolution AFM imaging. For high-resolution AFM imaging of tethered membrane proteins only very short linkers (<1 nm) have been used. Certainly, development of more sensitive AFM instrumentation and methodology is required to take advantage of these new sample preparation methods.

**3.4.3. Specific attachment for SMFS.** For SMFS, the specific attachment of atomic force microscope styluses to membrane proteins may be beneficial. For example, a well-defined anchoring point would allow a more precise alignment of the F–D curves. This would improve allocating the force peaks to the primary structure of the protein. However, only a few non-covalent interactions are strong enough to anchor membrane protein to the atomic force microscope stylus while bearing the forces required to unfold membrane proteins. The covalent Au–S bond between a gold-coated atomic force microscope stylus and a cysteine residue of a mutated bacteriorhodopsin was successfully used in SMFS experiments for specific attachment [68]. However, due to the covalent nature of the Au–S bond, the membrane proteins unfolded once remain bound to the atomic force microscope stylus and limit the number of membrane proteins that can be picked up by a single stylus. It may take a while until a better-suited approach for specific attachment of membrane proteins to the atomic force microscope stylus has been developed. One possibility may be linker molecules that recognize a specific region of the membrane protein and that can be ‘autocleaved’ after the membrane protein has been manipulated.

**3.4.4. SCFS.** SCFS uses a cell as a probe to measure its interactions with the environment. A living cell can set up numerous non-specific and specific interactions. Thus, the main problem in SCFS is to identify which cellular interactions are measured. One way to identify which cell surface receptor contributed to adhesion is to specifically block relevant receptors and to correlate changes in cell adhesion to receptor blocking. In addition, cell biological and genetic engineering tools may not only be used to control the functional state of the cell but also of individual receptors. This includes engineering cell lines deficient of certain genes or creating knock-down or knock-out cell lines. Alternatively, approaches to functionalize supports with specific ligands to bind only one or a few cell surface receptors would be beneficial.

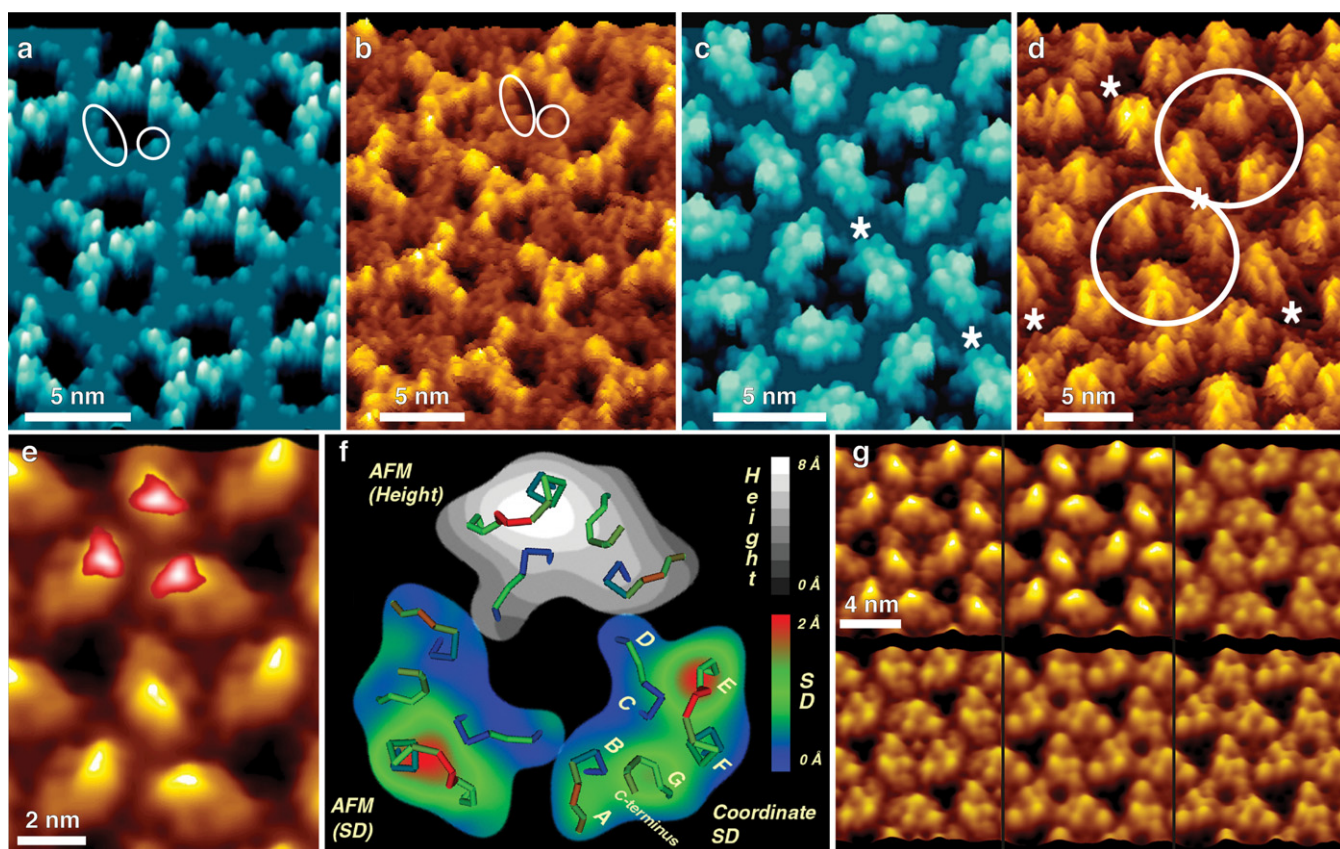


**Figure 8.** High-resolution AFM imaging. ((a)–(d)) Comparison of an atomic model of OmpF rendered to 3 Å ((a), (c)) and high-resolution AFM topographs of two-dimensional OmpF crystals ((b), (d)). The protrusions on the cytoplasmic surface are encircled in (a) and (b). The protrusions correspond to short turns connecting  $\beta$ -strands and are sometimes resolved in AFM topographs. Extracellular domains ((c), (d)) protrude 1.3 nm from the surface. These domains are formed from long, flexible polypeptide loops. Therefore, in AFM topographs the domains appear distorted (d). Two OmpF trimers are encircled while asterisks mark the location of the 2-fold symmetry center of the rectangular unit cell determined from cross-correlation with the atomic model. (e) Correlation average of the cytoplasmic surface of bacteriorhodopsin at an applied force of 100 pN. Regions with enhanced flexibility are derived from SD maps and superimposed in red to white shades. (f) Surface properties of bacteriorhodopsin. The backbone trace of the surface loops is shown and color-coded according to the backbone root mean square deviation (rmsd) calculated after averaging five different atomic models of bacteriorhodopsin [234]. The gray-scaled monomer (top) shows the height profile determined from (e). The prominent elevation corresponds to the EF loop. The colored monomers show the coordinate SD between the different atomic models (bottom right) and the SD of the height measured by AFM (bottom left). (g) Force-induced conformational changes in the cytoplasmic surface by applying various imaging forces: 80 pN (top left), 100 pN (top middle) and 150 pN (top right). At 150 pN, the atomic force microscope stylus displaces the EF loop and thus renders shorter loops on the cytoplasmic surface visible. Bottom row: three different center conformations of bacteriorhodopsin trimers observed at  $\approx 180$  pN. The full color scale corresponds to 1.5 nm in (b) and (d) and 1 nm in (e) and (g), respectively.

#### 4. Imaging native membrane proteins at work

Whereas some membrane proteins act as monomers, others require formation of higher order complexes to function. In many examples such homo- and heteromeric assemblies modulate the functional state of membrane proteins [221–225]. The structural stoichiometry, arrangement and conformation of such complex assemblies are often unknown. Switching the functional state often requires changing the protein's conformation. For example translocation [226–228], signal transduction [229, 230] and regulatory processes [231, 232] require membrane proteins to interconvert between different conformational states. Some of these conformational changes are rather small and for example include only the reorientation of a polypeptide loop whereas others require the protein structure to change considerably. To observe

even subtle conformational changes, high-resolution imaging AFM approaching  $\leq 1$  nm lateral resolution is required. In the following we describe examples of applying AFM imaging to identify membrane proteins and to observe their oligomeric assembly and functionally related conformational changes.

##### 4.1. Imaging native membrane proteins at sub-nanometer resolution

The trimeric porin OmpF is an *E. coli* outer membrane protein that has been structurally and functionally well characterized. It is composed of 16 antiparallel  $\beta$ -strands lining a water-filled aqueous transmembrane pore [233]. Figure 8 shows the atomic model of OmpF trimers reconstituted into the lipid membrane and assembled into two-dimensional crystals. These models were rendered to 3 Å to allow their comparison

with OmpF trimers imaged using CM AFM in buffer solution. At the periplasmic surface short polypeptide loops protruding the lipid bilayer connect consecutive  $\beta$ -strands (figure 8(a)). Even loops being only a few ( $\approx 2$ –3) amino acids long can be resolved in AFM topographs (figure 8(b)). Similarly, the surface topography of the extracellular OmpF surface (figure 8(d)) nicely corresponds to the atomic model (figure 8(c)). The characteristic substructure of the long and flexible extracellular polypeptide loops that protrude  $\approx 1.3$  nm from the bilayer surface is recorded [125].

The cytoplasmic surface of purple membrane can undergo structural changes upon AFM imaging. At an imaging force of  $\approx 100$  pN the bacteriorhodopsin surface is observed in an unperturbed conformation [55] (figure 8(e)). The topography obtained by CM AFM imaging correlates well with atomic models [234] (figure 8(f)). The EF loop connecting transmembrane  $\alpha$ -helices E and F corresponds to the prominent protrusion in the AFM topographs. At a slightly increased imaging force of  $\approx 150$  pN the atomic force microscope stylus displaces the flexible EF loops and shorter loops connecting transmembrane  $\alpha$ -helices A and B and C and D as well as the C-terminal region of bacteriorhodopsin becomes visible (figure 8(g)). Re-imaging the same surface at low imaging force ( $\approx 100$  pN) shows undistorted bacteriorhodopsin molecules, indicating the reversibility of the force-induced conformational change. During the photocycle this intrinsic flexibility of the EF loop is necessary to allow transmembrane  $\alpha$ -helix F to undergo conformational changes [235]. The standard deviation (SD) map obtained by correlation averaging of single bacteriorhodopsin molecules underlines this flexibility (figure 8(e)).

These examples show that AFM is well suited to image membrane proteins at sub-nanometer resolution and underscores the sensitivity of AFM to observe the unperturbed conformation of single polypeptide loops. Moreover, AFM imaging allows the manipulation of these structures in a controlled manner.

#### 4.2. Identifying membrane proteins and their structural details

Although AFM topographs of native membrane proteins can be acquired routinely at high resolution ( $\approx 1$  nm) additional information is required to identify the surface and subdomains of the protein. If complementary structural data are available, the comparison with AFM topographs allows identification of surface structures (figures 8(a)–(d)). If no such structural information is available other approaches for identification have to be used. In general, antibodies seem appealing as they specifically recognize their antigen. However, being often larger than the membrane protein, antibodies are not suited to identify protein substructures in AFM topographs. On the other hand, antibodies may be used to determine the orientation of membrane proteins within the lipid bilayer. In the following, we will present an overview of alternative methods that can be applied to identify the substructural details of membrane proteins.

**4.2.1. Antibody labeling.** Similar to conventional immunostaining in optical and electron microscopy, antibodies raised against the cytoplasmic C-terminus of bacteriorhodopsin were used to distinguish the extracellular from the cytoplasmic surface of purple membrane [236]. In the absence of antibodies individual purple membranes adsorbed to mica were smooth and did not show topographic differences. The surrounding mica surface was atomically flat and clean. Upon addition of antibodies, a fraction of membranes exhibited a rough textured surface whereas the remainder of membranes stayed as smooth as untreated samples. To confirm the specificity of the antibody, the C-terminus of bacteriorhodopsin was digested by papain. AFM topographs of papain-digested and antibody-treated purple membrane revealed only smooth and unlabeled membrane patches [236]. Thus, untreated purple membrane patches that were decorated with antibodies exposed their cytoplasmic surface toward the atomic force microscope stylus.

**4.2.2. Alterations in surface-exposed polypeptide loops.** AFM topographs commonly observe the membrane proteins' polypeptide loops protruding from the lipid bilayer. Thus, changing the loop can result in topographical changes that can be readily monitored by AFM. In one such example, 24 residues from the third loop of bovine rhodopsin replace the eight amino acids long EF loop of bacteriorhodopsin. In rhodopsin, the third loop is important for signal transduction to the G-protein (transducin), interacts with rhodopsin kinase and arrestin, and is supposed to protrude far from the membrane. High-resolution AFM imaging of the bacteriorhodopsin chimera revealed a much larger protrusion of the replaced EF loop projecting toward the C-terminus [237].

As an alternative to increasing the size of a loop, reducing the size of loops can also cause structural changes observable by high-resolution AFM imaging. Enzymatic removal of the third rhodopsin loop from chimeric bacteriorhodopsin using V8 protease did not affect purple membrane crystallinity but changed the appearance of the cytoplasmic surface. The prominent cytoplasmic protrusion of the EF loop seen in wild-type and chimeric bacteriorhodopsin disappeared and the ends of transmembrane  $\alpha$ -helices E and F became clearly visible [237]. Indeed, the topography of the V8 protease-treated bacteriorhodopsin mutant was similar to that obtained when mechanically displacing the EF loop with the atomic force microscope stylus (figure 8(g)).

**4.2.3. Digestion of polypeptide termini.** Digestion of terminal sequences of membrane proteins can be used to identify the corresponding surfaces and the structures formed by these sequences. This strategy was applied to the major intrinsic protein (MIP; also known as aquaporin 0, AQP0) from sheep lenses [238], bovine and human aquaporin 1 (AQP1) [239] and aquaporin Z (AqpZ) from *E. coli* [240]. High-resolution AFM imaging of two-dimensional crystallized AQP0 revealed a globular protrusion of  $0.8 \pm 0.1$  nm. This structural feature could be assigned to the C-terminus on the cytoplasmic surface because carboxypeptidase Y treatment removed it. At the same time, the height of the cytoplasmic

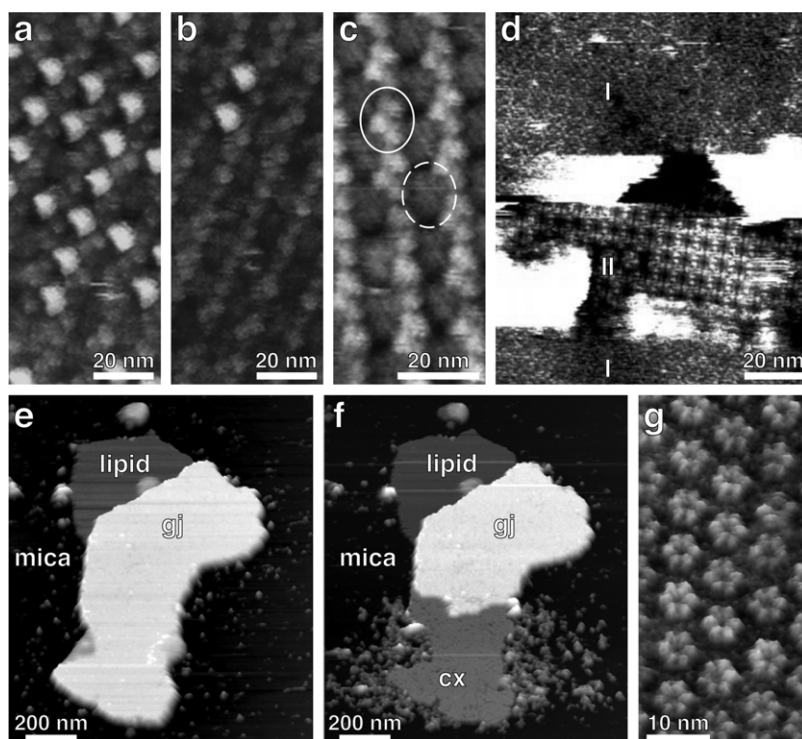


**Figure 9.** Dissecting membrane proteins by AFM. (a) Topograph of PSI complexes reconstituted into a two-dimensional lattice. PSI complexes are arranged in an up-and-down orientation. The extrinsic subunits PsaC, PsaD and PsaE located on the stromal side of the complex cause the high protrusions. (b) Repeatedly scanning the atomic force microscope stylus across the PSI complexes removes the extrinsic subunits and exposes the stromal surface of the reaction center core. (c) At higher magnification, the stromal (broken ellipse) and luminal (ellipse) surfaces of the reaction centers are clearly visible. (d) Nanodissecting double-layered membranes of AQP0. After removing the upper AQP0 membrane by the atomic force microscope stylus, both the cytoplasmic (I) and extracellular (II) surfaces of crystallized AQP0 proteins are visible. (e) Overview of an intact Cx26 gap junction plaque (marked gj). (f) Same gap junction plaque partially dissected. The upper connexon membrane of the plaque was partially removed by applying a slightly enhanced force to the scanning atomic force microscope stylus. This nanodissection exposed the extracellular surface of a single-layered connexon membrane (marked cx). (g) High-resolution topograph of the extracellular connexon surface after nanodissection. Six connexins forming individual connexon channels are clearly observed. The full gray range corresponds to a vertical scale of 4 nm in (a) and (b), 2 nm in (c), 1.8 nm in (d), 25 nm in (e) and (f) and 3 nm in (g). All topographs were recorded using CM AFM.

surface protruding from the lipid membrane reduced to  $0.6 \pm 0.1$  nm. As a result of carboxypeptidase Y treatment a cavity in the center of the AQP0 tetramer was formed [238]. In a similar experiment, removal of the 26 amino acid long N-terminal segment of AqpZ and subsequent investigation of the structural changes by high-resolution AFM imaging allowed identification of the cytoplasmic surface [240]. In both cases, the extracellular surface was not structurally affected by removal of peptide segments located at the opposite side of the membrane.

**4.2.4. Nanodissecting membrane proteins.** To elucidate the topography of membrane proteins, their surface has to be accessible to the atomic force microscope stylus. Extracellular portions of some membrane proteins can mediate specific cell-cell interactions. Native or reconstituted preparations of such proteins often exhibit sandwiched structures in which these extracellular surfaces are buried [238, 241, 242]. Binding of soluble proteins to form functional multi-protein complexes can also mask the membrane proteins' surface as in the case of the *Synechococcus sp.* reaction center photosystem I (PSI) [243]. To make these 'hidden' surfaces available for AFM

imaging, the atomic force microscope stylus can be used as a nanoscalpel to dissect sandwiched structures and complexes.

*Dissecting water-soluble subunits from PSI complexes.* Three extrinsic subunits bind to the stromal side of the membrane embedded PSI complex [243]. In AFM topographs of up-and-down oriented two-dimensional PSI crystals, these subunits appear as  $\approx 3.5$  nm high protrusions (figure 9(a)). Repeated scanning of the same area dissociates the subunits from the core complex (figure 9(b)) rendering the previously hidden surface accessible to the atomic force microscope stylus for high-resolution CM AFM imaging (figure 9(c)) [244]. This approach reveals the surface topography of both the intact and the (partially) dissected complex.

*Observing sandwiched surfaces of membrane proteins.* AQP0 from lens membranes has dual functions. It is both a water channel and a cell-cell adhesion molecule that organizes in thin junctional domains through interactions of the extracellular protein domains. Mutations in AQP0 are known to cause cataracts [245]. *In vitro*, reconstituted AQP0 favorably forms double layers, thus hiding its extracellular surface [246]. Increasing the imaging force while scanning

the surface removed a small part of the upper layer of the double-layered crystals rendering the extracellular surface accessible (figure 9(d)) [238]. The resulting high-resolution topographs revealed that in double-layered two-dimensional crystals AQP0s from the upper and lower layer are precisely superimposed and interact in a tongue-and-groove fashion via specific interactions between the extracellular surfaces of opposing AQP0s [238]. Atomistic insights into which polypeptide loops and amino acids facilitate these interactions were provided later on using electron microscopy and diffraction [247, 248].

*In vivo*, gap junctions connect cells via two stacked layers of plasma membrane. Connexons of opposing membranes dock via their extracellular surfaces forming a communication channel bridging the intercellular space between neighboring cells [249, 250]. Therefore, the extracellular connexon surface of gap junction plaques is initially hidden from the atomic force microscope stylus (figure 9(e)) [116, 241, 251]. Scanning gap junction plaques with increased imaging forces of  $\approx 1\text{--}1.5$  nN using CM AFM displaces the upper connexon membrane (figure 9(f)). This exposes the extracellular surface of the lower connexon layer for high-resolution AFM imaging (figure 9(g)) and functional studies [116, 251].

#### 4.3. Imaging the oligomeric state of native membrane proteins

Oligomerization is an abundant phenomenon in membrane proteins. It might occur due to unspecific interactions favored by the high local concentration of membrane proteins in cellular membranes, their confinement to a pseudo-two-dimensional space, and their predefined orientation within the lipid bilayer. Oligomerization may be also supported by hydrophobic mismatch, interactions between amino acids of membrane proteins, the membrane protein's functional state or by the composition of the membrane. These factors lead to an at least  $10^6$ -fold higher propensity to form dimers and higher oligomers compared with water-soluble proteins [252]. Despite this natural affinity of membrane proteins oligomerization often has functional implications [253–256].

AFM imaging has been used to observe the oligomeric state of various membrane proteins. Examples include  $\alpha$ -hemolysin [257] and cholera toxin [258] as well as various bacterial and vertebrate rhodopsins [69, 117, 256, 259], ion-driven rotors of  $F_0F_1$ -ATP synthases from different organisms [260–266] or a voltage gated anion channel (VDAC) [33].

**4.3.1. Rhodopsins show different stoichiometries.** The examples of different bacterial and vertebrate rhodopsins show that the resolution of AFM topographs can be sufficiently high to identify individual monomers within oligomers (figure 10(a)). Interestingly, the assemblies of rhodopsins from different archaea and eukarya differ in their stoichiometry, which ranges from dimeric to hexameric [69, 117, 259, 267]. These differences supposedly have structural and functional origins [256, 268]. In the case of proteorhodopsin from marine bacteria the circular arrangement of proteorhodopsin monomers was speculated to reflect an

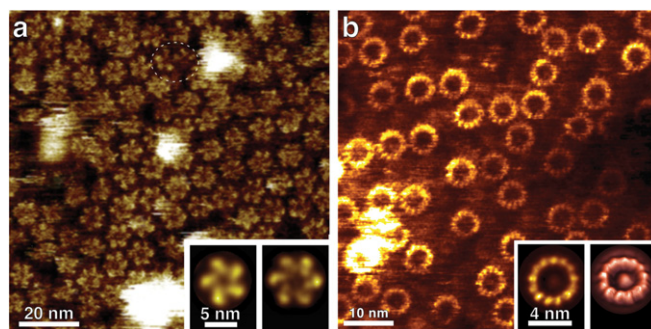


**Figure 10.** High-resolution AFM imaging reveals the stoichiometry of oligomeric membrane protein complexes. (a) High-resolution topograph of proteorhodopsin. In samples of reconstituted densely packed proteorhodopsin populations of both penta- and hexameric complexes can be observed. The insets show correlation averages of the pentameric (left) and hexameric (right) assemblies. (b) Reconstituted densely packed *Bacillus sp.* TA2.A1  $c_{13}$ -rings. In the overview images c-rings exposing their wide end (bright rings) toward the membrane surface protrude and c-rings exposing the narrow end (dark, weakly contrasted rings). A single-particle correlation average of the wide end of the c-ring is shown in top view (left) and perspective view (right). Particles exhibit 13-fold symmetry. The full color range of AFM topographs corresponds to a vertical scale of 2 nm (a) and 1.8 nm (b).

adaptation to the polarized light in the sea. The radial arrangement would thus increase the chance for one out of six differently oriented monomers to absorb light and thus contribute to the life-sustaining proton gradient across the membrane [259].

**4.3.2. Organism-specific  $F_0F_1$ -ATP synthase c-ring stoichiometry.** Other interesting examples of variations in the oligomeric state are the c-rings of ATP synthases from different organisms. ATP synthase is an enzyme that can synthesize and hydrolyze ATP. The flow of ions (protons or  $\text{Na}^+$ ) fuels the rotation of a membrane-spanning rotor (c-ring) of identical subunits. The number of subunits constituting a c-ring determines the number of ions required to produce three ATP molecules. While the number of subunits was assumed to be 12 [269–271], high-resolution AFM imaging could show that c-rings from different organisms exhibit varying stoichiometries of 11, 13 (figure 10(b)), 14 and 15 [260–262, 264, 272]. These numbers directly impact the ion-to-ATP ratio of an ATP synthase. It is discussed, whether the variable c-ring stoichiometry corresponds to the strength of the proton motive force established in different organisms and thus reflects an adaptation to optimize the energy used to synthesize ATP.

#### 4.4. Oligomeric assembly can alter surface structures of membrane proteins

AFM topographs of bacteriorhodopsin recorded at a lateral and vertical resolution of  $\approx 0.5$  nm and  $\approx 0.1$  nm, respectively, revealed that the surface structure of individual monomers depends on the oligomeric state [55]. Bacteriorhodopsin assembled in dimeric and trimeric forms showed different orientations of its polypeptide loops protruding from the

lipid bilayer [55]. As this conformational difference was unexpected, it may indicate that also other membrane proteins undergo structural changes upon oligomerization. Such changes could be very important especially for regulatory purposes.

#### 4.5. Imaging the supramolecular assembly of membrane proteins

Observing membrane proteins in the membrane of the living cell reflects the physiologically most relevant state. However, so far AFM could never reach sufficiently high resolution to image single membrane proteins of an intact cell [273–276]. Therefore, to approach the ‘native’ assembly of membrane proteins, membrane fragments are extracted from the cell, adsorbed to a flat support and then imaged at high resolution by AFM. Historically, the first AFM topography of such a native membrane was that of purple membrane extracted from *H. salinarum* [277]. The AFM topographs of native purple membranes, with a lateral resolution  $\leq 1$  nm, showed that the observed structural details match those from electron microscopy and x-ray crystallography [234, 278]. The first high-resolution AFM topographs of murine rhodopsin in native disk membranes that were extracted from rod outer segments of the eye surprisingly revealed that rhodopsins are organized in dimers (figures 11(a) and (b)) [117, 279, 280]. Based on these AFM topographs a three-dimensional model of a rhodopsin dimer was developed [281]. In this model the rhodopsin arrangement is compatible with binding of the G protein transducin [282] and the regulatory protein arrestin [283].

The supramolecular assembly of membrane proteins is a dynamic process and depends on the environment and functional state of the cell. Changes in the boundary conditions, e.g. changes in electrolyte concentration, temperature and pH or formation of functional membrane compartments, may cause rearrangement of membrane protein assemblies. The first experiment that could directly observe such rearrangements was AFM imaging of high- and low-light-adapted photosynthetic membranes that have been extracted from *Rhodospirillum photometricum* (figures 11(c) and (d)) [284]. These AFM topographs revealed that the ratio of light harvesting II complex to core complex increases when switching from the high-light- to the low-light-adapted state. Other AFM imaging studies showed the assembly of reaction centers in light harvesting I complexes in great detail [118, 285].

#### 4.6. Imaging membrane protein dynamics using time-lapse AFM

The fluid mosaic model of Singer and Nicolson proposes the lipid bilayer to be a two-dimensional fluid in which lipids and proteins freely diffuse [286]. However, it turned out over the past decades that membranes are ‘more mosaic than fluid’ [287]. Due to lipid microdomains that may exclude or concentrate certain membrane proteins [288], molecular crowding [289–291], organization in supramolecular complexes and anchoring to the cytoskeleton [292], the diffusion of membrane proteins is often hindered.

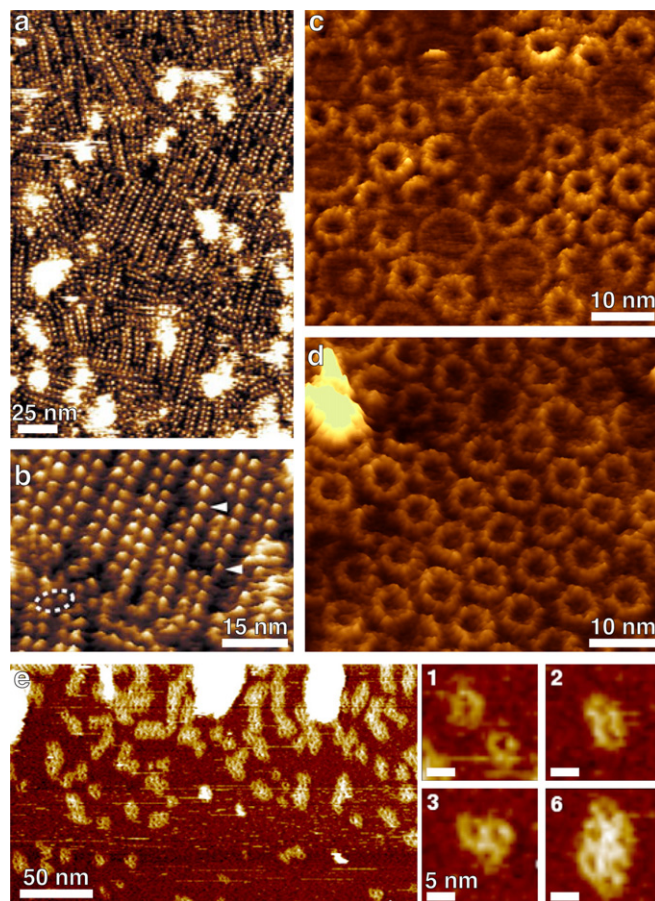


**Figure 11.** High-resolution AFM imaging of native assemblies of membrane proteins. (a) Paracrystalline arrangement of murine rhodopsin in the native ROS disc membrane. (b) At higher magnification the rhodopsin assembly is revealed in detail. Rhodopsins preferably assemble in dimers (encircled by a dashed line) and only occasionally occur as individual monomers (arrowheads). The rhodopsin dimers predominantly assemble into rows and protrude  $1.4 \pm 0.2$  nm ( $n = 111$ ) from the membrane. (c) Photosynthetic membranes of high-light-adapted *Rhodospirillum photometricum*. (d) Photosynthetic membranes of low-light-adapted *Rsp. photometricum*. Some areas of the membrane lack core complexes (large donuts) while LH2 (small donuts) shows a paracrystalline arrangement. (e) High-resolution NC frequency modulation AFM topograph of native VDAC in the outer mitochondrial membrane. The topographs reveal the native supramolecular assembly with different oligomeric states. The gallery on the right side shows four different oligomeric states. Numbers in the gallery indicate the oligomeric state. The full color range of AFM topographs corresponds to a vertical scale of 1.6 nm in (a) and (b), 4 nm in (c) and (d), and 2.3 nm in (e), respectively. Panels (a) and (b) adapted from [117] by permission from Macmillan Publishers Ltd. Panels (c) and (d) by courtesy of Simon Scheuring, Institute Curie, Paris. Panel (e) adapted from [33] with permission from Elsevier.

Today, measuring diffusion of membrane proteins relies on optical methods [293, 294], which require labeling and thus preselect a sub-set of proteins for observation. Such labels, however, might influence the diffusion behavior of the molecule [295, 296]. For precise tracking of single particles it is necessary to dilute the number of labeled molecules to prevent overlapping of the optical point spread functions detected for the fluorescence-emitting labels.

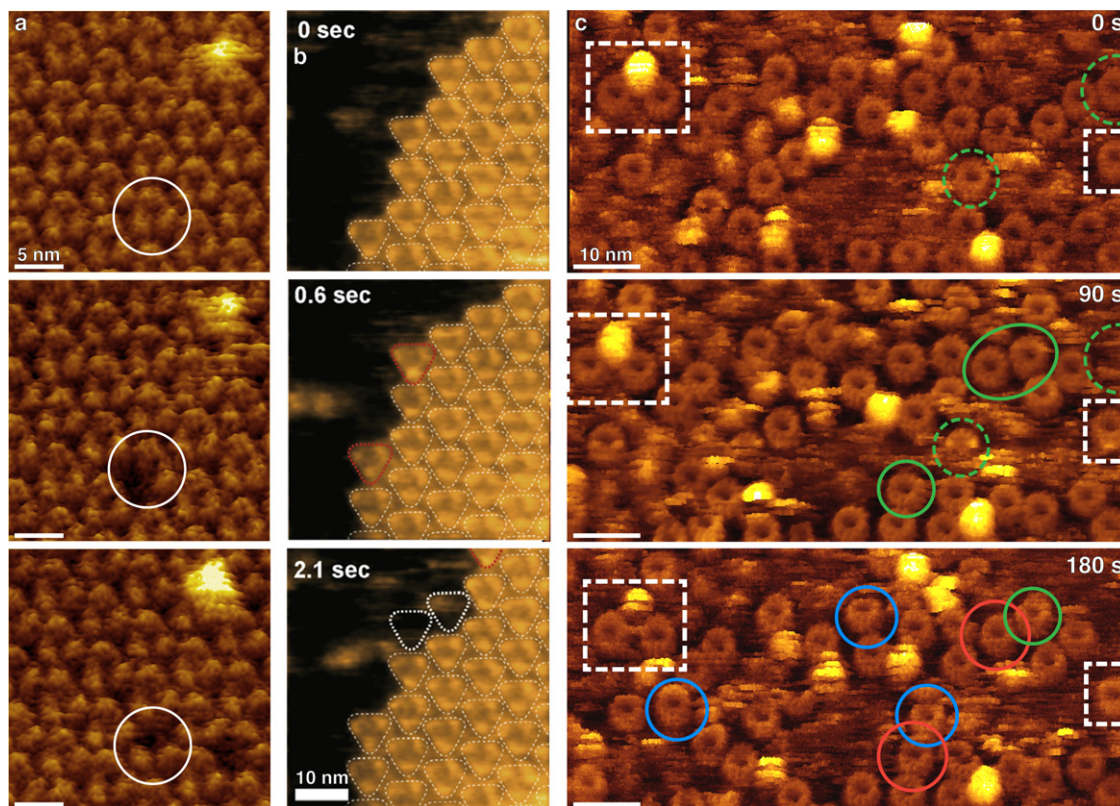


**Figure 12.** Following the motions of membrane proteins. (a) Cytoplasmic surface of purple membrane (top panel). After imaging the surface, a single bacteriorhodopsin molecule was removed by SMFS. Re-imaging reveals a vacancy corresponding to one bacteriorhodopsin (encircled, middle panel). Imaging the same area at a later time point revealed reorganization of the remaining two bacteriorhodopsin molecules being confined by surrounding bacteriorhodopsins (bottom panel). (b) High-speed AFM time-lapse topographs of the border separating crystalline and non-crystalline areas of purple membrane. Red (middle panel) and white (bottom panel) dotted triangles indicate newly and previously bound bacteriorhodopsin trimers, respectively. (c) Diffusion of single  $\text{Na}^+$ -driven ATP synthase rotors from *Ilyobacter tartaricus*. Subunits of individual rotors embedded in the lipid bilayer can be observed (top panel). The same area imaged after 90 s (middle panel). Some of the rotors changed their position (green circles) while others remained at the same location (white boxes). After another 90 s (bottom panel) some rotors moving in the previous image could be found at the same location (outlined red). Others began (outlined blue) or continued (outlined green) to move. Some rotors did not change their location throughout the time course (white boxes). Panel (b) adapted from [53] with permission from Elsevier.

Membrane proteins can be imaged for hours by AFM without destroying them or disturbing their assembly. The position of single proteins can be easily determined and tracked with sub-nanometer accuracy. Because AFM imaging is a label-free high-resolution technique, relocation of many proteins in a crowded environment can be investigated simultaneously.

**4.6.1. Dynamic assembly of purple membrane.** High-resolution topographs of purple membrane missing a single bacteriorhodopsin show the remaining bacteriorhodopsin molecules changing their position (figure 12(a)) [297]. As the available space is confined within the crystal lattice the bacteriorhodopsins rotated around the three-fold axis of the trimer. A recent study employing high-speed AFM imaging investigated the dynamics of purple membrane with a time resolution of  $\approx 40$  ms [53]. The dynamic association and dissociation of bacteriorhodopsin monomers, dimers and trimers (figure 12(b)) at the edges of crystalline areas were observed. Predominantly trimers associated with and dissociated from the crystalline area of purple

membrane. Occasionally, the association and dissociation of bacteriorhodopsin dimers or monomers could be observed. Analysis of the binding kinetics yielded an estimate for the free energy of a single inter-trimer bond of  $-0.9$  kcal mol $^{-1}$ . Moreover, AFM images suggest that such an inter-trimer bond could act as a pivot point for the rotational motion of bacteriorhodopsin trimers [53].

**4.6.2. Observation of membrane protein diffusion.** High-resolution time-lapse AFM imaging of reconstituted  $\text{Na}^+$ -driven rotors from bacterial ATP synthase allowed following the association of single rotors as well as their diffusion trajectories (figure 12(c)) [130]. Different modes of diffusion could be readily distinguished. Even within a single trajectory both hindered and free diffusion could be found. Compared with non-supported membranes, diffusion of rotors in these mica-supported lipid bilayers was slowed down by orders of magnitude. This example nicely points out the interactions of the close proximity between lipid bilayer and supporting surface (see section 3.2). In this case the interactions were weak and reduced but did not hinder the free diffusion of the proteins in the lipid membrane.

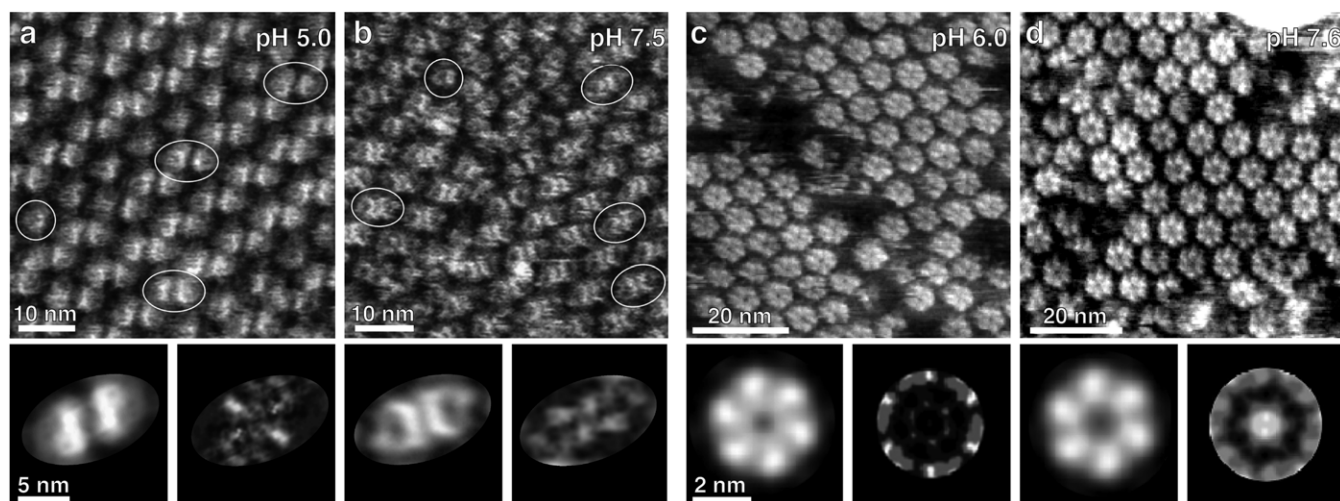


**Figure 13.** Functionally related conformational changes in membrane proteins observed by high-resolution AFM imaging. ((a), (b)) Topographs of the periplasmic surface of *E. coli* porin OmpG in the closed (a) and open state (b). Topographs show that OmpG mainly assembles as a dimer (outlined by an ellipse) but also rows of monomers (outlined by a circle) are frequently observed. The lower panels in (a) and (b) show correlation averages (left) and SD maps (right) obtained from the topographs shown in the upper panel. ((c), (d)) Extracellular surface of hexameric connexin26 (Cx26) hemichannels in a closed (c) and open (d) state. The lower panels in (c) and (d) show single-particle correlation averages (left) and SD maps (right), respectively. The full gray scale corresponds to a vertical range of 2.5 nm (topographs in (a) and (b)), 2 nm (correlation averages in (a) and (b)) and 0.6 nm and 1 nm for the SD maps of (a) and (b), respectively. The full gray scale in (c) and (d) corresponds to a vertical scale of 3 nm (topographs and correlation averages) and 0.35 nm (SD maps).

#### 4.7. Imaging membrane proteins at work

Membrane proteins often undergo functionally related conformational changes. In order to understand how membrane proteins work, it is important to characterize their different conformations. Currently, acquisition of an AFM topograph using a commercial atomic force microscope requires  $>90$  s. Most biological processes, however, occur on much faster timescales. Therefore, membrane protein conformations have to be kinetically trapped for AFM imaging or AFM imaging has to be significantly accelerated. Several membrane proteins have been imaged at work using time-lapse AFM [116, 125, 251, 298, 299].

**4.7.1. Voltage- and pH-induced conformational changes in Omps.** The first functionally related conformational change observed by AFM imaging was that of OmpF porin. OmpF opens and closes its transmembrane pore depending on the membrane potential applied and the pH of the buffer solution. When implementing conditions that switch the functional state of OmpF porin, the large extracellular loop reversibly collapsed onto the OmpF channel entrance [125]. Later, this unexpected motion was underscored by results obtained for porins of the same family of outer membrane proteins [300, 232]. Lately, reversible pH-induced conformational changes in the outer membrane protein G (OmpG), which is also an *E. coli* porin, was visualized by AFM [301]. At acidic pH, the channel entrance is obstructed (figure 13(a)) while it is wide open at neutral pH (figure 13(b)). The topographic changes observed correlate well with the results from x-ray crystallography [232] and support the finding that the extracellular loop L6 folds onto and closes the OmpG channel entrance.

**4.7.2. Communication channel gating.** Connexin-based gap junctions provide intercellular communication and are regulated on several levels [302]. The communication channels are composed of two end-to-end docked hemichannels located in the plasma membrane of opposing cells. After nanodissecting the upper membrane of a Cx26 gap junction patch, the extracellular surface of hemichannels became visible (figures 9(e) and (f)). Topographs revealed the hexameric hemichannels with an open pore entrance (figures 9(g)). In the presence of  $\text{Ca}^{2+}$ , the hemichannel surface structures moved radially toward the pore center thus closing the entrance [116]. Removing  $\text{Ca}^{2+}$  reversed the pore closure. In the presence of aminosulfonate compounds, such as HEPES, gating of Cx26 hemichannels is pH-dependent. While the communication channel is closed at acidic pH of 6.0 (figure 13(c)) it opens like a camera iris shutter upon approaching a neutral pH of 7.6 (figure 13(d)) [251]. Both gating mechanisms are crucial for proper intercellular communication and mutations impairing them often cause severe inheritable diseases [303, 304].

**4.7.3. Dynamics of bacteriorhodopsin during the photocycle.** The advent of high-speed AFM has led to a dramatically increased time resolution, which makes imaging of processes taking place on the sub-second time range possible. Recently, high-speed AFM imaging revealed dynamic processes in the photoactivated bacteriorhodopsin mutant D96N [54]. Upon photoactivation of bacteriorhodopsin the polypeptide loop connecting transmembrane  $\alpha$ -helices E and F was observed to undergo a conformational change. Interestingly, this EF loop can be forced to undergo similar conformational changes by slightly elevating the imaging force used in CM AFM [55, 298, 305]. This indicates that the EF loop shows an enhanced structural flexibility, such as required to allow

transmembrane  $\alpha$ -helices E and F to tilt relative to each other in the photocycle of bacteriorhodopsin [306].

#### 4.8. Current limitations, challenges and perspectives

AFM imaging is a valuable tool to evaluate the surface topography of membrane proteins in their native membrane and exposed to physiological buffer. So far AFM imaging has been mostly applied to determine the stoichiometry and supramolecular architecture of membrane protein complexes, and observe membrane proteins at work. Most of these studies have been performed on purified and reconstituted samples or on preparations of membrane proteins that form densely packed or two-dimensional arrays *in vivo*. In the future, applying AFM imaging to more complex assemblies of many different membrane proteins would be desirable, as only these provide further insight into their interplay in the native cellular membrane. In an attempt to get closer to physiological conditions, AFM imaging of membrane proteins in free spanning or cushioned membranes will be required [297].

The rapid improvements of high-speed AFM in terms of time and spatial resolution will push functional studies on membrane proteins forward. So far unresolved dynamic processes will be observable, giving new insights into membrane protein assembly, movement and function. Further development of high-speed AFM to reach even higher imaging rates will be a demanding task.

More importantly, in the future new ways to characterize the manifold structural and functional properties of membrane proteins will be required. Recognition and adhesion imaging are attempts to investigate more complex samples or to correlate adhesion strengths with topography. Multi-frequency imaging techniques try to correlate physical and mechanical properties of specimens with their topography. Also, AFM applications have been developed to simultaneously image structure and conductivity of cell membranes [307].

These examples point out that the future is open to multifunctional AFM approaches. Such methods would ideally allow simultaneous acquisition of topography, mechanical (e.g. deformation or stiffness), physical (e.g. hydrophobicity or electrostatics), chemical and biological parameters of membrane proteins at high resolution. This would provide further insight into the functional mechanisms of e.g. ligand-binding, functional assembly or conformational flexibility of individual membrane proteins.

## 5. Quantifying and locating interactions of membrane proteins

### 5.1. Pick and play with single membrane proteins

Atomic force microscope styluses are not only capable of imaging membrane protein topography at very high resolution but also provide a tool to pick up and manipulate single membrane proteins. In SMFS experiments, the atomic force microscope stylus is used to pick up membrane proteins and to characterize how the proteins respond under an external force. This approach offers exciting insights into the interactions that stabilize the membrane protein and determine its functional

state. As SMFS is conducted in buffer solution, the method can be used to characterize the influence of environmental conditions on the interactions established in membrane proteins. Consequently, the interactions stabilizing individual secondary structure elements of membrane proteins have been probed in dependence on temperature [308], pH [309], electrolyte [310], oligomeric state [311] and in the context of protein–protein interactions [312]. First experiments characterizing the unfolding and refolding pathways of single membrane proteins into the lipid membrane have been performed [67, 313, 314]. Throwing light on the energy landscape of membrane proteins, DFS offers a more detailed understanding of how interactions shape protein structure and function.

### 5.2. Unfolding individual membrane proteins

**5.2.1. F–D curves reflect unfolding of single membrane proteins.** Bacteriorhodopsin was the first membrane protein characterized by SMFS. Oesterhelt *et al* [68] obtained reproducible F–D curves by repeatedly bringing the atomic force microscope stylus into contact with purple membrane and subsequently retracting it with constant velocity (see section 2.5). In  $\approx 5$ –10% of all attempts, a bacteriorhodopsin molecule adhered to the atomic force microscope stylus giving rise to an F–D curve like the one shown in figure 2(c) (bottom panel). These F–D curves showed a reproducible pattern of several force peaks at stylus–sample separations up to  $\approx 75$  nm. This length corresponds to the length of the fully unfolded and stretched polypeptide of bacteriorhodopsin. High-resolution imaging of purple membrane before (figure 2(c), upper left panel) and after (figure 2(c), upper right panel) an approach–retract cycle confirmed that an F–D curve is a record of the extraction and unfolding of a bacteriorhodopsin molecule from purple membrane.

**5.2.2. Water-soluble and membrane proteins unfold differently.** Significant differences become evident when comparing the force-induced unfolding of a membrane protein with that of a water-soluble protein. Water-soluble proteins commonly unfold cooperatively, i.e. the structural integrity of the entire protein is disrupted upon reaching a critical force level [71, 315, 316]. In corresponding F–D curves, a single force peak reflects the unfolding of a single protein [71]. In contrast, F–D curves recorded upon unfolding a membrane protein show a set of force peaks, each one indicating an unfolding intermediate. Each unfolding step transforms one unfolding intermediate into the next one and characterizes the unfolding of a structural segment. Generally speaking, when exposed to mechanical stress, water-soluble proteins unfold in one main event, whereas membrane proteins unfold from the lipid bilayer in multiple sequential steps.

### 5.3. Quantifying and mapping interactions of membrane proteins

**5.3.1. What information is stored in F–D curves?** F–D curves of membrane proteins reveal different information: (i) the pulling distance locating the force peak, (ii) the sequence

at which force peaks occur and (iii) the magnitude of the force peak. The distance between force peaks in an F–D curve describes the length of the polypeptide segment unfolded upon transformation of one unfolding intermediate into the next one. Fitting a force peak with the WLC model (equation (5)) [73, 78, 79] approximates the contour length of a fully stretched polypeptide [71, 317]. Subtracting this contour length from the protein terminus to which the atomic force microscope stylus attached allows assignment of the beginning of the stable structural segment that established the unfolding barrier. Fitting all force peaks of an F–D curve locates all unfolding barriers and describes the populated unfolding intermediates (figure 14(a)). Fitting every force peak in hundreds of F–D curves allows the occurrence of each unfolding intermediate to be estimated. While some force peaks (unfolding barriers) appear in almost every F–D curve, the occurrence of others is of  $\leq 10\%$ . Finally, the location of the unfolding barriers can be mapped onto the primary, secondary (figure 14(c)) or tertiary structure of the membrane protein.

The sequence of unfolding events in an F–D curve defines the unfolding pathway the membrane protein took. As the probability of peak occurrence varies, manifold unfolding pathways co-exist (figure 14(b)) [68]. So far, multiple unfolding pathways have been observed for all membrane proteins subjected to SMFS, including bacteriorhodopsin [309] and halorhodopsin [69] from *H. salinarum*, sensory rhodopsin II from *Natronomonas pharaonis* [312], the sodium/proton antiporters NhaA from *E. coli* [67] and MjNhaP1 from *Methanococcus jannaschii* [66], the amino acid antiporter SteT from *E. coli* [318], OmpG from *E. coli* [203], as well as bovine [319] and murine [320] rhodopsin.

Molecular interactions within a stable structural segment establish unfolding barriers counteracting the externally applied force by SMFS. It is not yet known how many interactions and amino acids are required to set up an unfolding barrier. The lengths of stable structural segments vary between 4 and more than 40 amino acids indicating that a few amino acids are sufficient to establish an unfolding barrier. However, this does not mean that only a few amino acids of a segment contribute to the stability of a large structural segment. Probably, the interactions established by all amino acids in a stable segment sum up. To what extent individual amino acids contribute to the interactions that stabilize a structural segment remains to be determined.

5.3.2. *Environmental factors favor certain unfolding pathways.* The probability of populating certain unfolding pathways sensitively depends on the environmental conditions, for example pH, electrolyte, protein assembly state and the presence of small molecules that interact with the membrane protein [310, 311, 321, 322]. In bacteriorhodopsin, for example, the probability of pairwise unfolding of transmembrane  $\alpha$ -helices increases with temperature [308] but decreases with pulling velocity [323]. This indicates that changing the environmental conditions causes membrane proteins to choose different trajectories on their unfolding energy landscape. DFS studies of wild type and mutant bacteriorhodopsin support this notion. Single point mutations

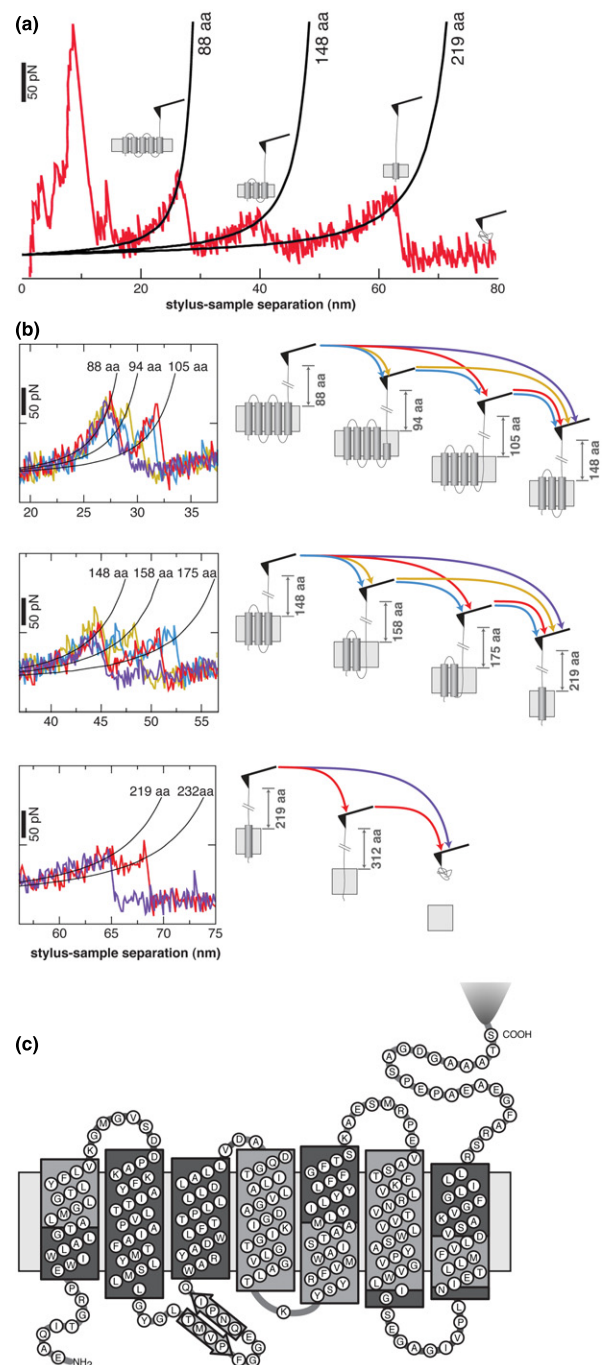


**Figure 14.** Mapping unfolding, pathways and interactions within membrane proteins. (a) F–D curve obtained upon unfolding a bacteriorhodopsin molecule. Black curves are WLC fits of force peaks. The contour length of the stretched polypeptide is indicated next to the WLC curves and given in amino acids. The cartoons scrutinize the major unfolding intermediates. (b) Detailed analysis of the unfolding pathways that bacteriorhodopsin can choose. Boxes on the left display sections from F–D curves that show a reproducible variability of force peaks. Each force peak denotes the unfolding of a structural segment. The probabilities at which individual force peaks occur give the probability of a structural element to unfold in a single step. Fewer force peaks assign fewer unfolding events and thus indicate cooperative unfolding of structural segments. (c) Stable structural segments that establish unfolding barriers are mapped onto the secondary structure of bacteriorhodopsin (alternately colored in light and dark gray). The atomic force microscope stylus indicates the terminus from which the protein was mechanically unfolded.

are sufficient to reshape the unfolding energy landscape and, at the same time, redistribute the probability at which certain unfolding pathways are chosen [324].

**5.3.3. Interactions of membrane proteins with the support are weak.** The amplitude of a force peak characterizes the strength of the interactions stabilizing a structural segment. Stabilization of a structural segment may involve a number of different interactions that are established within the membrane protein but also between the membrane protein and its environment. For SMFS the protein membrane is usually adsorbed to a solid support. The interactions between membrane protein and support could influence the interactions stabilizing a structural segment. To rule out such biasing interactions, force peak position and height of the same membrane protein adsorbed to different supporting materials, such as mica, gold, HOPG and glass, can be compared. The unfolding forces of bacteriorhodopsin from purple membrane adsorbed to mica, HOPG and another purple membrane did not differ [68]. Similarly, the forces required to unfold the sodium/proton antiporter NhaA adsorbed to freshly cleaved mica or another layer of protein membrane did not show any variation [67]. These results are in agreement with high-resolution AFM images that revealed freely diffusing membrane proteins embedded into a supported lipid membrane [130]. Consequently, the interactions stabilizing the unfolding intermediates of bacteriorhodopsin and NhaA are intrinsic to the membrane proteins. It may, however, not be excluded that more sensitive SMFS methods may detect such influences.

#### 5.4. Refolding membrane proteins

**5.4.1. Current models of membrane protein insertion and folding.** Over the past decades, the field of protein folding has contributed a lot toward understanding the folding mechanisms of water-soluble proteins [325–328]. However, elucidation of membrane protein folding mechanisms has progressed much slower. Although the three-stage model by Popot and Engelman describes the insertion and folding of membrane proteins into a lipid bilayer [329, 330], it does not describe the important step of transmembrane  $\alpha$ -helix formation in detail. Wimley and White proposed a thermodynamic model of membrane protein folding. Their model includes (i) partitioning of the peptide to the membrane interface, (ii) formation of  $\alpha$ -helices, (iii) insertion into the lipid bilayer and (iv) association of transmembrane segments. The main driving force behind all folding steps is the hydrophobic effect [331, 332]. The so-called four-step model is based on biophysical measurements using small peptides. The concepts derived from those experiments turned out to hold true *in vivo* [333, 334]. Noteworthy is that in addition to bacteriorhodopsin [335], the folding mechanism of only a few membrane proteins has been addressed experimentally [330, 336, 337]. Therefore, developing assays to study the folding of complex membrane proteins seems an exigent task.

**5.4.2. Problems and challenges encountered by conventional unfolding experiments.** In conventional unfolding experiments using thermal or chemical denaturation, the denatured state of a protein is both structurally and terminologically not well defined. The term ‘denatured’ is used to describe both inactive and (partially) unfolded proteins. Denatured proteins often populate an ensemble of multiple conformations. As the conformation of the denatured state can influence the folding pathway of a protein [338, 339], it seems important for membrane protein folding studies to start from a well-defined topology. Moreover, membrane proteins are commonly unfolded in the absence of their lipid bilayer and in the presence of detergents. Such conditions do not occur in the living cell. Consequently, the folding of membrane proteins should be studied under conditions mimicking their native environment as closely as possible.

**5.4.3. Refolding single membrane proteins into membranes.** Since 1997, SMFS has been used to study un- and refolding of single water-soluble proteins [71]. Similar approaches have been applied to bacteriorhodopsin [314] and NhaA [67, 313]. Figure 15(a) shows the experimental cycle of such a refolding experiment in which the membrane protein is partially unfolded. Some domains remain inserted in the membrane and act as an anchor. The unfolded portion of the membrane protein is stretched by the atomic force microscope stylus. From this well-defined conformation, the membrane protein is allowed to refold. Thereto, the atomic force microscope stylus is approached close to the membrane surface ( $\approx 5$  nm). After a pre-defined folding time, the cantilever is again retracted from the membrane (figure 15(a)). F–D curves acquired after refolding frequently show one or more force peaks exceeding 50 pN (figure 15(c)). These peaks locate interactions that stabilize refolding intermediates. Thorough analysis revealed that these interactions were identical in both strength and location to those observed in the correctly folded membrane protein. This indicates that the polypeptide spontaneously folded into the membrane and established interactions and structural intermediates similar to those detected when initially unfolding the membrane protein.

**5.4.4. Refolding kinetics from single membrane protein experiments.** Insight into the refolding kinetics of individual structural segments of NhaA was revealed by time-resolved SMFS refolding studies [313]. In these experiments, the refolding time was systematically increased from 10 ms to 15 s. The number of force peaks and thus the complexity of the F–D curves increased with refolding time (figure 15(c)). Careful analysis revealed that each structural segment refolded with a characteristic rate, ranging from  $\approx 0.3^1$  to  $\approx 50$  s<sup>-1</sup>. At short refolding times, the forces stabilizing structural elements were lower compared with initial unfolding. With increasing refolding time, these forces reached the strength measured upon initial unfolding. This indicates that the formation of interactions within a structural segment and between structural segments requires time.

Similar to the mechanically induced stepwise unfolding of membrane proteins, membrane proteins refold stepwise.

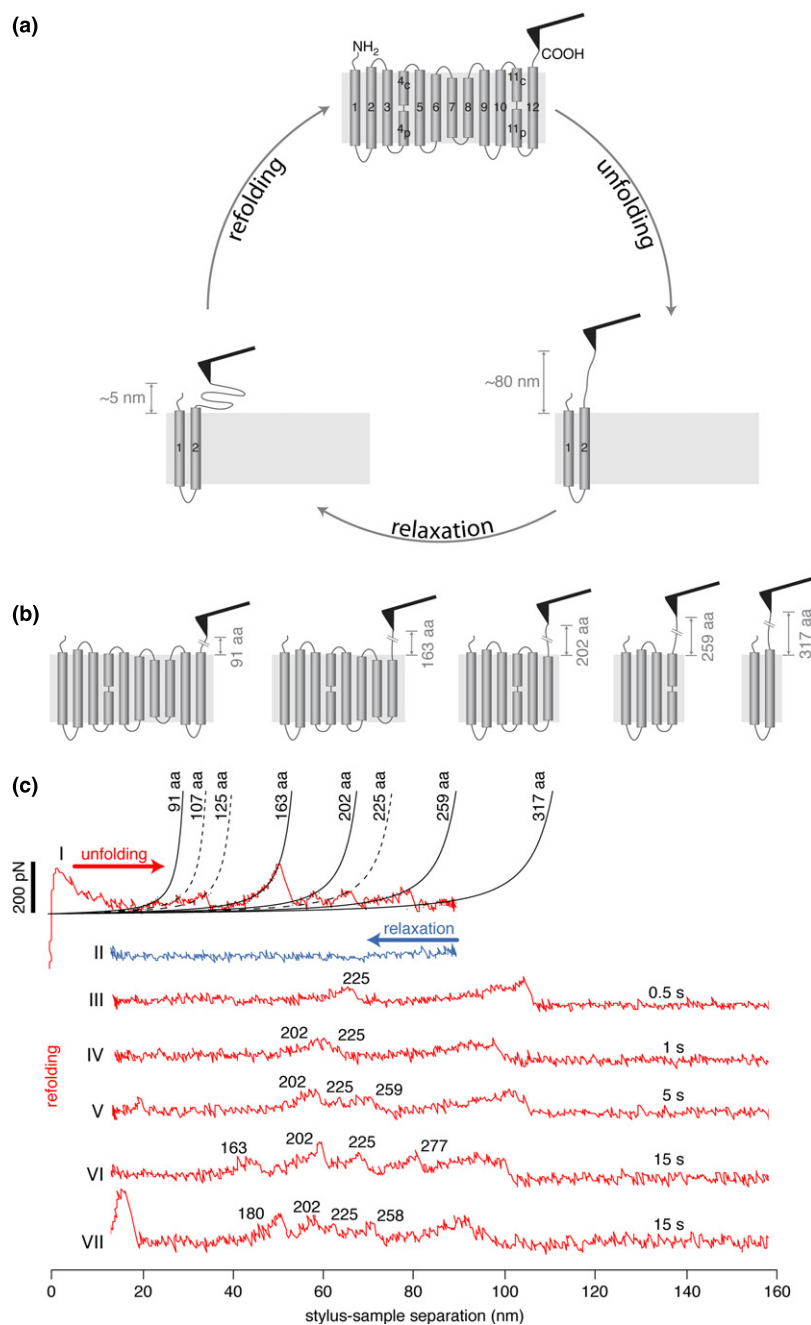


**Figure 15.** Refolding single membrane proteins. (a) Experimental cycle. Initially, ten out of twelve transmembrane  $\alpha$ -helices of NhaA are unfolded and extracted from the lipid bilayer. Subsequently, the atomic force microscope stylus is approached toward the lipid bilayer, thus relaxing the unfolded polypeptide. During the pre-defined waiting time the unfolded polypeptide is allowed to refold into the membrane before the stylus is withdrawn again to probe which structural segments of NhaA refolded. (b) Cartoon of the major unfolding intermediates populated during mechanical unfolding of NhaA. The numbers indicate the contour length (in amino acids) of the polypeptide that has been unfolded and extracted from the membrane. (c) F–D curves showing initial unfolding (I) and subsequent relaxation (II) of the polypeptide. The extent of NhaA refolding depends on the time given for refolding. Representative F–D curves obtained after 0.5 s (III), 1 s (IV), 5 s (V) and 15 s (VI and VII) refolding are shown. The numbers indicate the contour length (in amino acids) of the polypeptide deduced from the peaks in the initial F–D curve and the F–D curves obtained after refolding, respectively.

In contrast to unfolding however, folding does not occur sequentially along the polypeptide sequence but still follows a distinct order of events [67]. The first and fastest refolding intermediate ( $\approx 50 \text{ s}^{-1}$ ) of NhaA was a structural segment within transmembrane  $\alpha$ -helix V. The folding of this segment proceeded even against an applied force of  $\approx 30 \text{ pN}$ . The subsequent insertion of the  $\alpha$ -helical pair V and VI depended on this first folding event. All other structural segments

inserted independently of each other. Still, two transmembrane  $\alpha$ -helices that are connected by a polypeptide loop, which is located on the opposite side of the membrane, tended to fold and insert together. Such pairwise insertion might be energetically favored because it increases the number of hydrogen-bonded peptide bonds in the polypeptide backbone. After refolding, a new force peak could be occasionally detected that was not observed during initial unfolding of the

antiporter. The corresponding structural segment indicated a new folding intermediate that kinetically trapped the refolding polypeptide. Thus, it was assumed that this unfolding peak indicated a misfolding intermediate [67].

### 5.5. Mapping energy barriers and reconstructing the energy landscape of membrane proteins

**5.5.1. Concept of dynamic free energy landscapes.** Free energy minimization is the driving force behind many biomolecular processes. To reach a state of minimal energy, molecular interactions are often sequentially altered. Folding of an unstructured polypeptide into a stable, functional protein is the result of stepwise formation of interactions. Similarly, protein unfolding is a stepwise process. The sequence of the interaction events defines the reaction pathway of a process. As in protein (un-)folding, interactions shape reaction pathways that guide processes such as signal transduction, molecular translocation, ligand or inhibitor binding and conformational change.

The concept of energy landscapes is a powerful tool to understand such dynamic processes [86, 340–342]. In the framework of this concept, biomolecular reactions navigate a route downhill on a funnel-shaped energy landscape. In many cases, not only a single well-defined pathway but multiple independent pathways coexist on the energy landscape (figures 14(a) and (b)) [343–345]. The bottom of a free energy funnel is rough exhibiting multiple local energy minima. For example, the ensemble of conformational states that a protein can adopt is determined by the widths of the local minima and the height of the energy barriers separating the minima. Although multiple reaction pathways and conformations can be populated, the probability at which they are populated may vary. Furthermore, energy landscapes are dynamic and adapt to the environmental conditions. Thus, the concept of energy landscapes is appealing to explain both protein folding and function [344, 346–348].

**5.5.2. Probing energy landscape barriers with force.** In contrast to conventional SMFS, which localizes interactions in membrane proteins, DFS reveals the characteristic equilibrium parameters  $x_u$  and  $k_0$  of energy landscapes that are shaped by these interactions (figure 2, section 2.6). Applied to membrane protein unfolding, DFS gains insights into the interactions and energy barriers stabilizing individual structural segments. So far, DFS has been exploited to investigate the energy landscapes of a variety of membrane proteins including bacteriorhodopsin [323], bovine and murine rhodopsin [320, 349], NhaA [350], SteT [318] and the ADP/ATP carrier Aac3p from *Saccharomyces cerevisiae* [322]. In the following we will review such examples in detail.

**Anchoring of short transmembrane peptides in lipid bilayers.** Hydrophobic or amphipathic peptides insert into or associate with lipid bilayers. Determining these interactions is important for membrane protein folding, assembly and function. According to current models, the formation of individually stable transmembrane  $\alpha$ -helices is the first step of membrane protein folding [329]. Moreover, many membrane proteins

involved in processes such as signal transduction or membrane fusion often contain only one transmembrane  $\alpha$ -helix acting as a membrane anchor.

Canchev *et al* investigated the insertion strength of the synthetic WALP23 peptide, which forms a transmembrane  $\alpha$ -helix in DOPC and DPPC bilayers [351]. The force required to extract a WALP23 transmembrane  $\alpha$ -helix from highly ordered striated domains formed in DPPC bilayers changed with the loading rate and ranged from  $\approx 55$  pN ( $0.1$  nN s<sup>-1</sup>) to  $\approx 95$  pN ( $45$  nN s<sup>-1</sup>). Extracting WALP23 peptides from either striated domains formed in DPPC or from liquid phase DOPC bilayers resulted in  $x_u$  values of  $\approx 0.75$  nm. Thus, displacing the transmembrane  $\alpha$ -helix by only  $\approx 0.75$  nm from its equilibrium position induced its unfolding.

### Energy landscapes of membrane proteins.

**Quantifying energy barriers.** Bacteriorhodopsin unfolds following a distinct set of unfolding pathways, which are characterized by the pairwise or stepwise unfolding of transmembrane  $\alpha$ -helices. Irrespective of the unfolding pathway the distance to the transition state,  $x_u$ , is in the range  $\approx 0.3$ – $0.9$  nm. However the lifetime,  $\tau_0 = 1/k_0$ , of paired transmembrane  $\alpha$ -helices is on average  $\approx 10^4$  s while a single transmembrane  $\alpha$ -helix lives for about 100 s [323]. These findings support the notion that individual transmembrane  $\alpha$ -helices can form stable intermediates during membrane protein folding [329].

Mutations or environmental changes can change the energy landscape of a membrane protein. For example, the probability of bacteriorhodopsin choosing a certain unfolding pathway depends on the loading rate. At high loading rates, predominantly pathways involving the unfolding of single transmembrane  $\alpha$ -helices are populated. In contrast, pathways showing pairwise unfolding of transmembrane  $\alpha$ -helices dominate at low loading rates. Extrapolating the probabilities of the different pathways to zero loading rate indicates that transmembrane  $\alpha$ -helices, in the absence of externally applied force, unfold almost exclusively pairwise [323]. Inserting mutations at single [324] or multiple [352] sites in bacteriorhodopsin showed that these can have different effects. As intuitively expected, the stability of the structural segment that hosts the mutations can be altered. However, the mutations can also influence other structural segments that are far away from the mutated site.

Interestingly, DFS data of wild type and mutant bacteriorhodopsin revealed Hammond behavior [353], i.e. the height of the energy barrier stabilizing an unfolding intermediate decreased concomitant with the distance separating the folded from the transition state [324]. Such behavior was also observed for temperature-dependent unfolding of bacteriorhodopsin [354] and ligand-induced stabilization of SteT [318].

While many structural segments of membrane proteins show  $x_u$  values of  $\leq 1$  nm, some structural segments of SteT and Aac3 show unexpected large  $x_u$  values of  $> 1$  nm [318, 322]. These indicate different unfolding mechanisms.  $x_u$  values  $< 1$  nm suggest that  $\alpha$ -helices unfold in the lipid bilayer by breaking intrahelical hydrogen bonds. In contrast,

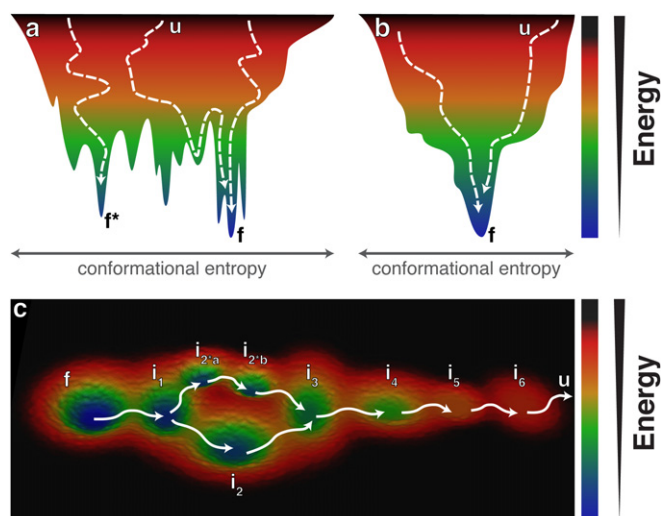


**Figure 16.** Cartoon of protein (un-)folding energy landscapes. (a) and (b) show cross-sections through funnel-shaped energy landscapes. The energy landscape can be corrugated (a), exhibiting many local minima in addition to the global minimum, or smooth (b), exhibiting a single global minimum. The width of the funnel represents the conformational entropy and the depth the free energy. On its way from an unfolded peptide (u) at the top of the energy funnel to a functionally folded protein (f) at the bottom of the funnel, the polypeptide can choose different pathways (indicated by dashed lines) and transiently populate local minima. Some of these folding routes may lead to misfolded conformations (f\*) that reside in a local minimum. (c) Cartoon of a hypothetical energy landscape of a membrane protein unfolded by SMFS. In its folded state (f), the protein resides at a low-energy conformation. Upon applying mechanical stress, the protein unfolds stepwise populating a series of unfolding intermediates (i<sub>x</sub>), each of which resides in a local energy minimum. After reaching i<sub>1</sub>, the protein can choose to unfold either via i<sub>2</sub> or via i<sub>2a</sub> and i<sub>2b</sub> before both pathways reach i<sub>3</sub> and subsequently populate the same intermediate states.

high  $x_u$  values indicate that  $\alpha$ -helices undergo large structural deformations ( $>1$  nm) prior unfolding. Their unfolding, for example, might be triggered after partial extraction from the lipid bilayer and concomitant weakening of the hydrophobic interactions stabilizing the transmembrane  $\alpha$ -helix.

**Energy landscape roughness.** The fine structure of an energy landscape determines the reaction kinetics. Proteins with a smooth energy landscape (figure 16(b)) fold faster while proteins with a rough energy landscape (figure 16(a)) require more time. In particular, transient trapping of folding intermediates in local energy minima impairs folding. Escape from these minima slows down the exploration of the conformational space, which finally allows locating the global energy minimum [343, 355]. The energy landscape roughness of individual transmembrane  $\alpha$ -helices of bacteriorhodopsin was investigated performing DFS at different temperatures [354]. The calculated roughness of  $\approx 5k_B T$  is in the range of the ones measured for protein–ligand interactions [356], small water-soluble proteins [99] and protein–protein interactions [357].

**Reconstructing energy landscapes.** Based on the information gathered about the unfolding energy barriers of individual

structural segments, the unfolding energy landscape of the membrane protein of interest can be reconstructed. Figure 16(c) sketches a reconstructed energy landscape of a membrane protein unfolded by SMFS. The model also emphasizes the possibility of choosing alternative unfolding pathways as indicated by the bifurcation of the unfolding pathway [358].

### 5.6. Current limitations, challenges and perspectives

Conventional experiments unfolding membrane proteins face a variety of problems. First, thermal unfolding of membrane proteins is often irreversible [359–362]. More importantly, membrane proteins mostly do not completely unfold upon thermal or chemical denaturation but retain a considerable amount of secondary structure [359, 363]. In particular, bilayer-exposed transmembrane  $\alpha$ -helices appear to remain folded or regain their structure [360, 364–367]. Thus, the term ‘unfolded’ is often used to describe the denatured, non-functional state of a membrane protein, not taking structural aspects into account. So far, all successful reversible unfolding experiments have been performed in the presence of non-physiological detergents [359–369]. Indeed, refolding often started from a set of secondary structure-containing, partially unfolded species [338, 339]. Without having a defined unfolded state, it is challenging to compare the results obtained from different proteins, denaturants or unfolding conditions because it remains unknown whether refolding is initiated from the same denatured state.

SMFS-based refolding experiments offer both more native-like conditions and well-defined denatured states. Experiments are performed in the absence of detergent and with a well-defined starting point for refolding, which is the unfolded and stretched polypeptide [67, 313, 314]. However, membrane proteins have never been completely extracted from the membrane in SMFS refolding experiments. Small segments always remained inserted in the membrane to anchor the polypeptide [67, 313, 314]. In the future, it may be better to completely unfold and extract a membrane protein prior to its refolding into the membrane. This way, the presence of a pre-existing folding core in the membrane that might facilitate the refolding process can be ruled out. *In vivo* membrane protein folding is initiated at the N-terminal part of the polypeptide, which is due to protein biosynthesis and co-translational membrane insertion. However, *in vitro* folding could be initiated at any other position of the polypeptide. SMFS-based refolding experiments would allow determining such nucleation sites and unraveling determinants for insertion of polypeptides into lipid bilayers.

## 6. Understanding function-related interactions in membrane proteins

Membrane proteins are dynamic entities that perform various functional tasks. To fulfil their function, they often undergo conformational changes and interact with membrane and water-soluble proteins as well as with small molecules. This molecular interplay is dynamic and functionally important.

Binding of a compound or another protein may trigger functional cycles, alter the energy landscape and regulate protein activity and functional state. Therefore, understanding the intra- and intermolecular interactions that determine both structure and function of a native membrane protein is of utmost importance.

### 6.1. Ligands establish specific interactions

Membrane proteins can selectively bind solutes from the intra- and extracellular environment. These ligands may be required for the function and the folding of the membrane protein or, as in the case of molecular transporters, serve as substrates that are translocated across the membrane. SMFS experiments have shown that bovine rhodopsin is stabilized in the presence of  $Zn^{2+}$  [370]. The effect is distributed over the entire protein and structurally not localized. This might be due to the fact that  $Zn^{2+}$  ions can bind to a number of different binding sites within bovine rhodopsin at a time. Interestingly, folding and functioning of rhodopsin are highly cooperative processes that involve long-range interactions [371]. Such interactions between spatially separated regions of the protein could transmit local effects to other structural regions and thus cause global stabilization of rhodopsin.

In contrast, ligand ( $Na^+$ )-binding to NhaA establishes localized interactions [310]. In its inactive state (low pH), NhaA cannot bind  $Na^+$ . The interactions detected in the inactive state are different from those in the active state (neutral pH, figures 17(a)–(c), encircled area). The prominent interaction established in the active state is localized at the  $Na^+$ -binding site of transmembrane  $\alpha$ -helix V (figure 17(f)) and disappears upon removing  $Na^+$  from the buffer solution (figure 17(d), encircled area). The interaction induced by  $Na^+$ -binding also revealed an early step in NhaA activation that takes place at  $\approx$ pH 5.5 (figure 17(e)), well before NhaA reaches its full activity at pH 7–8 [310]. Similar results have been obtained for another  $Na^+/H^+$  antiporter from *Methanococcus jannaschii* [66].

### 6.2. Inhibitors establish different interactions from ligands

Membrane proteins play a crucial role in drug development. Located at the interface between the interior and exterior of a cell, they mediate vital processes. About 70% of all drug targets are membrane proteins [372, 373]. In contrast to natural ligands, inhibitors must interact with membrane proteins in a different way to inhibit their function. Deciphering these interactions provides mechanistic insights into the inhibitor's mode of action.

SMFS experiments differentiated ligand- from inhibitor-binding to NhaA [321]. The inhibitor, 2-aminoperimidine (AP), competes with the ligand for the ligand-binding pocket and mimics its interactions (figures 18(a) and (b), boxed area). Beyond that, AP establishes additional interactions with NhaA (figures 18(a) and (b), encircled area). In particular, AP increases the stability of a structural segment in transmembrane  $\alpha$ -helix IX. This additional interaction is thought to inactivate NhaA. The ratio of inhibited NhaA to free NhaA depends on the AP concentration (figures 18(c)–(e)). High concentrations

of  $Na^+$  can displace AP from the binding site. Although far separated in the primary structure of NhaA, both the ligand-binding site and the stabilized transmembrane  $\alpha$ -helix IX are in close proximity in the folded protein (figure 18(f)).

Recently, Kedrov *et al* studied the binding of two related inhibitors, carboxy-atracyloside (CATR) and atracyloside (ATR), to ADP/ATP carriers. CATR and ATR differ by a single carboxylate group, which increases the affinity of CATR to the ADP/ATP carrier >10-fold [374]. SMFS experiments revealed that binding of both inhibitors takes place at the same location with similar strengths. However, interactions that stabilize transmembrane  $\alpha$ -helix H2 were more frequently detected in the CATR-bound state than in the ATR-inhibited state (53% vs 11%). Compared with ATR-binding, binding of CATR also increased the kinetic stability of transmembrane  $\alpha$ -helix H2 [322].

These examples demonstrate that SMFS can be exploited to detect subtle differences in the interactions established between a protein and a ligand or an inhibitor. Furthermore, differences in the binding mechanisms of closely related inhibitors can be revealed. Mapped to structural regions of the protein, these interactions can unravel mechanisms involved in ligand- and inhibitor-binding and functional activation of the membrane protein. In the future, more sensitive instrumentation will enable SMFS assays to provide more insights into the interaction mechanisms of membrane proteins with their binding partners.

### 6.3. How do interactions influence conformation?

The structure of proteins is governed by the inter- and intramolecular interactions set up during folding. Alterations in the interaction network of a membrane protein induced, for example, by ligand or inhibitor binding or (de-)protonation of functional groups can trigger conformational changes [232, 375].

Although SMFS and DFS can hardly be applied to solve protein structures, they allow us to describe the energy landscape and conformational entropy of the protein. The distance from the folded to the transition state estimates the width of the energy well. A broad energy well indicates larger conformational entropy of the protein. Accordingly, the folded protein can adopt more conformational sub-states than a folded structure stabilized by a narrow energy well.

The energy wells stabilizing the transmembrane  $\alpha$ -helices H5 and H6 of the ATR-bound mitochondrial ADP/ATP carrier Aac3 show an unusual high width of 21 Å and 15 Å, respectively. This indicates that both transmembrane  $\alpha$ -helices can adopt more conformational sub-states and exhibit an increased structural flexibility. Binding of CATR to the ADP/ATP carrier narrows the energy wells of transmembrane  $\alpha$ -helices H5 and H6 by  $\approx$ 4 Å and thus constrains their structural flexibility. The most confined transmembrane  $\alpha$ -helix H2 is directly involved in ATR- and CATR-binding to Aac3 [322]. Similarly, AP-binding inhibits NhaA and strongly restricts the conformational flexibility of transmembrane  $\alpha$ -helix IX [350]. These examples suggest that inhibitors tend to reduce the conformational flexibility of certain structural segments of membrane proteins, thus rendering them inactive.

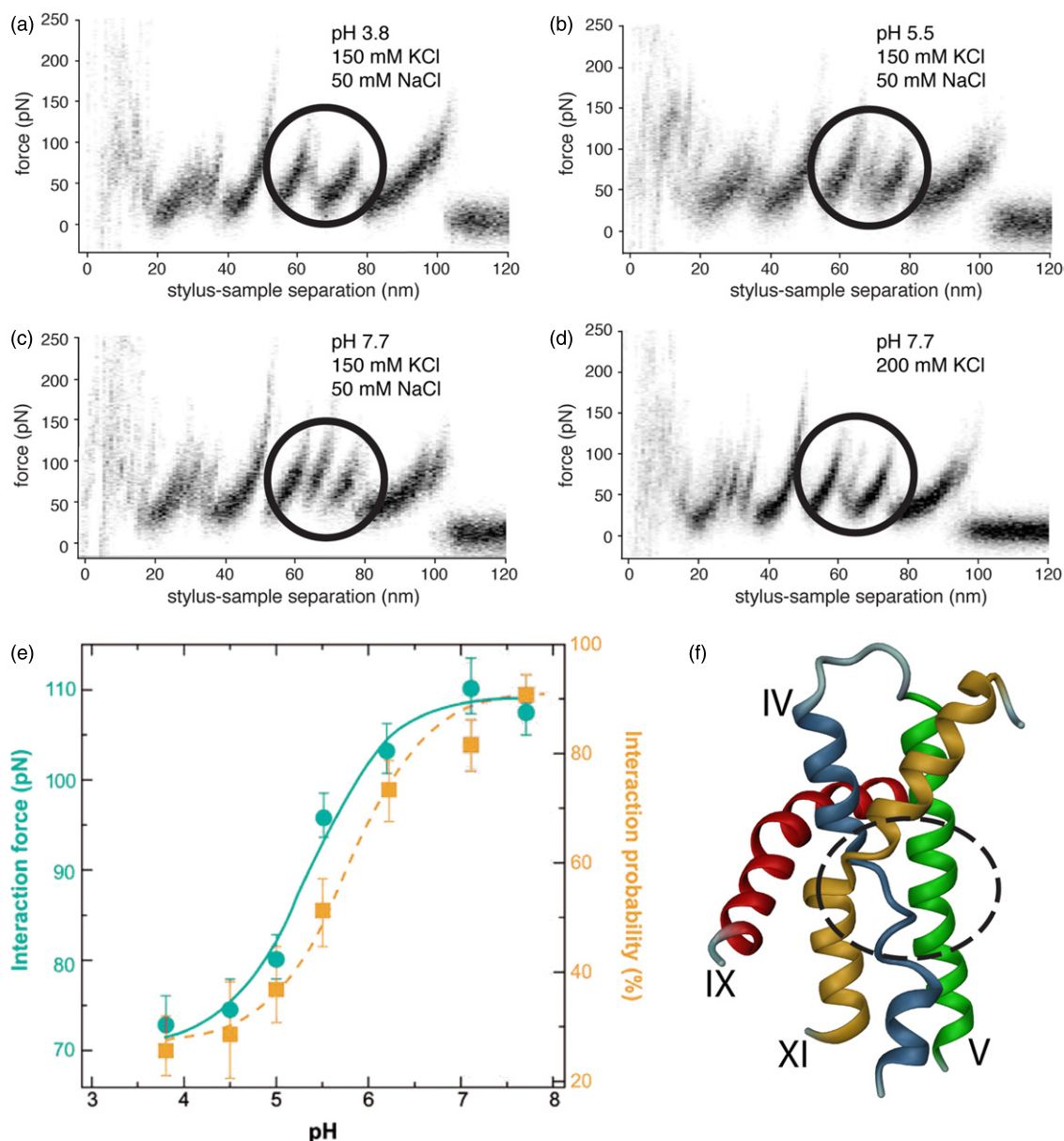


**Figure 17.**  $\text{Na}^+$ - and pH-dependent interactions within NhaA. Superimposition of 20 F–D curves recorded upon unfolding of single NhaA molecules at pH 3.8 (a), pH 5.5 (b) and pH 7.7 (c) in buffer solution containing 50 mM NaCl and 150 mM KCl. The pH-dependent peak (encircled) locates the interaction to the ligand-binding site. The superimposition of F–D curves recorded in the absence of the ligand ( $\text{Na}^+$ ) (d) shows that the molecular interaction at the ligand-binding site is reduced to that of inactive NhaA. (e) Strength and frequency of the interaction established at the ligand-binding site increase upon increasing pH from 5 to 6. The solid green and dashed orange lines represent sigmoid fits to the data points. (f) Cartoon locating the  $\text{Na}^+$ - and pH-dependent interactions at the ligand-binding site in transmembrane  $\alpha$ -helix V within the three-dimensional structure of NhaA.

In contrast to inhibitors that tend to trap a protein in an inactive conformation, natural ligands stimulate proteins to undergo functional conformational changes. In the absence of natural ligands, the amino acid antiporter SteT shows relatively narrow energy wells as judged by the  $x_u$  values ranging from 2.1 to 3.6 Å. In the presence of ligands, L-serine or L-threonine, the  $x_u$  values increased to 3.8–13.4 Å indicating a substantially enlarged flexibility of the antiporter [318]. During their functional cycle, antiporters switch between alternate conformations to sequentially expose ligand-binding sites to both faces of the membrane. However, in their unliganded state antiporters do not interconvert between the conformations

providing alternate access to the binding sites [226]. Thus, the increased flexibility in the liganded state reflects the increased probability of this state to interconvert [318]. Moreover, restricted conformations, as seen in the unliganded state of SteT, favor the specific binding of ligands [376].

#### 6.4. Quantifying how membrane proteins crosstalk

6.4.1. Cell-adhesion is a highly regulated process. Many membrane proteins are integrated into cellular networks that control and regulate their activity. Some membrane proteins are specialized in conveying adhesion to neighboring cells or

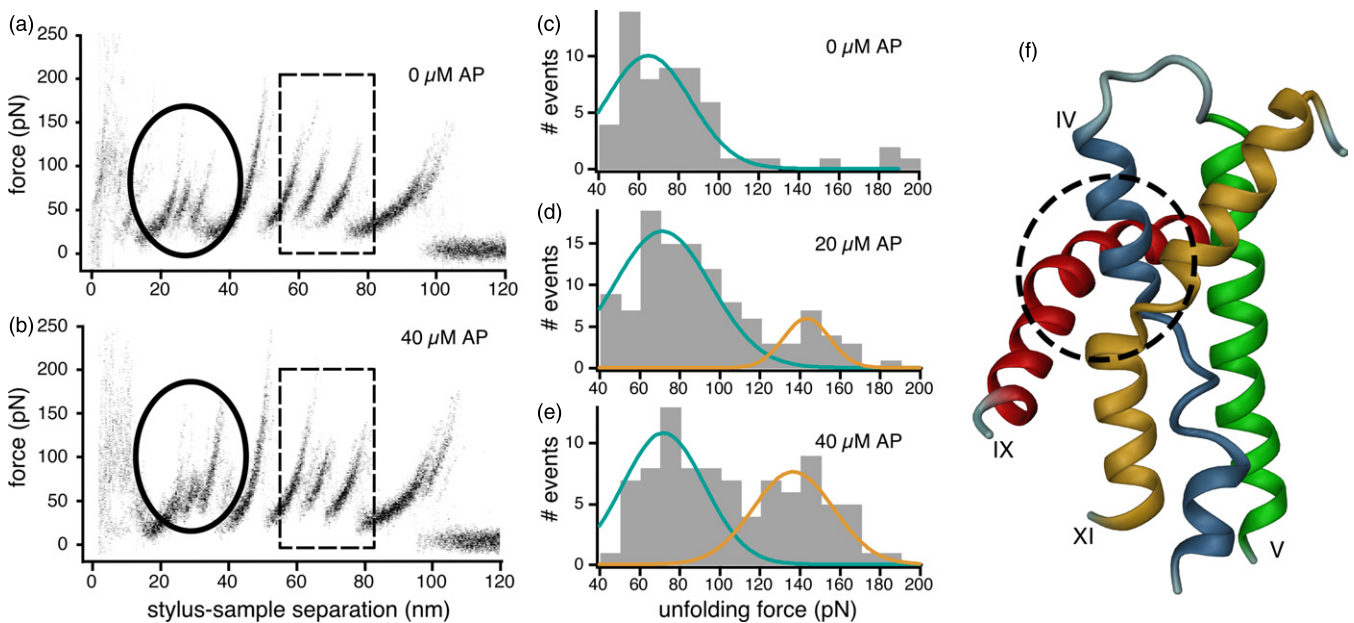


**Figure 18.** Inhibitor-binding changes interactions in NhaA. Superimposition of 20 F–D curves recorded upon unfolding of single NhaA in the absence (a) and the presence (b) of the inhibitor 2-aminoperimidine (AP). AP mimics the interactions established by the ligand ( $\text{Na}^+$ ) in transmembrane  $\alpha$ -helix V (boxed area) and locally increases the interactions in transmembrane  $\alpha$ -helix IX (encircled area). Distribution of unfolding forces detected at transmembrane  $\alpha$ -helix IX in the presence of 0 (c), 20 (d) and 40 (e)  $\mu\text{M}$  AP. Weak interactions were detected for free NhaA (green Gaussian fit) and enhanced interactions were observed for AP-inhibited NhaA (orange fit). Experiments were performed at pH 7.7 at which NhaA was not pH-inactivated. (f) Cartoon showing the location of the AP-enhanced interactions in transmembrane  $\alpha$ -helix IX within the three-dimensional structure of NhaA.

the extracellular matrix (ECM). Such CAM-mediated adhesive interactions play a crucial role in many biological processes and are tightly regulated [377, 378]. One way to control the adhesion to extracellular surfaces is to express a variety of different specialized CAMs. Integrins are the most important family of CAMs involved in adhesion to the ECM [377]. Composed of different  $\alpha$  and  $\beta$  subunits, integrins form 24 different heterodimers in mammals [379]. Because most integrins can bind to a set of ligands exposed by the ECM their binding specificity overlaps. *In vivo*, often several types of integrins are simultaneously expressed in a single cell. The complexity of the extracellular environment in living organisms asks for regulatory mechanisms to control the cell adhesion mediated by the different integrin receptors. Integrin crosstalk is another mechanism to regulate cell adhesion. In crosstalk, the binding of a ligand by one type of integrin regulates the behavior of a second type of integrin [377, 379, 380].

**6.4.2. sSCFS deciphers crosstalk of cell surface receptors.** SCFS quantifies the adhesion of a single cell at single receptor resolution [93]. Because the probing cell is alive, this approach allows us to detect how the adhesion of a receptor depends on the functional state of the cell. Recently, Friedrichs *et al* introduced a modified approach called stimulated SCFS (sSCFS) [216]. In sSCFS, cantilevers are functionalized with a component of the ECM (primary substrate, PS) to which HeLa cells adhere via integrin receptors. The cell is incubated on the cantilever to allow integrin-induced signaling cascades to take effect (figure 19(a)). Subsequently, adhesion of the cantilever-bound cell to a support coated with a

secondary substrate (SS) is probed. Control experiments probe the adhesion of the cell to the SS in the absence of any PS. The difference of both measurements reveals to what extent the PS modulates the binding of the cell to the SS. This approach disclosed a novel crosstalk between collagen I-binding integrin  $\alpha_1\beta_1$  and fibronectin-binding integrin  $\alpha_5\beta_1$  [216]. In particular, using collagen I as PS reduced the cellular adhesion to fibronectin coated SS (figure 19(b)). Interestingly, no differences in the adhesion strengths were observed when fibronectin was used as PS and collagen I as SS, indicating that the crosstalk is unidirectional. The  $\alpha_5\beta_1$ -mediated adhesion induced endocytosis of  $\alpha_1\beta_1$  [216].

In the future, sSCFS can be employed to unravel processes that regulate cell–substrate and cell–cell adhesion employing specific CAMs. Most importantly, this assay results in quantitative measurements of cell adhesion strengths.

### 6.5. Current limitations, challenges and perspectives

SMFS and SCFS provide information about the interactions that change the functional state of a protein or the interactions involved in regulatory signaling pathways. The integration of other techniques such as fluorescence microscopy or electrophysiological approaches into AFM-based force spectroscopy assays will open new horizons toward multifunctional characterization of both proteins and cells. Today, atomic force microscopes that are compatible with light microscopy are available. Yet, applications based on such combinations are still rare. One example is the analysis of focal adhesion structure by consecutive correlated AFM and fluorescence microscopy [381]. Other

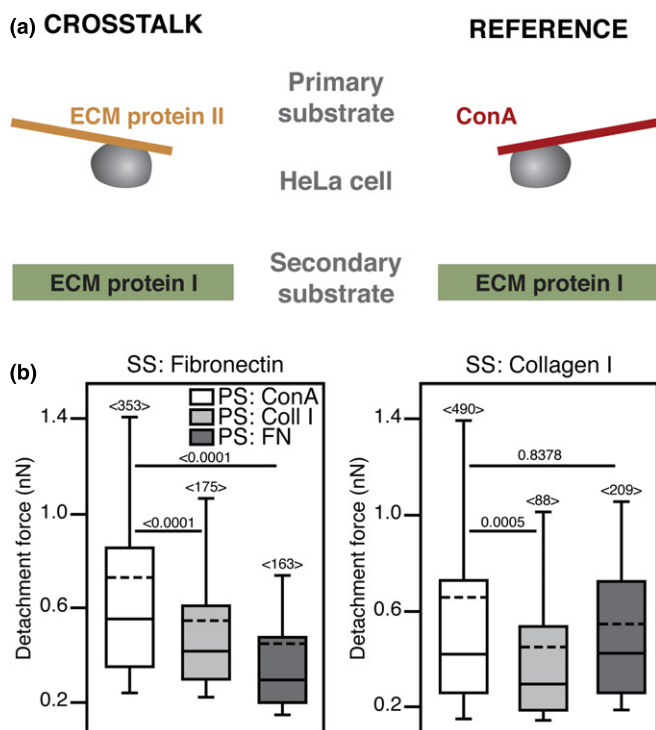


**Figure 19.** Stimulated SCFS (sSCFS) to quantify the crosstalk between cell adhesion receptors. (a) Experimental setup to detect integrin crosstalk. Cantilevers are either coated with ECM protein (left) or concavalin A (ConA, right) that serves as control as it does not induce signaling cascades [208]. ECM proteins allow specific attachment of HeLa cells to the atomic force microscope cantilever while ConA mediates non-specific attachment. SSs are ECM protein-coated supports. After firm attachment of HeLa cells to the functionalized cantilever, the adhesion to the SS is probed. (b) Adhesion strength of HeLa cells assayed by sSCFS. Box-whisker plots of peak forces required to detach HeLa cells from SS with respect to the PS (see legend in left plot; Coll I—collagen I; FN—fibronectin). Boxes and whiskers enclose 50% and 80% of the data points, respectively. Dashed and continuous black lines mark the mean and median. The number of analyzed F–D curves is given above the whiskers. Numbers between bars indicate significance  $p$ -values of Mann–Whitney tests.

examples combined AFM-based specific recognition imaging with fluorescence microscopy to localize membrane receptors *in vivo* [25]. In the future, sophisticated approaches such as single-molecule FRET [382, 383], confocal microscopy, or even super-resolution fluorescence microscopy [384, 385] will be increasingly combined with AFM-based methods. This will allow the characterization of dynamic processes in the cell membrane in real-time with high spatial resolution. The possibility to simultaneously manipulate and monitor complex biological systems offers new perspectives.

## 7. Conclusions and outlook

AFM-based methods become more and more valuable tools in membrane protein research. Performed under near-native conditions in buffer solution without the need for labeling or staining single membrane proteins can be imaged as they are,

embedded in their functionally important membrane bilayer. Although it can be quite challenging to extract membrane proteins from cells for AFM, the final sample preparation step for AFM imaging and spectroscopy is far less demanding than for other methods such as electron and x-ray crystallography. Nevertheless, improved sample preparation methods that mimic the native cellular environment of membrane proteins will be increasingly important and may become routinely available. Such improved native-like conditions will put AFM studies on membrane protein function, interaction and assembly forward. Other methods will enable integrated approaches combining AFM with other techniques.

For more than one decade, AFM imaging has been particularly successful in deciphering the stoichiometry of membrane protein complexes and of their supramolecular architecture. Even subtle function-related conformational changes in membrane proteins have been observed. With the advent of high-speed AFM imaging membrane proteins at much shorter time-scales became possible. Certainly, the current time-resolution of AFM imaging will improve further. Similarly, new AFM imaging modes will allow the extraction of additional biological, chemical and physical parameters characterizing the structure–function relationship of membrane proteins. Combined with high-resolution imaging, these insights will open ways to understand the structural and functional complexity of biological membranes. Multi-frequency dynamic AFM imaging modes build a first step toward such multifunctional imaging.

Due to the challenges set by the hydrophobicity of membrane proteins and their need to be exposed to the anisotropic bilayer environment, the investigation of membrane protein folding and stability is a rather unattended field. Most studies targeting this issue, however, employ model systems in which membrane proteins are exposed to an artificial, non-native environment. SMFS and DFS fill this gap. Membrane proteins embedded in their native membrane environment are probed by mechanical force. F–D traces record individual and common unfolding and refolding pathways of membrane proteins. Thorough analysis of F–D curves allows the assignment of unfolding and refolding intermediates as well as quantification and mapping of the interactions that stabilize these intermediates. These interactions can also be used to follow how interactions are established upon binding of ligands or inhibitors and thus functionally modulate the membrane protein. Characterizing the energy landscape of these interactions, DFS further increases our understanding of membrane protein folding, stability and function.

To put SMFS-based assays forward in the future, technological improvements increasing throughput and sensitivity will be required. First promising SMFS developments have been made to record equilibrium fluctuations at well-defined applied forces or peptide extensions. Thus, folding and refolding kinetics and energy landscape parameters could be determined at the same time. These approaches complement current models, which are based on non-equilibrium data, to reconstruct the free energy landscape.

## Acknowledgments

The authors thank S Kawamura, M Pfreundschuh and S Wegmann for critical reading of the manuscript. The ETH Zürich and the Deutsche Forschungsgemeinschaft (DFG) supported this work.

## References

- [1] Binnig G, Quate C F and Gerber C 1986 Atomic force microscope *Phys. Rev. Lett.* **56** 930
- [2] Gerber C and Lang H P 2006 How the doors to the nanoworld were opened *Nature Nanotechnol.* **1** 3–5
- [3] Muller D J 2008 AFM: a nanotool in membrane biology *Biochemistry* **47** 7986–98
- [4] Muller D J, Helenius J, Alsteens D and Dufrene Y F 2009 Force probing surfaces of living cells to molecular resolution *Nature Chem. Biol.* **5** 383–90
- [5] Israelachvili J N 2011 *Intermolecular and Surface Forces* 3rd edn (San Diego, CA: Academic)
- [6] Butt H-J 1992 Measuring local surface charge densities in electrolyte solutions with a scanning force microscope *Biophys. J.* **63** 578–82
- [7] Muller D J and Engel A 1997 The height of biomolecules measured with the atomic force microscope depends on electrostatic interactions *Biophys. J.* **73** 1633–44
- [8] Schabert F A and Engel A 1994 Reproducible acquisition of *Escherichia coli* porin surface topographs by atomic force microscopy *Biophys. J.* **67** 2394–3403
- [9] Muller D J, Fotiadis D, Scheuring S, Müller S A and Engel A 1999 Electrostatically balanced subnanometer imaging of biological specimens by atomic force microscope *Biophys. J.* **76** 1101–11
- [10] Moller C, Allen M, Elings V, Engel A and Muller D J 1999 Tapping-mode atomic force microscopy produces faithful high-resolution images of protein surfaces *Biophys. J.* **77** 1150–8
- [11] Olsen J D, Tucker J D, Timney J A, Qian P, Vassilev C and Hunter C N 2008 The organization of LH2 complexes in membranes from *Rhodobacter sphaeroides* *J. Biol. Chem.* **283** 30772–9
- [12] García R and Pérez R 2002 Dynamic atomic force microscopy methods *Surf. Sci. Rep.* **47** 197–301
- [13] Crittenden S, Raman A and Reifengerger R 2005 Probing attractive forces at the nanoscale using higher-harmonic dynamic force microscopy *Phys. Rev. B* **72** 235422
- [14] Gabai R, Segev L and Joselevich E 2005 Single polymer chains as specific transducers of molecular recognition in scanning probe microscopy *J. Am. Chem. Soc.* **127** 11390–8
- [15] Sahin O, Magonov S, Su C, Quate C F and Solgaard O 2007 An atomic force microscope tip designed to measure time-varying nanomechanical forces *Nature Nanotechnol.* **2** 507–14
- [16] Preiner J, Tang J, Pastushenko V and Hinterdorfer P 2007 Higher harmonic atomic force microscopy: imaging of biological membranes in liquid *Phys. Rev. Lett.* **99** 046102
- [17] Sahin O, Quate C F, Solgaard O and Atalar A 2004 Resonant harmonic response in tapping-mode atomic force microscopy *Phys. Rev. B* **69** 165416
- [18] Sugimoto Y, Innami S, Abe M, Culance O and Morita S 2007 Dynamic force spectroscopy using cantilever higher flexural modes *Appl. Phys. Lett.* **91** 093120
- [19] Proksch R 2006 Multifrequency, repulsive-mode amplitude-modulated atomic force microscopy *Appl. Phys. Lett.* **89** 113121
- [20] Lozano J R and Garcia R 2008 Theory of multifrequency atomic force microscopy *Phys. Rev. Lett.* **100** 076102
- [21] Jun Li Y, Takahashi K, Kobayashi N, Naitoh Y, Kageshima M and Sugawara Y 2010 Multifrequency high-speed phase-modulation atomic force microscopy in liquids *Ultramicroscopy* **110** 582–5
- [22] Basak S and Raman A 2007 Dynamics of tapping mode atomic force microscopy in liquids: theory and experiments *Appl. Phys. Lett.* **91** 064107
- [23] Patil S, Martinez N F, Lozano J R and Garcia R 2007 Force microscopy imaging of individual protein molecules with sub-pico newton force sensitivity *J. Mol. Recognit.* **20** 516–23
- [24] Dufrene Y and Hinterdorfer P 2008 Recent progress in AFM molecular recognition studies *Pflüg. Arch. Eur. J. Physiol.* **456** 237–45
- [25] Duman M *et al* 2010 Improved localization of cellular membrane receptors using combined fluorescence microscopy and simultaneous topography and recognition imaging *Nanotechnology* **21** 115504
- [26] Ahmad S, Chtcheglova L, Mayer B, Kuznetsov S and Hinterdorfer P 2010 Nanosensing of Fcγ receptors on macrophages *Anal. Bioanal. Chem.* **399** 2359–67
- [27] Tang J *et al* 2008 Recognition imaging and highly ordered molecular templating of bacterial S-layer nanoarrays containing affinity-tags *Nano Lett.* **8** 4312–9
- [28] Chtcheglova L A, Waschke J, Wildling L, Drenckhahn D and Hinterdorfer P 2007 Nano-scale dynamic recognition imaging on vascular endothelial cells *Biophys. J.* **93** L11–L3
- [29] Chtcheglova L, Atalar F, Ozbek U, Wildling L, Ebner A and Hinterdorfer P 2008 Localization of the ergtoxin-1 receptors on the voltage sensing domain of hERG K<sup>+</sup> channel by AFM recognition imaging *Pflüg. Arch. Eur. J. Physiol.* **456** 247–54
- [30] Jiang J, Hao X, Cai M, Shan Y, Shang X, Tang Z and Wang H 2009 Localization of Na<sup>+</sup>-K<sup>+</sup> ATPases in quasi-native cell membranes *Nano Lett.* **9** 4489–93
- [31] Giessibl F J 1995 Atomic resolution of the silicon (111)-(7 × 7) surface by atomic force microscopy *Science* **267** 68–71
- [32] Hoogenboom B W, Hug H J, Pellmont Y, Martin S, Frederix P L T M, Fotiadis D and Engel A 2006 Quantitative dynamic-mode scanning force microscopy in liquid *Appl. Phys. Lett.* **88** 193109
- [33] Hoogenboom B W, Suda K, Engel A and Fotiadis D 2007 The supramolecular assemblies of voltage-dependent anion channels in the native membrane *J. Mol. Biol.* **370** 246–55
- [34] Butt H-J, Siedle P, Seifert K, Fendler K, Seeger T, Bamberg E, Weisenhorn A L, Goldie K and Engel A 1993 Scan speed limit in atomic force microscopy *J. Microsc.* **169** 75–84
- [35] Viani M B *et al* 1999 Fast imaging and fast force spectroscopy of single biopolymers with a new atomic force microscope designed for small cantilevers *Rev. Sci. Instrum.* **70** 4300–3
- [36] Schitter G, Stark R W and Stemmer A 2004 Fast contact-mode atomic force microscopy on biological specimen by model-based control *Ultramicroscopy* **100** 253–7
- [37] Mahmood I A and Moheimani S O R 2009 Making a commercial atomic force microscope more accurate and faster using positive position feedback control *Rev. Sci. Instrum.* **80** 063705
- [38] Zhou Y, Shang G, Cai W and Yao J-E 2010 Cantilevered bimorph-based scanner for high speed atomic force microscopy with large scanning range *Rev. Sci. Instrum.* **81** 053708
- [39] Yan Y, Wu Y, Zou Q and Su C 2008 An integrated approach to piezoactuator positioning in high-speed atomic force microscope imaging *Rev. Sci. Instrum.* **79** 073704

- [40] Schitter G, Astrom K J, Demartini B E, Thurner P J, Turner K L and Hansma P K 2007 Design and modeling of a high-speed AFM-scanner *IEEE Trans. Contr. Sys.* **15** 906–15
- [41] Schitter G, Astrom K J, Demartini B, Fantner G E, Turner K, Thurner P J and Hansma P K 2006 Design and modeling of a high-speed scanner for atomic force microscopy *Proc. 2006 Am. Control Conf. (Minneapolis, MN, 14–16 June 2006)* vols 1–12, pp 502–7
- [42] Humphris A D L, Miles M J and Hobbs J K 2005 A mechanical microscope: high-speed atomic force microscopy *Appl. Phys. Lett.* **86** 034106
- [43] Humphris A D L, Hobbs J K and Miles M J 2003 Ultrahigh-speed scanning near-field optical microscopy capable of over 100 frames per second *Appl. Phys. Lett.* **83** 6–8
- [44] Picco L M, Bozec L, Ulcinas A, Engledew D J, Antognozzi M, Horton M A and Miles M J 2007 Breaking the speed limit with atomic force microscopy *Nanotechnology* **18** 044030
- [45] Fantner G E *et al* 2006 Components for high speed atomic force microscopy *Ultramicroscopy* **106** 881–7
- [46] Kindt J H, Fantner G E, Cutroni J A and Hansma P K 2004 Rigid design of fast scanning probe microscopes using finite element analysis *Ultramicroscopy* **100** 259–65
- [47] Fantner G E, Hegarty P, Kindt J H, Schitter G, Cidade G A G and Hansma P K 2005 Data acquisition system for high speed atomic force microscopy *Rev. Sci. Instrum.* **76** 026118
- [48] Hansma P K, Schitter G, Fantner G E and Prater C 2006 Applied physics—high-speed atomic force microscopy *Science* **314** 601–2
- [49] Ando T, Kodera N, Takai E, Maruyama D, Saito K and Toda A 2001 A high-speed atomic force microscope for studying biological macromolecules *Proc. Natl Acad. Sci. USA* **98** 12468–72
- [50] Ando T, Uchihashi T and Fukuma T 2008 High-speed atomic force microscopy for nano-visualization of dynamic biomolecular processes *Prog. Surf. Sci.* **83** 337–437
- [51] Yamamoto D, Uchihashi T, Kodera N and Ando T 2008 Anisotropic diffusion of point defects in a two-dimensional crystal of streptavidin observed by high-speed atomic force microscopy *Nanotechnology* **19** 384009
- [52] Kodera N, Yamamoto D, Ishikawa R and Ando T 2010 Video imaging of walking myosin V by high-speed atomic force microscopy *Nature* **468** 72–6
- [53] Yamashita H, Voitchovsky K, Uchihashi T, Contera S A, Ryan J F and Ando T 2009 Dynamics of bacteriorhodopsin 2D crystal observed by high-speed atomic force microscopy *J. Struct. Biol.* **167** 153–8
- [54] Shibata M, Yamashita H, Uchihashi T, Kandori H and Ando T 2010 High-speed atomic force microscopy shows dynamic molecular processes in photoactivated bacteriorhodopsin *Nature Nanotechnol.* **5** 208–12
- [55] Muller D J, Sass H-J, Muller S A, Büldt G and Engel A 1999 Surface structures of native bacteriorhodopsin depend on the molecular packing arrangement in the membrane *J. Mol. Biol.* **285** 1903–9
- [56] Beyder A and Sachs F 2006 Microfabricated torsion levers optimized for low force and high-frequency operation in fluids *Ultramicroscopy* **106** 838–46
- [57] Benoit M, Gabriel D, Gerisch G and Gaub H E 2000 Discrete interactions in cell adhesion measured by single-molecule force spectroscopy *Nature Cell Biol.* **2** 313–7
- [58] Moy V, Florin E and Gaub H 1994 Intermolecular forces and energies between ligands and receptors *Science* **266** 257–9
- [59] Dufre ne Y F 2009 Atomic force microscopy: a powerful molecular toolkit in nanoproteomics *Proteomics* **9** 5400–5
- [60] Alsteens D, Dague E, Verbelen C, Andre G, Dupres V and Dufre ne Y F 2009 Nanoscale imaging of microbial pathogens using atomic force microscopy *WIREs Nanomed. Nanobiotechnol.* **1** 168–80
- [61] Sukharev S and Corey D P 2004 Mechanosensitive channels: multiplicity of families and gating paradigms *Sci. STKE* **2004** re4
- [62] Gillespie P G and M ller U 2009 Mechanotransduction by hair cells: models, molecules, and mechanisms *Cell* **139** 33–44
- [63] Vogel V 2006 Mechanotransduction involving multimodular proteins: converting force into biochemical signals *Annu. Rev. Biophys. Biomol. Struct.* **35** 459–88
- [64] Lee G, Abdi K, Jiang Y, Michaely P, Bennett V and Marszalek P E 2006 Nanospring behaviour of ankyrin repeats *Nature* **440** 246–9
- [65] Moffitt J R, Chemla Y R, Smith S B and Bustamante C 2008 Recent advances in optical tweezers *Annu. Rev. Biochem.* **77** 205–28
- [66] Kedrov A, Wegmann S, Smits S H J, Goswami P, Baumann H and Muller D J 2007 Detecting molecular interactions that stabilize, activate and guide ligand-binding of the sodium/proton antiporter MjNhaP1 from *Methanococcus jannaschii*. *J. Struct. Biol.* **159** 290–301
- [67] Kedrov A, Ziegler C, Janovjak H, K hlbrandt W and Muller D J 2004 Controlled unfolding and refolding of a single sodium-proton antiporter using atomic force microscopy *J. Mol. Biol.* **340** 1143–52
- [68] Oesterhelt F, Oesterhelt D, Pfeiffer M, Engel A, Gaub H E and Muller D J 2000 Unfolding pathways of individual bacteriorhodopsins *Science* **288** 143–6
- [69] Cisneros D A, Oesterhelt D and Muller D J 2005 Probing origins of molecular interactions stabilizing the membrane proteins halorhodopsin and bacteriorhodopsin *Structure* **13** 235–42
- [70] Howard J 2001 *Mechanics of Motor Proteins and the Cytoskeleton* (Sunderland, MA: Sinauer Associates)
- [71] Rief M, Gautel M, Oesterhelt F, Fernandez J M and Gaub H E 1997 Reversible unfolding of individual titin immunoglobulin domains by AFM *Science* **276** 1109–12
- [72] Rief M, Oesterhelt F, Heymann B and Gaub H E 1997 Single molecule force spectroscopy on polysaccharides by atomic force microscopy *Science* **275** 1295–7
- [73] Bustamante C, Marko J F, Siggia E D and Smith S 1994 Entropic elasticity of lambda-phage DNA *Science* **265** 1599–600
- [74] Clausen-Schaumann H, Seitz M, Krautbauer R and Gaub H E 2000 Force spectroscopy with single bio-molecules *Curr. Opin. Chem. Biol.* **4** 524–30
- [75] Cui Y and Bustamante C 2000 Pulling a single chromatin fiber reveals the forces that maintain its higher-order structure *Proc. Natl Acad. Sci. USA* **97** 127–32
- [76] Oesterhelt F, Rief M and Gaub H E 1999 Single molecule force spectroscopy by AFM indicates helical structure of poly(ethylene-glycol) in water *New J. Phys.* **1** 6
- [77] Yasumura K Y, Stowe T D, Chow E M, Pfaffman T, Kenny T W, Stipe B C and Rugar D 2000 Quality factors in micron- and submicron-thick cantilevers *J. Microelectromech. Syst.* **9** 117–25
- [78] Kratky O and Porod G 1949 R ntgenuntersuchung gel ster Fadenmolek le *Rec. Trav. Chim. Pays-Bas.* **68** 1106–22
- [79] Marko J F and Siggia E D 1995 Stretching DNA *Macromolecules* **28** 8759–70
- [80] Smith S B, Finzi L and Bustamante C 1992 Direct mechanical measurements of the elasticity of single DNA molecules by using magnetic beads *Science* **258** 1122–6
- [81] Bell G I 1978 Models for the specific adhesion of cells to cells *Science* **200** 618–27

- [82] Evans E 2001 Probing the relation between force-lifetime and chemistry in single molecular bonds *Annu. Rev. Biophys. Biomol. Struct.* **30** 105–28
- [83] Evans E and Ritchie K 1997 Dynamic strength of molecular adhesion bonds *Biophys. J.* **72** 1541–55
- [84] Evans E 1999 Energy landscapes of biomolecular adhesion and receptor anchoring at interfaces explored with dynamic force spectroscopy *Faraday Discuss.* **111** 1–16
- [85] Dill K A, Bromberg S, Yue K, Chan H S, Ftebig K M, Yee D P and Thomas P D 2008 Principles of protein folding—a perspective from simple exact models *Protein Sci.* **4** 561–602
- [86] Dill K A and Chan H S 1997 From Levinthal to pathways to funnels *Nature Struct. Biol.* **4** 10–9
- [87] Dill K 1999 Polymer principles and protein folding *Protein Sci.* **8** 1166–80
- [88] Onuchic J N, Wolynes P G, Luthey-Schulten Z and Socci N D 1995 Toward an outline of the topography of a realistic protein-folding funnel *Proc. Natl Acad. Sci. USA* **92** 3626–30
- [89] Merkel R, Nassoy P, Leung A, Ritchie K and Evans E 1999 Energy landscapes of receptor–ligand bonds explored with dynamic force spectroscopy *Nature* **397** 50–3
- [90] Kemler R 1992 Classical cadherins *Sem. Cell Biol.* **3** 149–55
- [91] Kaplanski G, Farnarier C, Tissot O, Pierres A, Benoliel A M, Alessi M C, Kaplanski S and Bongrand P 1993 Granulocyte-endothelium initial adhesion. Analysis of transient binding events mediated by E-selectin in a laminar shear flow *Biophys. J.* **64** 1922–33
- [92] Garcia A J, Ducheyne P and Boettiger D 1997 Quantification of cell adhesion using a spinning disc device and application to surface-reactive materials *Biomaterials* **18** 1091–8
- [93] Helenius J, Heisenberg C-P, Gaub H E and Muller D J 2008 Single-cell force spectroscopy *J. Cell Sci.* **121** 1785–91
- [94] Sun M, Graham J S, Hegedüs B, Marga F, Zhang Y, Forgacs G and Grandbois M 2005 Multiple membrane tethers probed by atomic force microscopy *Biophys. J.* **89** 4320–9
- [95] Krieg M, Helenius J, Heisenberg C P and Muller D J 2008 A bond for a lifetime: employing membrane nanotubes from living cells to determine receptor–ligand kinetics *Angew. Chem. Int. Edn Engl.* **47** 9775–7
- [96] Viani M B, Schaffer T E, Chand A, Rief M, Gaub H E and Hansma P K 1999 Small cantilevers for force spectroscopy of single molecules *J. Appl. Phys.* **86** 2258–62
- [97] Alcaraz J, Buscemi L, Puig-De-Morales M, Colchero J, Baró A and Navajas D 2002 Correction of microrheological measurements of soft samples with atomic force microscopy for the hydrodynamic drag on the cantilever *Langmuir* **18** 716–21
- [98] Janovjak H, Struckmeier J and Muller D J 2005 Hydrodynamic effects in fast AFM single-molecule force measurements *Eur. Biophys. J.* **34** 91–6
- [99] Schlierf M and Rief M 2005 Temperature softening of a protein in single-molecule experiments *J. Mol. Biol.* **354** 497–503
- [100] Junker J P, Ziegler F and Rief M 2009 Ligand-dependent equilibrium fluctuations of single calmodulin molecules *Science* **323** 633–7
- [101] Bullard B, Garcia T, Benes V, Leake M C, Linke W A and Oberhauser A F 2006 The molecular elasticity of the insect flight muscle proteins projectin and kettin *Proc. Natl Acad. Sci. USA* **103** 4451–6
- [102] King G M, Carter A R, Churnside A B, Eberle L S and Perkins T T 2009 Ultrastable atomic force microscopy: atomic-scale stability and registration in ambient conditions *Nano Lett.* **9** 1451–6
- [103] Struckmeier J, Wahl R, Leuschner M, Nunes J, Janovjak H, Geisler U, Hofmann G, Jahnke T and Muller D J 2008 Fully automated single-molecule force spectroscopy for screening applications *Nanotechnology* **19** 384020
- [104] Bosshart P D, Casagrande F, Frederix P L T M, Ratera M, Bippes C A, Muller D J, Palacin M, Engel A and Fotiadis D 2008 High-throughput single-molecule force spectroscopy for membrane proteins *Nanotechnology* **19** 384014
- [105] Kuhn M, Janovjak H, Hubain M and Muller D J 2005 Automated alignment and pattern recognition of single-molecule force spectroscopy data *J. Microsc.* **218** 125–32
- [106] Marsico A, Labudde D, Sapra T, Muller D J and Schroeder M 2007 A novel pattern recognition algorithm to classify membrane protein unfolding pathways with high-throughput single-molecule force spectroscopy *Bioinformatics* **23** e231–6
- [107] Mueller F, Muller D J and Labudde D 2006 Analysis assistant for single-molecule force spectroscopy data on membrane proteins—MPTV *Bioinformatics* **22** 1796–9
- [108] Aioanei D, Brucale M and Samori B 2011 Open source platform for the execution and analysis of mechanical refolding experiments *Bioinformatics* **27** 423–5
- [109] Sandal M, Benedetti F, Brucale M, Gomez-Casado A and Samori B 2009 Hooke: an open software platform for force spectroscopy *Bioinformatics* **25** 1428–30
- [110] van Meer G, Voelker D R and Feigenson G W 2008 Membrane lipids: where they are and how they behave *Nature Rev. Mol. Cell Biol.* **9** 112–24
- [111] Shevchenko A and Simons K 2010 Lipidomics: coming to grips with lipid diversity *Nature Rev. Mol. Cell Biol.* **11** 593–8
- [112] Rothman J E and Lenard J 1977 Membrane asymmetry *Science* **195** 743–53
- [113] Wiener M C and White S H 1992 Structure of a fluid dioleoylphosphatidylcholine bilayer determined by joint refinement of x-ray and neutron diffraction data: III. Complete structure *Biophys. J.* **61** 434–47
- [114] Oesterhelt D and Stoeckenius W 1974 Isolation of the cell membrane of *Halobacterium halobium* and its fractionation into red and purple membrane *Methods in Enzymology* ed L P Sidney Fleischer (New York: Academic) pp 667–78
- [115] Lal R, John S A, Laird D W and Arnsdorf M F 1995 Heart gap junction preparations reveal hemiplaques by atomic force microscopy *Am. J. Physiol. Cell Physiol.* **268** C968–77
- [116] Muller D J, Hand G M, Engel A and Sosinsky G E 2002 Conformational changes in surface structures of isolated connexin 26 gap junctions *EMBO J.* **21** 3598–607
- [117] Fotiadis D, Liang Y, Filipek S, Saperstein D A, Engel A and Palczewski K 2003 Atomic-force microscopy: rhodopsin dimers in native disc membranes *Nature* **421** 127–8
- [118] Scheuring S, Seguin J, Marco S, Lévy D, Robert B and Rigaud J-L 2003 Nanodissection and high-resolution imaging of the *Rhodospseudomonas viridis* photosynthetic core complex in native membranes by AFM *Proc. Natl Acad. Sci. USA* **100** 1690–3
- [119] Buzhynskyy N, Hite R K, Walz T and Scheuring S 2006 The supramolecular architecture of junctional microdomains in native lens membranes *EMBO Rep.* **8** 51–5
- [120] Bogdanov M, Mileykovskaya E and Dowhan W 2008 Lipids in the assembly of membrane proteins and organization of protein supercomplexes: implications for lipid-linked disorders *Subcell. Biochem.* **49** 197–239
- [121] Lee A G 2004 How lipids affect the activities of integral membrane proteins *Biochim. Biophys. Acta Biomembr.* **1666** 62–87

- [122] Opekarová M and Tanner W 2003 Specific lipid requirements of membrane proteins—a putative bottleneck in heterologous expression *Biochim. Biophys. Acta Biomembr.* **1610** 11–22
- [123] Muller D J, Amrein M and Engel A 1997 Adsorption of biological molecules to a solid support for scanning probe microscopy *J. Struct. Biol.* **119** 172–88
- [124] Cisneros D A, Muller D J, Daud S M and Lakey J H 2006 An approach to prepare membrane proteins for single-molecule imaging *Angew. Chem. Int. Edn Engl.* **45** 3252–6
- [125] Muller D J and Engel A 1999 Voltage and pH-induced channel closure of porin OmpF visualized by atomic force microscopy *J. Mol. Biol.* **285** 1347–51
- [126] Karrasch S, Dolder M, Schabert F, Ramsden J and Engel A 1993 Covalent binding of biological samples to solid supports for scanning probe microscopy in buffer solution *Biophys. J.* **65** 2437–46
- [127] Karrasch S, Hegerl R, Hoh J H, Baumeister W and Engel A 1994 Atomic force microscopy produces faithful high-resolution images of protein surfaces in an aqueous environment *Proc. Natl Acad. Sci. USA* **91** 836–8
- [128] Guthold M *et al* 1999 Direct observation of one-dimensional diffusion and transcription by *Escherichia coli* RNA polymerase *Biophys. J.* **77** 2284–94
- [129] Sackmann E 1996 Supported membranes: scientific and practical applications *Science* **271** 43–8
- [130] Muller D J, Engel A, Matthey U, Meier T, Dimroth P and Suda K 2003 Observing membrane protein diffusion at subnanometer resolution *J. Mol. Biol.* **327** 925–30
- [131] Hemmersam A G, Foss M, Chevallier J and Besenbacher F 2005 Adsorption of fibrinogen on tantalum oxide, titanium oxide and gold studied by the QCM-D technique *Colloids Surf. B* **43** 208–15
- [132] Agnihotri A and Siedlecki C A 2004 Time-dependent conformational changes in fibrinogen measured by atomic force microscopy *Langmuir* **20** 8846–52
- [133] Svaldo-Lanero T, Penco A, Prato M, Canepa M, Rolandi R and Cavalleri O 2008 Nanopatterning by protein unfolding *Soft Matter* **4** 965–7
- [134] Engel M F M, Visser A J W G and van Mierlo C P M 2004 Conformation and orientation of a protein folding intermediate trapped by adsorption *Proc. Natl Acad. Sci. USA* **101** 11316–21
- [135] Brewer S H, Glomm W R, Johnson M C, Knag M K and Franzen S 2005 Probing BSA binding to citrate-coated gold nanoparticles and surfaces *Langmuir* **21** 9303–7
- [136] Shimizu M, Kobayashi K, Morii H, Mitsui K, Knoll W and Nagamune T 2003 Secondary structure analyses of protein films on gold surfaces by circular dichroism *Biochem. Biophys. Res. Commun.* **310** 606–11
- [137] Hasler L, Heymann J B, Engel A, Kistler J and Walz T 1998 2D crystallization of membrane proteins: rationales and examples *J. Struct. Biol.* **121** 162–71
- [138] Stahlberg H, Fotiadis D, Scheuring S, Rémy H, Braun T, Mitsuoka K, Fujiyoshi Y and Engel A 2001 Two-dimensional crystals: a powerful approach to assess structure, function and dynamics of membrane proteins *FEBS Lett.* **504** 166–72
- [139] Milhiet P-E, Gubellini F, Berquand A, Dosset P, Rigaud J-L, Le Grimellec C and Lèvy D 2006 High-resolution AFM of membrane proteins directly incorporated at high density in planar lipid bilayer *Biophys. J.* **91** 3268–75
- [140] Rigaud J L 2002 Membrane proteins: functional and structural studies using reconstituted proteoliposomes and 2-D crystals *Braz. J. Med. Biol. Res.* **35** 753–66
- [141] Seddon A M, Curnow P and Booth P J 2004 Membrane proteins, lipids and detergents: not just a soap opera *Biochim. Biophys. Acta Biomembr.* **1666** 105–17
- [142] Salafsky J, Groves J T and Boxer S G 1996 Architecture and function of membrane proteins in planar supported bilayers: a study with photosynthetic reaction centers *Biochemistry* **35** 14773–81
- [143] Tanaka M and Sackmann E 2005 Polymer-supported membranes as models of the cell surface *Nature* **437** 656–63
- [144] Knotts T A IV, Rathore N and De Pablo J J 2008 An entropic perspective of protein stability on surfaces *Biophys. J.* **94** 4473–83
- [145] Friedel M, Baumketner A and Shea J-E 2007 Stability of a protein tethered to a surface *J. Chem. Phys.* **126** 095101
- [146] Knotts IV T A, Rathore N and De Pablo J J 2005 Structure and stability of a model three-helix-bundle protein on tailored surfaces *Proteins: Struct. Funct. Bioinf.* **61** 385–97
- [147] Wei S and Knotts IV T A 2010 Predicting stability of alpha-helical, orthogonal-bundle proteins on surfaces *J. Chem. Phys.* **133** 115102
- [148] Sinner E-K and Knoll W 2001 Functional tethered membranes *Curr. Opin. Chem. Biol.* **5** 705–11
- [149] Kufer S K, Dietz H, Albrecht C, Blank K, Kardinal A, Rief M and Gaub H E 2005 Covalent immobilization of recombinant fusion proteins with hAGT for single molecule force spectroscopy *Eur. Biophys. J.* **35** 72–8
- [150] Ebner A *et al* 2007 A new, simple method for linking of antibodies to atomic force microscopy tips *Bioconjug. Chem.* **18** 1176–84
- [151] Hinterdorfer P and Dufrene Y F 2006 Detection and localization of single molecular recognition events using atomic force microscopy *Nature Methods* **3** 347–55
- [152] Zimmermann J L, Nicolaus T, Neuert G and Blank K 2010 Thiol-based, site-specific and covalent immobilization of biomolecules for single-molecule experiments *Nature Protoc.* **5** 975–85
- [153] Friedel M, Baumketner A and Shea J-E 2006 Effects of surface tethering on protein folding mechanisms *Proc. Natl Acad. Sci. USA* **103** 8396–401
- [154] Rigler P, Ulrich W-P and Vogel H 2004 Controlled immobilization of membrane proteins to surfaces for fourier transform infrared investigations *Langmuir* **20** 7901–3
- [155] Tinazli A, Tang J, Valiokas R, Picuric S, Lata S, Piehler J, Liedberg B and Tampé R 2005 High-affinity chelator thiols for switchable and oriented immobilization of histidine-tagged proteins: a generic platform for protein chip technologies *Chem.—Eur. J.* **11** 5249–59
- [156] Rädler U, Mack J, Persike N, Jung G and Tampé R 2000 Design of supported membranes tethered via metal-affinity ligand–receptor pairs *Biophys. J.* **79** 3144–52
- [157] Giess F, Friedrich M G, Heberle J, Naumann R L and Knoll W 2004 The protein–tethered lipid bilayer: a novel mimic of the biological membrane *Biophys. J.* **87** 3213–20
- [158] Cornell B A, Braach-Maksvytis V L B, King L G, Osman P D J, Raguse B, Wiczorek L and Pace R J 1997 A biosensor that uses ion-channel switches *Nature* **387** 580–3
- [159] Hegner M, Wagner P and Semenza G 1993 Ultralarge atomically flat template-stripped Au surfaces for scanning probe microscopy *Surf. Sci.* **291** 39–46
- [160] Terrettaz S, Ulrich W-P, Vogel H, Hong Q, Dover L G and Lakey J H 2002 Stable self-assembly of a protein engineering scaffold on gold surfaces *Protein Sci.* **11** 1917–25
- [161] Knoll W, Frank C W, Heibel C, Naumann R, Offenhausser A, Ruhe J, Schmidt E K, Shen W W and Sinner A 2000 Functional tethered lipid bilayers *J. Biotechnol.* **74** 137–58
- [162] Zebrowska A and Krysinski P 2004 Incorporation of Na<sup>+</sup>,K<sup>+</sup>-ATP-ase into the thiolipid biomimetic assemblies via the fusion of proteoliposomes *Langmuir* **20** 11127–33

- [163] He L, Robertson J W, Li J, Karcher I, Schiller S M, Knoll W and Naumann R 2005 Tethered bilayer lipid membranes based on monolayers of thiolipids mixed with a complementary dilution molecule: I. Incorporation of channel peptides *Langmuir* **21** 11666–72
- [164] Purruicker O, Förtig A, Jordan R and Tanaka M 2004 Supported membranes with well-defined polymer tethers—incorporation of cell receptors *ChemPhysChem* **5** 327–35
- [165] Wagner M L and Tamm L K 2000 Tethered polymer-supported planar lipid bilayers for reconstitution of integral membrane proteins: silane-polyethyleneglycol-lipid as a cushion and covalent linker *Biophys. J.* **79** 1400–14
- [166] Lang H, Duschl C and Vogel H 1994 A new class of thiolipids for the attachment of lipid bilayers on gold surfaces *Langmuir* **10** 197–210
- [167] Schiller S M, Naumann R, Lovejoy K, Kunz H and Knoll W 2003 Archaea analogue thiolipids for tethered bilayer lipid membranes on ultrasmooth gold surfaces *Angew. Chem. Int. Edn Engl.* **42** 208–11
- [168] Bunjes N, Schmidt E K, Jonczyk A, Rippmann F, Beyer D, Ringsdorf H, Gräber P, Knoll W and Naumann R 1997 Thiopeptide-supported lipid layers on solid substrates *Langmuir* **13** 6188–94
- [169] Seitz P C, Reif M D, Kononov O V, Jordan R and Tanaka M 2009 Modulation of substrate–membrane interactions by linear poly(2-methyl-2-oxazoline) spacers revealed by x-ray reflectivity and ellipsometry *ChemPhysChem* **10** 2876–83
- [170] Sinner E-K, Reuning U, Kök F N, Saccà B, Moroder L, Knoll W and Oesterhelt D 2004 Incorporation of integrins into artificial planar lipid membranes: characterization by plasmon-enhanced fluorescence spectroscopy *Anal. Biochem.* **333** 216–24
- [171] Robelek R, Lemker E, Wiltschi B, Kirste V, Naumann R, Oesterhelt D and Sinner E K 2007 Incorporation of *in vitro* synthesized GPCR into a tethered artificial lipid membrane system *Angew. Chem. Int. Edn Engl.* **46** 605–8
- [172] Sackmann E and Bruinsma R F 2002 Cell adhesion as wetting transition? *ChemPhysChem* **3** 262–9
- [173] Goennenwein S, Tanaka M, Hu B, Moroder L and Sackmann E 2003 Functional incorporation of integrins into solid supported membranes on ultrathin films of cellulose: impact on adhesion *Biophys. J.* **85** 646–55
- [174] Marshall B T, Sarangapani K K, Wu J, Lawrence M B, McEver R P and Zhu C 2005 Measuring molecular elasticity by atomic force microscope cantilever fluctuations *Biophys. J.* **90** 681–92
- [175] Smith E A, Coym J W, Cowell S M, Tokimoto T, Hruby V J, Yamamura H I and Wirth M J 2005 Lipid bilayers on polyacrylamide brushes for inclusion of membrane proteins *Langmuir* **21** 9644–50
- [176] Jimenez J, Heim A J II, Matthews W G and Alcantar N 2006 Construction and characterization of soft-supported lipid bilayer membranes for biosensors application *Conf. Proc. IEEE Eng. Med. Biol. Soc.* **1** 4119–22
- [177] Renner L, Osaki T, Chiantia S, Schwille P, Pompe T and Werner C 2008 Supported lipid bilayers on spacious and pH-responsive polymer cushions with varied hydrophilicity *J. Phys. Chem. B* **112** 6373–8
- [178] Lee D-C, Chang B-J, Yu L, Frey S L, Lee K Y C, Patchipulusu S and Hall C 2004 Polymer cushions functionalized with lipid molecules *Langmuir* **20** 11297–300
- [179] Hillebrandt H, Wiegand G, Tanaka M and Sackmann E 1999 High electric resistance polymer/lipid composite films on indium-tin-oxide electrodes *Langmuir* **15** 8451–9
- [180] Elender G, Kuhner M and Sackmann E 1996 Functionalisation of Si/SiO<sub>2</sub> and glass surfaces with ultrathin dextran films and deposition of lipid bilayers *Biosensors Bioelectron.* **11** 565–77
- [181] Drexler J and Steinem C 2003 Pore-suspending lipid bilayers on porous alumina investigated by electrical impedance spectroscopy *J. Phys. Chem. B* **107** 11245–54
- [182] Favero G, Campanella L, Cavallo S, D'Annibale A, Perrella M, Mattei E and Ferri T 2005 Glutamate receptor incorporated in a mixed hybrid bilayer lipid membrane array, as a sensing element of a biosensor working under flowing conditions *J. Am. Chem. Soc.* **127** 8103–11
- [183] Hemmler R, Böse G, Wagner R and Peters R 2005 Nanopore unitary permeability measured by electrochemical and optical single transporter recording *Biophys. J.* **88** 4000–7
- [184] Hennesthal C, Drexler J and Steinem C 2002 Membrane-suspended nanocompartments based on ordered pores in alumina *ChemPhysChem* **3** 885–9
- [185] Hennesthal C and Steinem C 2000 Pore-spanning lipid bilayers visualized by scanning force microscopy *J. Am. Chem. Soc.* **122** 8085–6
- [186] Storm A J, Chen J H, Ling X S, Zandbergen H W and Dekker C 2003 Fabrication of solid-state nanopores with single-nanometre precision *Nature Mater.* **2** 537–40
- [187] Danelon C, Santschi C, Brugger J and Vogel H 2006 Fabrication and functionalization of nanochannels by electron-beam-induced silicon oxide deposition *Langmuir* **22** 10711–5
- [188] Romer W, Lam Y H, Fischer D, Watts A, Fischer W B, Goring P, Wehrspohn R B, Gosele U and Steinem C 2004 Channel activity of a viral transmembrane peptide in micro-BLMs: Vpu<sub>1-32</sub> from HIV-1 *J. Am. Chem. Soc.* **126** 16267–74
- [189] Romer W and Steinem C 2004 Impedance analysis and single-channel recordings on nano-black lipid membranes based on porous alumina *Biophys. J.* **86** 955–65
- [190] Schmitt E K, Vrouenraets M and Steinem C 2006 Channel activity of OmpF monitored in nano-BLMs *Biophys. J.* **91** 2163–71
- [191] De Boer J, Geyer N, Gösele U and Schmidt V 2009 Three-beam interference lithography: upgrading a Lloyd's interferometer for single-exposure hexagonal patterning *Opt. Lett.* **34** 1783–5
- [192] Nussio M R, Oncins G, Ridelis I, Szili E, Shapter J G, Sanz F and Voelcker N H 2009 Nanomechanical characterization of phospholipid bilayer islands on flat and porous substrates: a force spectroscopy study *J. Phys. Chem. B* **113** 10339–47
- [193] Kedrov A, Janovjak H, Sapra K T and Muller D J 2007 Deciphering molecular interactions of native membrane proteins by single-molecule force spectroscopy *Annu. Rev. Biophys. Biomol. Struct.* **36** 233–60
- [194] Grandbois M, Beyer M, Rief M, Clausen-Schaumann H and Gaub H E 1999 How strong is a covalent bond? *Science* **283** 1727–30
- [195] Hochuli E, Döbeli H and Schacher A 1987 New metal chelate adsorbent selective for proteins and peptides containing neighbouring histidine residues *J. Chromatogr. A* **411** 177–84
- [196] Nevo R, Stroh C, Kienberger F, Kaftan D, Brumfeld V, Elbaum M, Reich Z and Hinterdorfer P 2003 A molecular switch between alternative conformational states in the complex of Ran and importin  $\beta$ 1 *Nature Struct. Mol. Biol.* **10** 553–7
- [197] Berquand A, Xia N, Castner D G, Clare B H, Abbott N L, Dupres V, Adriaensen Y and Dufrene Y F 2005 Antigen binding forces of single antilysozyme Fv fragments explored by atomic force microscopy *Langmuir* **21** 5517–23

- [198] Dupres V, Menozzi F D, Locht C, Clare B H, Abbott N L, Cuenot S, Bompard C, Raze D and Dufrene Y F 2005 Nanoscale mapping and functional analysis of individual adhesins on living bacteria *Nature Methods* **2** 515–20
- [199] Conti M, Falini G and Samori B 2000 How strong is the coordination bond between a histidine tag and Ni—nitrilotriacetate? An experiment of mechanochemistry on single molecules *Angew. Chem. Int. Edn Engl.* **39** 215–8
- [200] Schmitt L, Ludwig M, Gaub H E and Tampe R 2000 A metal-chelating microscopy tip as a new toolbox for single-molecule experiments by atomic force microscopy *Biophys. J.* **78** 3275–85
- [201] Kienberger F, Kada G, Gruber H J, Pastushenko V P, Riener C, Trieb M, Knaus H-G, Schindler H and Hinterdorfer P 2000 Recognition force spectroscopy studies of the NTA-His6 bond *Single Molecules* **1** 59–65
- [202] Verbelen C, Gruber H J and Dufrene Y F 2007 The NTA-His<sub>6</sub> bond is strong enough for AFM single-molecular recognition studies *J. Mol. Recognit.* **20** 490–4
- [203] Sapra K T, Damaghi M, Koster S, Yildiz O, Kuhlbrandt W and Muller D J 2009 One beta hairpin after the other: exploring mechanical unfolding pathways of the transmembrane beta-barrel protein OmpG *Angew. Chem. Int. Edn Engl.* **48** 8306–8
- [204] Lee G U, Kidwell D A and Colton R J 1994 Sensing discrete streptavidin biotin interactions with atomic-force microscopy *Langmuir* **10** 354–7
- [205] Marshall B T, Long M, Piper J W, Yago T, Mcever R P and Zhu C 2003 Direct observation of catch bonds involving cell-adhesion molecules *Nature* **423** 190–3
- [206] Neuert G, Albrecht C, Pamir E and Gaub H E 2006 Dynamic force spectroscopy of the digoxigenin-antibody complex *FEBS Lett.* **580** 505–9
- [207] Tang J, Krajcikova D, Zhu R, Ebner A, Cutting S, Gruber H J, Barak I and Hinterdorfer P 2007 Atomic force microscopy imaging and single molecule recognition force spectroscopy of coat proteins on the surface of *Bacillus subtilis* spore *J. Mol. Recognit.* **20** 483–9
- [208] Watanabe Y, Tamura M, Osajima A, Anai H, Kabashima N, Serino R and Nakashima Y 2003 Integrins induce expression of monocyte chemoattractant protein-1 via focal adhesion kinase in mesangial cells *Kidney Int.* **64** 431–40
- [209] Goldstein I J and Iyer R N 1966 Interaction of concanavalin a, a phytohemagglutinin, with model substrates *Biochim. Biophys. Acta Gen. Subj.* **121** 197–200
- [210] Puech P H, Taubenberger A, Ulrich F, Krieg M, Muller D J and Heisenberg C P 2005 Measuring cell adhesion forces of primary gastrulating cells from zebrafish using atomic force microscopy *J. Cell Sci.* **118** 4199–206
- [211] Wojcikiewicz E P, Zhang X, Chen A and Moy V T 2003 Contributions of molecular binding events and cellular compliance to the modulation of leukocyte adhesion *J. Cell Sci.* **116** 2531–9
- [212] Friedrichs J, Helenius J and Muller D J 2010 Quantifying cellular adhesion to extracellular matrix components by single-cell force spectroscopy *Nature Protoc.* **5** 1353–61
- [213] Fredin N J, Broderick A H, Buck M E and Lynn D M 2009 Nanoimprinted thin films of reactive, azlactone-containing polymers: combining methods for the topographic patterning of cell substrates with opportunities for facile post-fabrication chemical functionalization *Biomacromolecules* **10** 994–1003
- [214] Li X, Koller G, Huang J, Di Silvio L, Renton T, Esat M, Bonfield W and Edirisinghe M 2010 A novel jet-based nano-hydroxyapatite patterning technique for osteoblast guidance *J. R. Soc. Interface* **7** 189–97
- [215] Spatz J P and Geiger B 2007 Molecular engineering of cellular environments: cell adhesion to nano-digital surfaces *Methods Cell Biol.* **83** 89–111
- [216] Friedrichs J, Helenius J and Muller D J 2010 Stimulated single-cell force spectroscopy to quantify cell adhesion receptor crosstalk *Proteomics* **10** 1455–62
- [217] Loll P J 2003 Membrane protein structural biology: the high throughput challenge *J. Struct. Biol.* **142** 144–53
- [218] Takai K, Sawasaki T and Endo Y 2008 Development of key technologies for high-throughput cell-free protein production with the extract from wheat embryos *Advances in Protein Chemistry and Structural Biology* (New York: Academic) chapter 2, pp 53–84
- [219] Schneider B, Junge F, Shirokov V A, Durst F, Schwarz D, Dotsch V and Bernhard F 2010 Membrane protein expression in cell-free systems *Methods Mol. Biol.* **601** 165–86
- [220] Junge F, Schneider B, Reckel S, Schwarz D, Dotsch V and Bernhard F 2008 Large-scale production of functional membrane proteins *Cell. Mol. Life Sci.* **65** 1729–55
- [221] Franco R, Casadó V, Cortés A, Mallol J, Ciruela F, Ferré S, Lluís C and Canela E I 2008 G-protein-coupled receptor heteromers: function and ligand pharmacology *Br. J. Pharmacol.* **153** S90–S98
- [222] Fuxe K *et al* 2008 Receptor–receptor interactions within receptor mosaics. Impact on neuropsychopharmacology *Brain Res. Rev.* **58** 415–52
- [223] Franco R, Casadó V, Cortés A, Pèrez-Capote K, Mallol J, Canela E, Ferré S and Lluís C 2008 Novel pharmacological targets based on receptor heteromers *Brain Res. Rev.* **58** 475–82
- [224] Gotti C, Moretti M, Gaimarri A, Zanardi A, Clementi F and Zoli M 2007 Heterogeneity and complexity of native brain nicotinic receptors *Biochem. Pharmacol.* **74** 1102–11
- [225] van Rijn R M, Whistler J L and Waldhoer M 2010 Opioid-receptor-heteromer-specific trafficking and pharmacology *Curr. Opin. Pharmacol.* **10** 73–9
- [226] West I C 1997 Ligand conduction and the gated-pore mechanism of transmembrane transport *Biochim. Biophys. Acta Rev. Biomembr.* **1331** 213–34
- [227] Law C J, Maloney P C and Wang D-N 2008 Ins and outs of major facilitator superfamily antiporters *Annu. Rev. Microbiol.* **62** 289–305
- [228] Hollenstein K, Dawson R J P and Locher K P 2007 Structure and mechanism of ABC transporter proteins *Curr. Opin. Struct. Biol.* **17** 412–8
- [229] Arnaout M A, Mahalingam B and Xiong J-P 2005 Integrin structure, allostery, and bidirectional signaling *Annu. Rev. Cell Dev. Biol.* **21** 381–410
- [230] Scheerer P, Park J H, Hildebrand P W, Kim Y J, Krauss N, Choe H W, Hofmann K P and Ernst O P 2008 Crystal structure of opsin in its G-protein-interacting conformation *Nature* **455** 497–502
- [231] Harris A L 2001 Emerging issues of connexin channels: biophysics fills the gap *Q. Rev. Biophys.* **34** 325–472
- [232] Yildiz O, Vinothkumar K R, Goswami P and Kuhlbrandt W 2006 Structure of the monomeric outer-membrane porin OmpG in the open and closed conformation *EMBO J.* **25** 3702–13
- [233] Cowan S W, Schirmer T, Rummel G, Steiert M, Ghosh R, Pauptit R A, Jansonius J N and Rosenbusch J P 1992 Crystal structures explain functional properties of two *E. coli* porins *Nature* **358** 727–33
- [234] Heymann J B, Muller D J, Landau E M, Rosenbusch J P, Pebay-Peyroula E, Büldt G and Engel A 1999 Charting the surfaces of the purple membrane *J. Struct. Biol.* **128** 243–9
- [235] Pfeiffer M, Rink T, Gerwert K, Oesterheld D and Steinhoff H J 1999 Site-directed spin-labeling reveals the

- orientation of the amino acid side-chains in the E-F loop of bacteriorhodopsin *J. Mol. Biol.* **287** 163–71
- [236] Muller D J, Schoenenberger C A, Büldt G and Engel A 1996 Immuno-atomic force microscopy of purple membrane *Biophys. J.* **70** 1796–802
- [237] Heymann J B, Pfeiffer M, Hildebrandt V, Kaback H R, Fotiadis D, Groot B, Engel A, Oesterhelt D and Muller D J 2000 Conformations of the rhodopsin third cytoplasmic loop grafted onto bacteriorhodopsin *Structure* **8** 643–53
- [238] Fotiadis D, Hasler L, Muller D J, Stahlberg H, Kistler J and Engel A 2000 Surface tongue-and-groove contours on lens MIP facilitate cell-to-cell adherence *J. Mol. Biol.* **300** 779–89
- [239] Fotiadis D, Suda K, Tittmann P, Jenö P, Philippsen A, Muller D J, Gross H and Engel A 2002 Identification and structure of a putative Ca<sup>2+</sup>-binding domain at the C terminus of AQP1 *J. Mol. Biol.* **318** 1381–94
- [240] Scheuring S, Ringler P, Borgnia M, Stahlberg H, Muller D J, Agre P and Engel A 1999 High resolution AFM topographs of the *Escherichia coli* water channel aquaporin Z *EMBO J.* **18** 4981–7
- [241] Hoh J H, Lal R, John S A, Revel J-P and Arnsdorf M F 1991 Atomic force microscopy and dissection of gap junctions *Science* **253** 1405–8
- [242] Schabert F A, Henn C and Engel A 1995 Native *Escherichia coli* OmpF porin surfaces probed by atomic force microscopy *Science* **268** 92–4
- [243] Schubert W D, Klukas O, Krauss N, Saenger W, Fromme P and Witt H T 1997 Photosystem I of *Synechococcus elongatus* at 4 Å resolution: comprehensive structure analysis *J. Mol. Biol.* **272** 741–69
- [244] Fotiadis D, Muller D J, Tsiotis G, Hasler L, Tittmann P, Mini T, Jenö P, Gross H and Engel A 1998 Surface analysis of the photosystem I complex by electron and atomic force microscopy *J. Mol. Biol.* **283** 83–94
- [245] Chpelinsky A B 2009 Structural function of MIP/aquaporin 0 in the eye lens; genetic defects lead to congenital inherited cataracts *Aquaporins* ed E Beitz (Berlin: Springer) pp 265–97
- [246] Hasler L, Walz T, Tittmann P, Gross H, Kistler J and Engel A 1998 Purified lens major intrinsic protein (MIP) forms highly ordered tetragonal two-dimensional arrays by reconstitution *J. Mol. Biol.* **279** 855–64
- [247] Gonen T, Sliz P, Kistler J, Cheng Y and Walz T 2004 Aquaporin-0 membrane junctions reveal the structure of a closed water pore *Nature* **429** 193–7
- [248] Gonen T, Cheng Y, Sliz P, Hiroaki Y, Fujiyoshi Y, Harrison S C and Walz T 2005 Lipid-protein interactions in double-layered two-dimensional AQP0 crystals *Nature* **438** 633–8
- [249] Yeager M and Harris A L 2007 Gap junction channel structure in the early 21st century: facts and fantasies *Curr. Opin. Cell Biol.* **19** 521–8
- [250] Sosinsky G E and Nicholson B J 2005 Structural organization of gap junction channels *Biochim. Biophys. Acta Biomembr.* **1711** 99–125
- [251] Yu J, Bippes C A, Hand G M, Muller D J and Sosinsky G E 2007 Aminosulfonate modulated pH-induced conformational changes in connexin26 hemichannels *J. Biol. Chem.* **282** 8895–904
- [252] Grasberger B, Minton A P, Delisi C and Metzger H 1986 Interaction between proteins localized in membranes *Proc. Natl Acad. Sci. USA* **83** 6258–62
- [253] Panetta R and Greenwood M T 2008 Physiological relevance of GPCR oligomerization and its impact on drug discovery *Drug Discov. Today* **13** 1059–66
- [254] Mo W and Zhang J-T 2009 Oligomerization of human ATP-binding cassette transporters and its potential significance in human disease *Expert Opin. Drug Metab. Toxicol.* **5** 1049–63
- [255] Meng G, Fronzes R M, Chandran V, Remaut H and Waksman G 2009 Protein oligomerization in the bacterial outer membrane *Mol. Membr. Biol.* **26** 136–45
- [256] Fotiadis D, Jastrzebska B, Philippsen A, Muller D J, Palczewski K and Engel A 2006 Structure of the rhodopsin dimer: a working model for G-protein-coupled receptors *Curr. Opin. Struct. Biol.* **16** 252–9
- [257] Czajkowsky D M, Sheng S and Shao Z 1998 Staphylococcal  $\alpha$ -hemolysin can form hexamers in phospholipid bilayers *J. Mol. Biol.* **276** 325–30
- [258] Mou J, Yang J and Shao Z 1995 Atomic force microscopy of cholera toxin B-oligomers bound to bilayers of biologically relevant lipids *J. Mol. Biol.* **248** 507–12
- [259] Klyszejko A L, Shastri S, Mari S A, Grubmuller H, Muller D J and Glaubitz C 2007 Folding and assembly of proteorhodopsin *J. Mol. Biol.* **376** 35–41
- [260] Seelert H, Poetsch A, Dencher N A, Engel A, Stahlberg H and Muller D J 2000 Structural biology. Proton-powered turbine of a plant motor *Nature* **405** 418–9
- [261] Stahlberg H, Muller D J, Suda K, Fotiadis D, Engel A, Meier T, Matthey U and Dimroth P 2001 Bacterial Na<sup>+</sup>-ATP synthase has an undecameric rotor *EMBO Rep.* **2** 229–33
- [262] Pogoryelov D, Yu J, Meier T, Vonck J, Dimroth P and Muller D J 2005 The c15 ring of the *Spirulina platensis* F<sub>1</sub>/F<sub>0</sub> ATP synthase: F<sub>1</sub>/F<sub>0</sub> symmetry mismatch is not obligatory *EMBO Rep.* **6** 1040–4
- [263] Meier T, Yu J, Raschle T, Henzen F, Dimroth P and Muller D J 2005 Structural evidence for a constant c11 ring stoichiometry in the sodium F-ATP synthase *FEBS J.* **272** 5474–83
- [264] Pogoryelov D, Reichen C, Klyszejko A L, Brunisholz R, Muller D J, Dimroth P and Meier T 2007 The oligomeric state of c rings from cyanobacterial F-ATP synthases varies from 13 to 15 *J. Bacteriol.* **189** 5895–902
- [265] Fritz M, Klyszejko A L, Morgner N, Vonck J, Brutschy B, Muller D J, Meier T and Müller V 2008 An intermediate step in the evolution of atpases - a hybrid F<sub>0</sub>-V<sub>0</sub> rotor in a bacterial Na<sup>+</sup> F<sub>1</sub>F<sub>0</sub> ATP synthase *FEBS J.* **275** 1999–2007
- [266] Matthies D, Preiss L, Klyszejko A L, Muller D J, Cook G M, Vonck J and Meier T 2009 The c13 ring from a thermoalkaliphilic ATP synthase reveals an extended diameter due to a special structural region *J. Mol. Biol.* **388** 611–8
- [267] Muller D J, Schabert F A, Büldt G and Engel A 1995 Imaging purple membranes in aqueous solutions at sub-nanometer resolution by atomic force microscopy *Biophys. J.* **68** 1681–6
- [268] Oesterhelt D 1998 The structure and mechanism of the family of retinal proteins from halophilic archaea *Curr. Opin. Struct. Biol.* **8** 489–500
- [269] Junge W 1999 ATP synthase and other motor proteins *Proc. Natl Acad. Sci. USA* **96** 4735–7
- [270] Rastogi V K and Girvin M E 1999 Structural changes linked to proton translocation by subunit c of the ATP synthase *Nature* **402** 263–8
- [271] Dimroth P, Wang H, Grabe M and Oster G 1999 Energy transduction in the sodium F-ATPase of *Propionigenium modestum* *Proc. Natl Acad. Sci. USA* **96** 4924–9
- [272] Meier T, Matthey U, Henzen F, Dimroth P and Muller D J 2001 The central plug in the reconstituted undecameric c cylinder of a bacterial ATP synthase consists of phospholipids *FEBS Lett.* **505** 353–6
- [273] Kienberger F *et al* 2003 Dynamic force microscopy imaging of native membranes *Ultramicroscopy* **97** 229–37

- [274] Greif D, Wesner D, Regtmeier J and Anselmetti D 2010 High resolution imaging of surface patterns of single bacterial cells *Ultramicroscopy* **110** 1290–6
- [275] You H X and Yu L 1999 Atomic force microscopy imaging of living cells: progress, problems and prospects *Methods Cell Sci.* **21** 1–17
- [276] Dupres V, Alsteens D, Andre G and Dufr ne Y F 2010 Microbial nanoscopy: a closer look at microbial cell surfaces *Trends Microbiol.* **18** 397–405
- [277] Butt H J, Downing K H and Hansma P K 1990 Imaging the membrane protein bacteriorhodopsin with the atomic force microscope *Biophys. J.* **58** 1473–80
- [278] Heymann J B, Muller D J, Mitsuoka K and Engel A 1997 Electron and atomic force microscopy of membrane proteins *Curr. Opin. Struct. Biol.* **7** 543–9
- [279] Liang Y, Fotiadis D, Filipek S  , Saperstein D A, Palczewski K and Engel A 2003 Organization of the G protein-coupled receptors rhodopsin and opsin in native membranes *J. Biol. Chem.* **278** 21655–62
- [280] Liang Y, Fotiadis D, Maeda T, Maeda A, Modzelewska A, Filipek S, Saperstein D A, Engel A and Palczewski K 2004 Rhodopsin signaling and organization in heterozygote rhodopsin knockout mice *J. Biol. Chem.* **279** 48189–96
- [281] Fotiadis D, Liang Y, Filipek S, Saperstein D A, Engel A and Palczewski K 2004 The G protein-coupled receptor rhodopsin in the native membrane *FEBS Lett.* **564** 281–8
- [282] Filipek S, Krzysko K A, Fotiadis D, Liang Y, Saperstein D A, Engel A and Palczewski K 2004 A concept for G protein activation by G protein-coupled receptor dimers: the transducin/rhodopsin interface *Photochem. Photobiol. Sci.* **3** 628–38
- [283] Modzelewska A, Filipek S, Palczewski K and Park P S 2006 Arrestin interaction with rhodopsin: conceptual models *Cell Biochem. Biophys.* **46** 1–15
- [284] Scheuring S and Sturgis J N 2005 Chromatic adaptation of photosynthetic membranes *Science* **309** 484–7
- [285] Fotiadis D, Qian P, Philippsen A, Bullough P A, Engel A and Hunter C N 2004 Structural analysis of the reaction center light-harvesting complex I photosynthetic core complex of *Rhodospirillum rubrum* using atomic force microscopy *J. Biol. Chem.* **279** 2063–8
- [286] Singer S J and Nicolson G L 1972 The fluid mosaic model of the structure of cell membranes *Science* **175** 720–31
- [287] Engelman D M 2005 Membranes are more mosaic than fluid *Nature* **438** 578–80
- [288] Lingwood D and Simons K 2010 Lipid rafts as a membrane-organizing principle *Science* **327** 46–50
- [289] Zinser E, Sperka-Gottlieb C D, Fasch E V, Kohlwein S D, Paltauf F and Daum G 1991 Phospholipid synthesis and lipid composition of subcellular membranes in the unicellular eukaryote *Saccharomyces cerevisiae* *J. Bacteriol.* **173** 2026–34
- [290] Frick M, Schmidt K and Nichols B J 2007 Modulation of lateral diffusion in the plasma membrane by protein density *Curr. Biol.* **17** 462–7
- [291] Ramadurai S, Holt A, Krasnikov V, van Den Bogaart G, Killian J A and Poolman B 2009 Lateral diffusion of membrane proteins *J. Am. Chem. Soc.* **131** 12650–6
- [292] Kahya N and Schwille P 2006 Fluorescence correlation studies of lipid domains in model membranes (review) *Mol. Membr. Biol.* **23** 29–39
- [293] Chen Y, Lagerholm B C, Yang B and Jacobson K 2006 Methods to measure the lateral diffusion of membrane lipids and proteins *Methods* **39** 147–53
- [294] Jaskolski F and Henley J M 2009 Synaptic receptor trafficking: the lateral point of view *Neuroscience* **158** 19–24
- [295] Schmidt T, Schutz G J, Baumgartner W, Gruber H J and Schindler H 1996 Imaging of single molecule diffusion *Proc. Natl Acad. Sci. USA* **93** 2926–9
- [296] Weiss S 1999 Fluorescence spectroscopy of single biomolecules *Science* **283** 1676–83
- [297] Muller D J and Engel A 2008 Strategies to prepare and characterize native membrane proteins and protein membranes by AFM *Curr. Opin. Colloid Interface Sci.* **13** 338–50
- [298] Engel A and Muller D J 2000 Observing single biomolecules at work with the atomic force microscope *Nature Struct. Biol.* **7** 715–8
- [299] Muller D J, Baumeister W and Engel A 1996 Conformational change of the hexagonally packed intermediate layer of *Deinococcus radiodurans* monitored by atomic force microscopy *J. Bacteriol.* **178** 3025–30
- [300] Andersen C, Schiffler B, Charbit A and Benz R 2002 pH-induced collapse of the extracellular loops closes *Escherichia coli* maltoporin and allows the study of asymmetric sugar binding *J. Biol. Chem.* **277** 41318–25
- [301] Mari S A, Koster S, Bippes C A, Yildiz O, Kuhlbrandt W and Muller D J 2010 pH-induced conformational change of the  $\beta$ -barrel-forming protein OmpG reconstituted into native *E. coli* lipids *J. Mol. Biol.* **396** 610–6
- [302] Goodenough D A and Paul D L 2009 Gap junctions *Cold Spring Harbor Perspect. Biol.* **1** a002576
- [303] Chang E H, Van Camp G and Smith R J 2003 The role of connexins in human disease *Ear Hear.* **24** 314–23
- [304] Dermietzel R and Hofst dter F 1998 Gap junctions in health and disease *Virchows Arch.* **432** 177–86
- [305] Muller D J, B ldt G and Engel A 1995 Force-induced conformational change of bacteriorhodopsin *J. Mol. Biol.* **249** 239–43
- [306] Muller D J, Heymann J B, Oesterhelt F, M ller C, Gaub H, B ldt G and Engel A 2000 Atomic force microscopy of native purple membrane *Biochim. Biophys. Acta Bioenerg.* **1460** 27–38
- [307] Frederix P L T M, Gullo M R, Akiyama T, Tonin A, Rooij N F D, Staufner U and Engel A 2005 Assessment of insulated conductive cantilevers for biology and electrochemistry *Nanotechnology* **16** 997–1005
- [308] Janovjak H, Kessler M, Oesterhelt D, Gaub H and Muller D J 2003 Unfolding pathways of native bacteriorhodopsin depend on temperature *EMBO J.* **22** 5220–9
- [309] Muller D J, Kessler M, Oesterhelt F, M ller C, Oesterhelt D and Gaub H 2002 Stability of bacteriorhodopsin  $\alpha$ -helices and loops analyzed by single-molecule force spectroscopy *Biophys. J.* **83** 3578–88
- [310] Kedrov A, Krieg M, Ziegler C, Kuhlbrandt W and Muller D J 2005 Locating ligand binding and activation of a single antiporter *EMBO Rep.* **6** 668–74
- [311] Sapra K T, Besir H, Oesterhelt D and Muller D J 2006 Characterizing molecular interactions in different bacteriorhodopsin assemblies by single-molecule force spectroscopy *J. Mol. Biol.* **355** 640–50
- [312] Cisneros D A, Oberbarnscheidt L, Pannier A, Klare J P, Helenius J, Engelhard M, Oesterhelt F and Muller D J 2008 Transducer binding establishes localized interactions to tune sensory rhodopsin II *Structure* **16** 1206–13
- [313] Kedrov A, Janovjak H, Ziegler C, Kuhlbrandt W and Muller D J 2006 Observing folding pathways and kinetics of a single sodium-proton antiporter from *Escherichia coli* *J. Mol. Biol.* **355** 2–8
- [314] Kessler M, Gottschalk K E, Janovjak H, Muller D J and Gaub H E 2006 Bacteriorhodopsin folds into the membrane against an external force *J. Mol. Biol.* **357** 644–54

- [315] Tskhovrebova L, Trinick J, Sleep J A and Simmons R M 1997 Elasticity and unfolding of single molecules of the giant muscle protein titin *Nature* **387** 308–12
- [316] Kellermayer M S S Z, Smith S B, Granzier H L and Bustamante C 1997 Folding–unfolding transitions in single titin molecules characterized with laser tweezers *Science* **276** 1112–6
- [317] Janshoff A, Neitzert M, Oberdörfer Y and Fuchs H 2000 Force spectroscopy of molecular systems—single molecule spectroscopy of polymers and biomolecules *Angew. Chem. Int. Edn Engl.* **39** 3212–37
- [318] Bippes C A, Zeltina A, Casagrande F, Ratera M, Palacin M, Muller D J and Fotiadis D 2009 Substrate binding tunes conformational flexibility and kinetic stability of an amino acid antiporter *J. Biol. Chem.* **284** 18651–63
- [319] Sapra K T, Park P S, Filipek S, Engel A, Muller D J and Palczewski K 2006 Detecting molecular interactions that stabilize native bovine rhodopsin *J. Mol. Biol.* **358** 255–69
- [320] Kawamura S, Colozo A T, Muller D J and Park P S H 2010 Conservation of molecular interactions stabilizing bovine and mouse rhodopsin *Biochemistry* **49** 10412–20
- [321] Kedrov A, Ziegler C and Muller D J 2006 Differentiating ligand and inhibitor interactions of a single antiporter *J. Mol. Biol.* **362** 925–32
- [322] Kedrov A, Hellawell A M, Klosin A, Broadhurst R B, Kunji E R S and Müller D J 2010 Probing the interactions of carboxy-atractyloside and atractyloside with the yeast mitochondrial ADP/ATP carrier *Structure* **18** 39–46
- [323] Janovjak H, Struckmeier J, Hubain M, Kedrov A, Kessler M and Muller D J 2004 Probing the energy landscape of the membrane protein bacteriorhodopsin *Structure* **12** 871–9
- [324] Sapra K T, Balasubramanian G P, Labudde D, Bowie J U and Muller D J 2008 Point mutations in membrane proteins reshape energy landscape and populate different unfolding pathways *J. Mol. Biol.* **376** 1076–90
- [325] Anfinsen C B 1973 Principles that govern the folding of protein chains *Science* **181** 223–30
- [326] Dill K A, Ozkan S B, Shell M S and Weikl T R 2008 The protein folding problem *Annu. Rev. Biophys.* **37** 289–316
- [327] Fersht A R 2008 From the first protein structures to our current knowledge of protein folding: delights and scepticisms *Nature Rev. Mol. Cell Biol.* **9** 650–4
- [328] Schaeffer R D, Fersht A and Daggett V 2008 Combining experiment and simulation in protein folding: closing the gap for small model systems *Curr. Opin. Struct. Biol.* **18** 4–9
- [329] Engelman D M *et al* 2003 Membrane protein folding: beyond the two stage model *FEBS Lett.* **555** 122–5
- [330] MacKenzie K R 2006 Folding and stability of  $\alpha$ -helical integral membrane proteins *Chem. Rev.* **106** 1931–77
- [331] White S H and Wimley W C 1999 Membrane protein folding and stability: physical principles *Annu. Rev. Biophys. Biomol. Struct.* **28** 319–65
- [332] White S H and von Heijne G 2005 Transmembrane helices before, during, and after insertion *Curr. Opin. Struct. Biol.* **15** 378–86
- [333] Hessa T, Kim H, Bihlmaier K, Lundin C, Boekel J, Andersson H, Nilsson I, White S H and von Heijne G 2005 Recognition of transmembrane helices by the endoplasmic reticulum translocon *Nature* **433** 377–81
- [334] Hessa T, Meindl-Beinker N M, Bernsel A, Kim H, Sato Y, Lerch-Bader M, Nilsson I, White S H and von Heijne G 2007 Molecular code for transmembrane-helix recognition by the Sec61 translocon *Nature* **450** 1026–30
- [335] Booth P J 2000 Unravelling the folding of bacteriorhodopsin *Biochim. Biophys. Acta Bioenerg.* **1460** 4–14
- [336] Tamm L K, Hong H and Liang B 2004 Folding and assembly of  $\beta$ -barrel membrane proteins *Biochim. Biophys. Acta Biomembr.* **1666** 250–63
- [337] Booth P J, Templer R H, Meijberg W, Allen S J, Curran A R and Lorch M 2001 *In vitro* studies of membrane protein folding *Crit. Rev. Biochem. Mol. Biol.* **36** 501–603
- [338] Shortle D 2002 The expanded denatured state: an ensemble of conformations trapped in a locally encoded topological space *Adv. Protein Chem.* **62** 1–23
- [339] Smith C R, Mateljevic N and Bowler B E 2002 Effects of topology and excluded volume on protein denatured state conformational properties *Biochemistry* **41** 10173–81
- [340] Bryngelson J D and Wolynes P G 1989 Intermediates and barrier crossing in a random energy model (with applications to protein folding) *J. Phys. Chem.* **93** 6902–15
- [341] Wolynes P G, Onuchic J N and Thirumalai D 1995 Navigating the folding routes *Science* **267** 1619–20
- [342] Frauenfelder H, Sligar S G and Wolynes P G 1991 The energy landscapes and motions of proteins *Science* **254** 1598–603
- [343] Bryngelson J D, Onuchic J N, Socci N D and Wolynes P G 1995 Funnels, pathways, and the energy landscape of protein folding: a synthesis *Proteins: Struct. Funct. Genet.* **21** 167–95
- [344] Henzler-Wildman K and Kern D 2007 Dynamic personalities of proteins *Nature* **450** 964–72
- [345] Jahn T R and Radford SE 2005 The yin and yang of protein folding *FEBS J.* **272** 5962–70
- [346] Frederick K K, Marlow M S, Valentine K G and Wand A J 2007 Conformational entropy in molecular recognition by proteins *Nature* **448** 325–9
- [347] Boehr D D, McElheny D, Dyson H J and Wright P E 2006 The dynamic energy landscape of dihydrofolate reductase catalysis *Science* **313** 1638–42
- [348] Ma B, Kumar S, Tsai C-J, Hu Z and Nussinov R 2000 Transition-state ensemble in enzyme catalysis: possibility, reality, or necessity? *J. Theor. Biol.* **203** 383–97
- [349] Sapra K T, Park P S H, Palczewski K and Muller D J 2008 Mechanical properties of bovine rhodopsin and bacteriorhodopsin: possible roles in folding and function *Langmuir* **24** 1330–7
- [350] Kedrov A, Appel M, Baumann H, Ziegler C and Muller D J 2008 Examining the dynamic energy landscape of an antiporter upon inhibitor binding *J. Mol. Biol.* **375** 1258–66
- [351] Ganchev D N, Rijkers D T S, Snel M M E, Killian J A and De Kruijff B 2004 Strength of integration of transmembrane  $\alpha$ -helical peptides in lipid bilayers as determined by atomic force spectroscopy *Biochemistry* **43** 14987–93
- [352] Sapra K T, Doehner J, Renugopalakrishnan V, Padros E and Muller D J 2008 Role of extracellular glutamic acids in the stability and energy landscape of bacteriorhodopsin *Biophys. J.* **95** 3407–18
- [353] Hammond G S 1955 A correlation of reaction rates *J. Am. Chem. Soc.* **77** 334–8
- [354] Janovjak H, Knaus H and Muller D J 2007 Transmembrane helices have rough energy surfaces *J. Am. Chem. Soc.* **129** 246–7
- [355] Wolynes P G 2005 Energy landscapes and solved protein-folding problems *Phil. Trans. R. Soc. A* **363** 453–67
- [356] Rico F and Moy V T 2007 Energy landscape roughness of the streptavidin–biotin interaction *J. Mol. Recognit.* **20** 495–501
- [357] Nevo R, Brumfeld V, Kapon R, Hinterdorfer P and Reich Z 2005 Direct measurement of protein energy landscape roughness *EMBO Rep.* **6** 482–6

- [358] Damaghi M, Bippes C, Koster S, Yildiz O, Mari S A, Kuhlbrandt W and Muller D J 2010 pH-dependent interactions guide the folding and gate the transmembrane pore of the  $\beta$ -barrel membrane protein OmpG *J. Mol. Biol.* **397** 878–82
- [359] Brouillette C G, Muccio D D and Finney T K 1987 pH dependence of bacteriorhodopsin thermal unfolding *Biochemistry* **26** 7431–8
- [360] Epand R F, Epand R M and Jung C Y 1999 Glucose-induced thermal stabilization of the native conformation of GLUT 1 *Biochemistry* **38** 454–8
- [361] Landin J S, Katragadda M and Albert A D 2001 Thermal destabilization of rhodopsin and opsin by proteolytic cleavage in bovine rod outer segment disk membranes *Biochemistry* **40** 11176–83
- [362] Morin P E, Diggs D and Freire E 1990 Thermal stability of membrane-reconstituted yeast cytochrome c oxidase *Biochemistry* **29** 781–8
- [363] Taneva S G, Caaveiro J M, Muga A and Goñi F M 1995 A pathway for the thermal destabilization of bacteriorhodopsin *FEBS Lett.* **367** 297–300
- [364] Haltia T and Freire E 1995 Forces and factors that contribute to the structural stability of membrane proteins *Biochim. Biophys. Acta Rev. Biomembr.* **1241** 295–322
- [365] Lau F W and Bowie J U 1997 A method for assessing the stability of a membrane protein *Biochemistry* **36** 5884–92
- [366] London E and Khorana H G 1982 Denaturation and renaturation of bacteriorhodopsin in detergents and lipid–detergent mixtures *J. Biol. Chem.* **257** 7003–11
- [367] Pervushin K V, Orekhov V, Popov A I, Musina L and Arseniev A S 1994 Three-dimensional structure of (1–71)bacterioopsin solubilized in methanol/chloroform and SDS micelles determined by  $^{15}\text{N}$ - $^1\text{H}$  heteronuclear NMR spectroscopy *Eur. J. Biochem.* **219** 571–83
- [368] Huang K S, Bayley H, Liao M J, London E and Khorana H G 1981 Refolding of an integral membrane protein. Denaturation, renaturation, and reconstitution of intact bacteriorhodopsin and two proteolytic fragments *J. Biol. Chem.* **256** 3802–9
- [369] Valiyaveetil F I, Zhou Y and Mackinnon R 2002 Lipids in the structure, folding, and function of the KcsA  $\text{K}^+$  channel *Biochemistry* **41** 10771–7
- [370] Park P S H, Sapra K T, Kolinski M, Filipek S, Palczewski K and Muller D J 2007 Stabilizing effect of  $\text{Zn}^{2+}$  in native bovine rhodopsin *J. Biol. Chem.* **282** 11377–85
- [371] Klein-Seetharaman J 2005 Dual role of interactions between membranous and soluble portions of helical membrane receptors for folding and signaling *Trends Pharmacol. Sci.* **26** 183–9
- [372] Pestourie C, Cerchia L, Gombert K, Aissouni Y, Boulay J, De Franciscis V, Libri D, Tavitian B and Duconge F 2006 Comparison of different strategies to select aptamers against a transmembrane protein target *Oligonucleotides* **16** 323–35
- [373] Yildirim M A, Goh K-I, Cusick M E, Barabasi A-L and Vidal M 2007 Drug–target network *Nature Biotechnol.* **25** 1119–26
- [374] Vignais P V, Douce R, Lauquin G J M and Vignais P M 1976 Binding of radioactively labeled carboxyatractyloside, atractyloside and bongkreic acid to the ADP translocator of potato mitochondria *Biochim. Biophys. Acta Bioenerg.* **440** 688–96
- [375] Kobilka B K and Deupi X 2007 Conformational complexity of G-protein-coupled receptors *Trends Pharmacol. Sci.* **28** 397–406
- [376] Tsai C J, Kumar S, Ma B and Nussinov R 1999 Folding funnels, binding funnels, and protein function *Protein Sci.* **8** 1181–90
- [377] Hynes R O 1992 Integrins: versatility, modulation, and signaling in cell adhesion *Cell* **69** 11–25
- [378] Costa P and Parsons M 2010 New insights into the dynamics of cell adhesions *Int. Rev. Cell Molec. Biol.* **283** 57–91
- [379] Humphries J D, Byron A and Humphries M J 2006 Integrin ligands at a glance *J. Cell Sci.* **119** 3901–3
- [380] Geiger B, Bershadsky A, Pankov R and Yamada K M 2001 Transmembrane crosstalk between the extracellular matrix–cytoskeleton crosstalk *Nature Rev. Mol. Cell Biol.* **2** 793–805
- [381] Franz C M and Muller D J 2005 Analyzing focal adhesion structure by atomic force microscopy *J. Cell Sci.* **118** 5315–23
- [382] Grashoff C *et al* 2010 Measuring mechanical tension across vinculin reveals regulation of focal adhesion dynamics *Nature* **466** 263–6
- [383] Roy R, Hohng S and Ha T 2008 A practical guide to single-molecule FRET *Nature Methods* **5** 507–16
- [384] Fernandez-Suarez M and Ting A Y 2008 Fluorescent probes for super-resolution imaging in living cells *Nature Rev. Mol. Cell Biol.* **9** 929–43
- [385] Hell S W 2007 Far-field optical nanoscopy *Science* **316** 1153–8